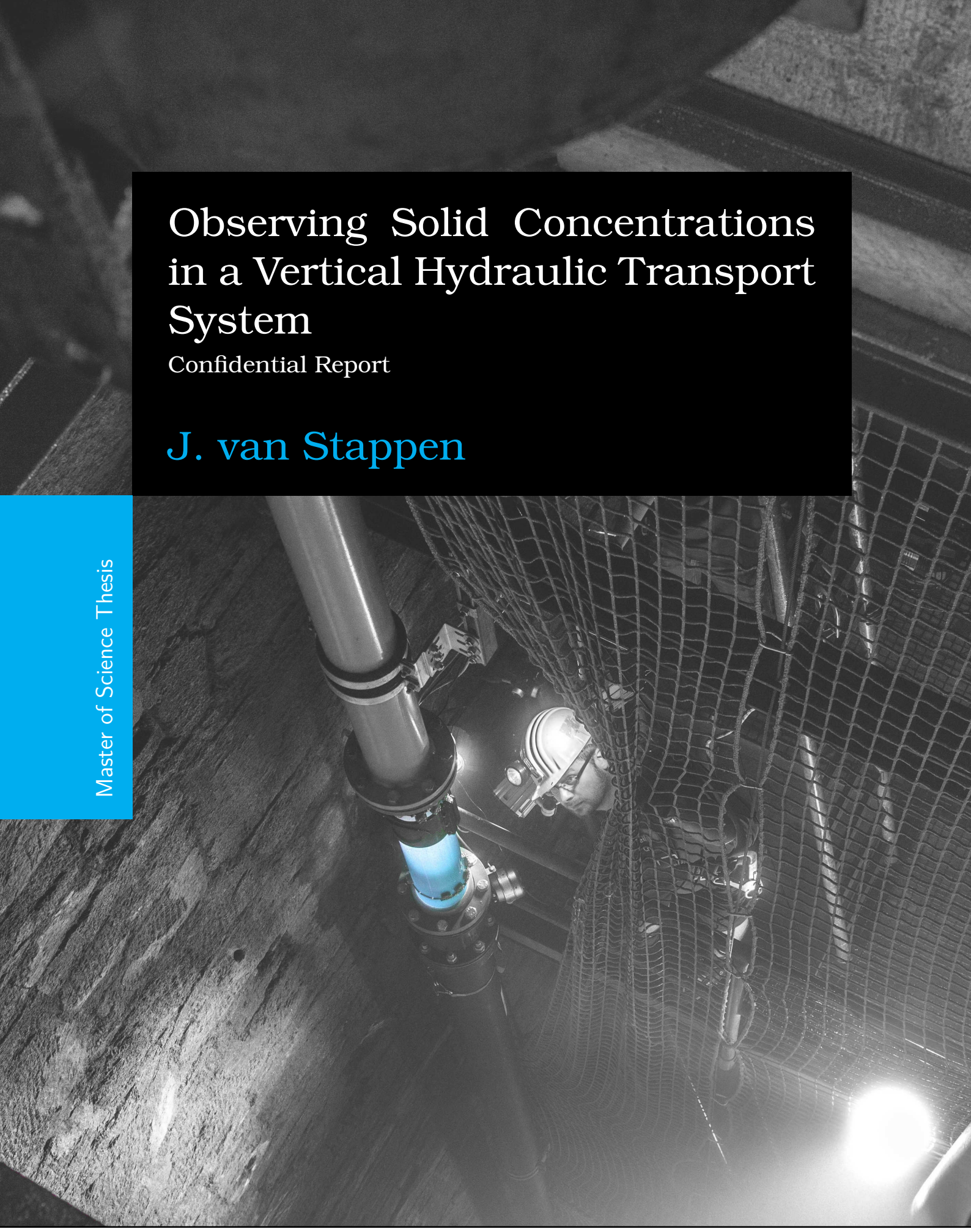

Observing Solid Concentrations in a Vertical Hydraulic Transport System

Confidential Report

J. van Stappen

Master of Science Thesis

TU Delft Delft University of Technology

Observing Solid Concentrations in a Vertical Hydraulic Transport System

Confidential Report

Master of Science Thesis

For the degree of Master of Science in Offshore & Dredging Engineering and Systems & Control at Delft University of Technology

J. van Stappen

March 13, 2018

Faculty of Mechanical, Maritime and Materials Engineering (3mE) · Delft University of Technology

Graduation Committee TU Delft: Prof. dr. ir. J.W. van Wingerden
Dr. ir. S. A. Miedema
Ir. B.M. Doekemeijer
Ir. T.D. Schouten

Graduation Committee Royal IHC: Dr. ir. J.M. van Wijk
Ir. W.B.A. Boomsma

The research presented in this thesis has been financed by Royal IHC, The Netherlands and the European Union Seventh Framework Programme for research, technological development and demonstration under Grant Agreement no. 604500:

Cover: Dipl.-ing. T. Mueller inspecting the riser used for the experiments of this research.

TU Delft Delft University of Technology

Abstract

As the world's population rises and the application of electronics increases, the demand for rare earth metals such as Cobalt and Nickel grows. Deposits of these metals can be found on land but with the increasing demand there is a great probability that these reserves will not be sufficient in the future. It therefore becomes interesting to investigate the possibility of mining these metals out of the ocean. At large depths ($\approx 5000m$) manganese nodules are formed by nature, these are rock shaped objects that contain various rare earth metals, Royal IHC is currently developing equipment to bring these manganese nodules to the shore. A collector is developed which retrieves the nodules from the sea bed, from there the nodules will be transported to the water surface using a Vertical Transport System (VTS). By means of vertical hydraulic transport in the VTS the nodules will be transported to the water surface where they are collected on a vessel.

An important demand of the VTS is that insight of the location of solid concentrations inside the riser is available, this information is required for different reasons: Monitoring the propagation of solid concentrations will enable anticipation of the coming flow at the vessel, it is required for controlling the pumps, it will indicate where plugs are likely to be formed and furthermore it will indicate if the aimed production is achieved. For the vertical transport system it has been proposed to measure the volumetric concentration of solids inside the booster stations located every 1000m and predict the propagation of solids in between these measurements, it was found that this configuration has the disadvantage that measurement error in the booster stations results in an error of the concentration estimation over the whole length of a riser section. An important aspect of the slurry flow is the particle diameter of the collected solids which is identified to be an unknown input of the system, this parameter influences the transport velocity of the solids and therefore needs to be estimated. These two topics gave rise to the following question: "How can the observation of solid concentrations inside a riser be improved?".

In order to evaluate this research question an observer is designed for a scaled test setup of the vertical transport system, on this setup designed improvements will be tested. The basic 1D Vertical Hydraulic Transport system developed at IHC has been chosen to form the basis of the observer, this model simulates the propagation of solids in a riser and is suitable for on-line use. Started is with an observability analysis of this model in order to

find an improved measurement configuration for estimating the solid concentration in the riser, it was found that pressure difference measurements over a large distance of the riser will increase the observability of the system. In order to apply the observer to the test setup it has been investigated how the pressure difference measurements translate into a measured concentration, it was found that the pressure drop created by the wall friction of the mixture can be approximated with the pressure drop due to wall friction under liquid only conditions. Using this knowledge about the measurements a cascade structure observer is designed. First an observer is designed for the fluid velocity in the test setup, the Extended Kalman Filter is found to be suitable for this purpose. The Ensemble Kalman Filter (Enkf) was used to observer the concentration through the riser, using simulations different configurations of this filter were tuned. It was found that an increased performance can be attained if the artificial model perturbations of the Enkf are modelled relative to the ensemble mean. The third part of the observer is an estimator for the particle diameter, a method to estimate the particle diameter is investigated by evaluating what the effect of the particle diameter is on the slurry flow. It is found that the particle diameter can be correlated to the time to travel through a riser section, a proposal for an observer is therefore to adapt the particle diameter by using a proportional integral of the lag found between the concentration estimate over a large distance and the concentration measurement at that point.

The observer has been applied to the test setup which features a scaled riser section of $140m$, first it was evaluated how different pressure difference configurations affect the concentration observation. It was found that by using a pressure difference measurement over the whole section of a riser, by which the mean concentration is measured, the concentration observation at the top of the riser can by significantly improved. With a different configuration the estimation of the particle diameter was investigated, using the observer designed it has been made possible to distinguish mixtures containing different combinations of solids fractions. There are errors in the outcome of the particle diameter estimate due to the fact that at the conditions of the test setup the influence of the particle diameter is only subtle and therefore hard to measure, however it has been proven that by applying the particle diameter observer an improvement can be seen in the concentration observation. A sensitivity of the observer was found to be the relation of the pressure difference measurement to the changing wall roughness of the riser, the effect of this change needs to be accounted for by periodically redetermining the wall roughness.

Using the scaled test setup it was concluded that the long-range pressure difference configuration yields an improved observation of the concentration of solids, furthermore the particle diameter observation has shown to improve the observation as well. Besides the improvements of the observation it has also been proven that over the course of $100m$ the concentration inside the riser can accurately be measured. In order to find these results measurements related to the slurry were conducted and a design for an observer was created based on these measurements, this observer design can be used for implementation in the full scale VTS.

Table of Contents

Preface

The past year I have had the opportunity to perform research at Royal IHC, being involved with conducting one of the largest Vertical Hydraulic Transport experiments ever have made this an unforgettable and educational experience. Since this is a thesis performed in order to obtain two different master degrees some time was spent gathering with everyone who was involved, I would therefore like to thank my supervisors Ir. W.B.A. Boomsma, Dr. ir. Sape Miedema, Dr. ir. J.M. van Wijk and Prof. Dr. ir. J.W. van Wingerden for taking the time and guiding me in the right direction during this research. Also I would like to thank the colleagues from IHC MTI and IHC Mining for making the days at the office always a pleasure. Last but not least, thank you Conny for supporting me during this process.

Delft, University of Technology — J. van Stappen
March 13, 2018

Chapter 1

Introduction

In this chapter background information regarding the thesis subject is provided which is followed by an elaboration on the research question of this thesis. This chapter ends with an explanation of the approach that is used for this research, along with a layout for this thesis.

1-1 Background

As the world's population rises and the application of electronics increases, the demand for rare earth metals such as Cobalt and Nickel grows. Deposits of these metals can be found on land but with the increasing demand there is a great probability that these reserves will not be sufficient in the future. It therefore becomes interesting to investigate the possibility of mining these metals out of the ocean.

In the 19th century it was found that in large area's in earth's oceans so called *polymetallic nodules* are present, these rock like objects are also called *manganese nodules* and contain concentrations of various rare earth metals. Manganese is the main component of the nodules and besides this they also contain various other metals of which nickel, copper, and cobalt are the most valuable [1]. Polymetallic nodules are slowly formed by bacteria and consists of iron and manganese hydroxides, it is estimated that the diameter of a nodule increases with a rate of $0.1mm$ per 1000 years, the diameter of the nodules can be up to $10cm$.

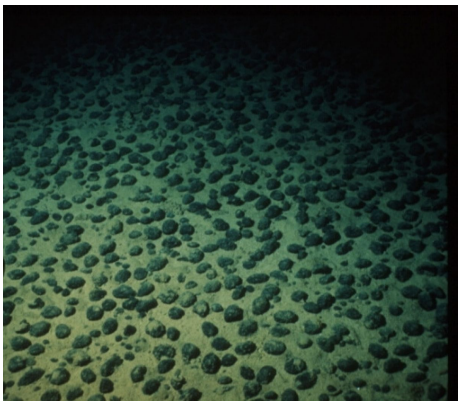

Figure 1-1: Poly-metallic nodules laying on the see floor, source: IHC

Polymetallic nodules are formed in deep sea, large concentrations can be found at depths ranging from 4000-6000m and the concentration of a field can reach values up to $15kg/m^2$. In Figure 1-1 it can be seen how nodules are spread on the sea bed.

Currently a way to retrieve these nodules from the sea floor is being investigated by IHC. Besides developing a collector that harvests the nodules, a Vertical Transport System (VTS) is designed to bring the nodules to the water surface where they are collected at a vessel. The method of vertical hydraulic transport is favoured by IHC for this purpose: Water is pumped through a riser using centrifugal pumps and at the bottom of the riser the solids are added to the system. Due to drag forces the nodules are transported to the surface along with the carrying fluid. In Figure 1-2 a schematic representation of the riser is presented.

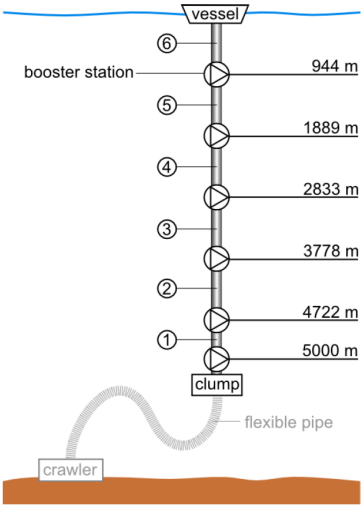

Figure 1-2: Vertical Transport System (VTS)

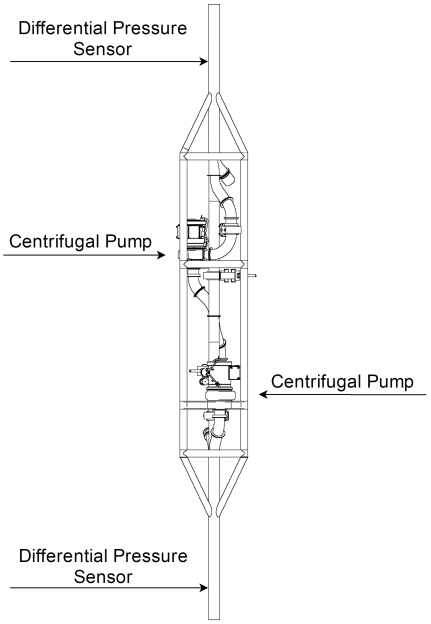

Figure 1-3: Booster Station

As is seen in the figure the riser is divided into different riser sections that have a length of approximately $1000m$, between every riser section a booster station is present, of which a larger image is shown in Figure 1-3. Every booster station contains two centrifugal pumps, these pumps are the driving force of the the vertical transport system.

An important demand of the VTS is that insight of the location of solid concentrations inside the riser is available, this information is required for different reasons: Monitoring the propagation of solid concentrations will enable anticipation of the coming flow at the vessel, it is required for controlling the pumps, it will indicate where plugs are likely to be formed and furthermore it will indicate if the aimed production is achieved. Before and after every booster station a differential pressure sensor is placed which measures the pressure drop over a section of $6m$, this setup has been chosen to be a suitabele way to measure the volumetric concentration at the location of the booster stations [2].

It has been proposed to use the concentration measurements at the booster stations and predict the propagation of the solids through the riser [2], for this purpose a model describing vertical hydraulic transport has been developed [3] and it has been adjusted for real time estimation [2]. Problems encountered with this configuration is that if the concentration is not measured correctly at a booster station the observation of concentration over the whole section of a riser is influenced. A second issue with this configuration is that the propagation of solids needs to be predicted over a long section, the accuracy of this prediction depends on the correctness of the model. An unknown input of the model is the particle diameter of the transported solids, a good estimate of this parameter is important to predict the velocity of solids through the riser.

IHC has designed and built a test setup to investigate phenomena related to Vertical Hydraulic Transport of solids, experiments are conducted in a circuit that features a riser section of approximately $140m$. In the circuit pressure sensors will be installed which make this an ideal set-up for investigating the observation of solid concentrations in a riser, the measurement data of this test program will be used for this research.

1-2 Research Question

Using pressure difference measurements the volumetric concentration of solids within the vertical transport system needs to be monitored, at IHC a proposal for an observer was made based on the Ensemble Kalman Filter but the configuration of this proposed observer has the issue that the estimate of the concentration of a whole riser section is dependent on the measurement in the booster station below that section.

The particle diameter is identified as an unknown input of the system, this parameter influences the velocity of solids in the riser with respect to the velocity of the carrying fluid and is therefore required to estimate the concentration of solids in between the riser section. A method to observe this parameter has not yet been developed, these two aspects have lead to the following research question:

"How can the observation of solid concentrations inside a riser be improved?"

A literature survey has been conducted in order to map relevant literature regarding Vertical Hydraulic transport and observer structures [4]. It is found that the pressure drop of a vertical section is influenced by the mixture wall shear stress, and that there are different models describing this effect. This phenomena needs to accounted for when measuring the volumetric concentration from the pressure difference measurements. No method was found to measure the particle diameter on-line in a vertical flow, however it might be possible to observer this parameter if a physical relation with the measurements in the riser can be found. Also it was found that the efficiency of the pump is influenced by the particle diameter which may provide a method to measure this parameter.

A scaled Vertical Transport System is available to evaluate the research question of this thesis, the following sub-questions are defined to answer this question:

- How significant is the contribution of the solids to the pressure drop created by wall friction in a vertical pipe?
- Is the particle diameter of the solids measurable in the performance of a centrifugal pump?
- What are the problems previously encountered with the Ensemble Kalman filter? How are they mitigated?
- Is it possible to measure the particle diameter in a vertical flow using pressure difference measurements, combined with fluid velocity measurements?
- How do results of scaled experiments translate into a conclusion for a full scale vertical transport system?

1-3 Approach and Thesis Structure

Insight of the volumetric concentration of solids throughout the riser is aimed for which is why a so called *observer* is designed: a method to estimate this concentration. The goal of this research is to find a solution to the problems that were elaborated, for this purpose two tools will be available:

- Simulations of an 1D Vertical Hydraulic Transport model
- A scaled test setup of a Vertical Transport System

The full scale VTS is divided in sections of approximately $1000m$ and before and after these sections a booster stations is present where the concentration can be measured. The aim of the observer is therefore to measure the concentration over the length of $1000m$, if this can be done it will also be feasible to observer the concentration in all the other riser sections too.

An observer design is made in order to evaluate the effect of designed improvements, this observer will be tested on the simulations and the scaled test setup that is available. At this point an early design of the observer can already be proposed. The output of the observer will be the concentration throughout the riser, and it is known that the observations will consist out of pressure difference measurements which are therefore the input of the observer. An observation of the fluid velocity needs to be made which will be used to determine the propagation of solids in between the Δp measurements, furthermore based on the results of the concentration measurements the particle diameter is corrected. A simplified observer structure is made which will be used throughout this report, in Chapter 5 the structure underneath this scheme is further elaborated:

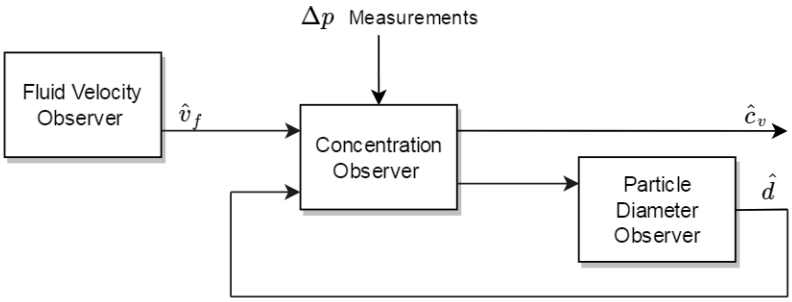

Figure 1-4: Simplified Observer Structure

The structure of this thesis is as follows: Chapter 2 will provide an elaboration on vertical transport models available, with the structure of these models it is evaluated what kind of measurement configuration will yield the best observability conditions for measuring the volumetric concentration throughout the riser. Also simulations will be elaborated of a full size VTS section, which will be used to test the observer on.

In Chapter 3 the test setup that is used to conduct experiments is explained. A list of conducted measurements is provided along with an explanation of the measurement procedure. Furthermore, a comparison is made between the scaled test setup and the full scale VTS.

Using the data of the measurements it is elaborated what will be the input of the observer, and how this signals will be used: in chapter 4 it is investigated how Δp measurements will translate into a measured concentration, and what the effect is of different solid types on these measurements. Furthermore it is investigated what useful information about the slurry can be retrieved from measuring the decrease in pump efficiency.

In Chapter 5 the observer design is explained according to the structure shown in Figure 1-4. Methods to measure the fluid velocity are compared, and based on simulations a concentration observer and a particle diameter observer are designed and tested. At the end of the chapter it is explained how this observer design will be suitable for both the test setup VTS and the full scale VTS.

The results of observing solid concentrations in the scaled vertical transport system are shown in Chapter 6. With these results it is investigated whether made improvements of the observer can be considered effective. Chapter 7 provides provides the answers to the research questions and recommendations for further research.

Chapter 2

Model Description

In this chapter the models that are relevant for the observer are described. An elaboration is provided about the 1DVHT model which simulates the propagation of solids in a riser, and the b1DVHT model is explained which is a simplification of this model designed for on-line use in an observer. An observability analysis is performed based on the b1DVHT model, with this analysis it will be determined if there is a measurement construction that improves the observability of the system. Furthermore it will be determined if the particle diameter can be observed from the measurements. The last section of this chapter is dedicated to simulations of the 1DVHT model which will be used for the design of the observer in chapter 5.

2-1 Vertical Hydraulic Transport Models

The principles of vertical transport have been elaborated in the literature survey [4]. 2 vertical transport models have been created at IHC: a 1D-Vertical Hydraulic Transport Model (1DVHT model) which has been validated and a simplification of this model designed for online use, the basic 1D-Vertical Hydraulic Transport Model (b1DVHT model). Both models can be represented with the following input-output structure, where only the information important for this research is considered:

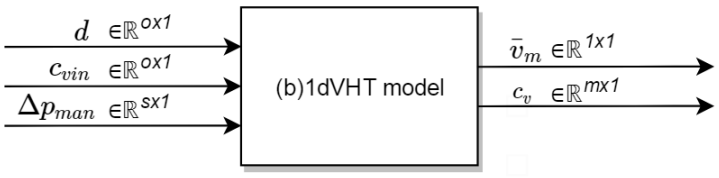

Figure 2-1: Input-output scheme of the (b)1DVHT model

There are o solid fractions which are added to the riser at the bottom with a corresponding particle diameter $d[mm] \in \mathbb{R}^{o\times 1}$ and an inlet concentration $c_{vin}[-] \in \mathbb{R}^{o\times 1}$. The slurry is

brought into motion by the centrifugal pumps, of which a number of s is installed creating each a manometric pressure $\Delta p_{man}[Pa] \in \mathbb{R}^{s\times 1}$. The result is a mixture bulk velocity $\bar{v}_m[m/s] \in \mathbb{R}^{1\times 1}$ which is equal through the whole riser, the riser is spatially discretised into m states and at every state a volumetric concentration of solids $c_v \in \mathbb{R}^{m\times 1}$ is determined.

The definition of the volumetric concentration ($c_v[-]$) is important for this research, it is aimed to observer this parameter in the slurry. The volumetric concentration in a riser cell is the volume that is occupied by solids, this parameter can be expressed using the density of the mixture $\rho_m[kg/m^3]$ that is measured, the density of the solids $\rho_s[kg/m^3]$ and the density of water $\rho_f[kg/m^3]$:

$$c_v = \frac{\rho_m - \rho_f}{\rho_s - \rho_f} \tag{2-1}$$

2-1-1 1D Vertical Hydraulic Transport model

A thesis has been dedicated investigating the vertical transport of manganese nodules [3], the conclusion of this thesis is that there is a possibility of plug formation of solids in the VTS which has been the motive to investigate the monitoring of concentrations. Part of the work done for this thesis is the design of the 1DVHT model *1D vertical hydraulic transport model*. This model simulates propagations of solid concentrations in one dimension driven by a vertical flow of water. It takes into account the effect of multiple fractions of particle diameters present in the flow, and solves the following equation numerically which accounts for both advection and diffusion:

$$\frac{\partial c_v}{\partial t} + \frac{\partial c_v v_s}{\partial z} = \frac{\partial}{\partial z}\left(\epsilon_z \frac{\partial c_v}{\partial z}\right) \tag{2-2}$$

The momentum equation is solved using the implicit Adam-Bashfort 2-time integration scheme, the pressure distribution is then solved using a succesove overrelaxation method. Outcome of the model has been validated by making use of a sedimentation test, the results have shown good agreement between the model and the experiments.

2-1-2 Basic 1D Vertical Hydraulic Transport model

The 1DVHT model is too computationally intensive to run realtime and it has therefore been investigated how the complexity of the model can be decreased. Simplifications of the model have been investigated that aim on reducing the computational power needed while maintaining a model that approaches the output of the 1DVHT model [2]. The simplified model is called the b1DVHT model (basic 1D Vertical Hydraulic Transport), in this model the implicit scheme used to solve the momentum equation is changed into an explicit scheme. Furthermore it was found that simulations of the 1DVHT model where a full Particle Size Distribution (PSD) was used to simulate the slurry could be represented as a reduced PSD of 1 or 2 representative solid fractions.

The equations describing the model are elaborated, the b1DVHT model can be expressed as a state space model such that:

$$\begin{aligned} x(k+1) &= f(x(k), u(k)) + w(k) \\ y(k) &= h(x(k)) + v(k) \end{aligned} \tag{2-3}$$

Process and measurement noise are represented as $w(k)$ and $v(k)$ with the following gaussian distributions: $p(w) \sim N(0, Q)$, $p(v) \sim N(0, R)$. For a system where 1 fraction of solids is present, and one pump is installed this yields the following state space model:

$$x(k) = \begin{bmatrix} \bar{v}_m(k) \\ c_{v1}(k) \\ c_{v2}(k) \\ c_{v3}(k) \\ \vdots \\ c_{vm}(k) \end{bmatrix}, y(k) = h(x(k)) = \begin{bmatrix} \bar{v}_m \\ c_v \\ \vdots \end{bmatrix}, u(k) = \begin{bmatrix} c_{vin}(k) \\ p_{man}(k) \end{bmatrix} \tag{2-4}$$

The state update of $\bar{v}_m$ for a riser is described in [2] however this model is not valid for the test setup that will be used, a velocity model suitable for the test setup is therefore elaborated in Chapter 5. Using the bulk mixture velocity, the concentration and a measured fluid velocity the following equation is solved:

$$\bar{v}_m = c_v \cdot v_s + (1 - c_v) \cdot v_f \tag{2-5}$$

To solve this equatiun the solids velocity v_s needs to be known, this parameter has a certain slip with respect to the fluid velocity v_f which is where the influence of the particle diameter is seen. The slip is the hindered settling velocity, which is a result of the terminal (maximum) settling velocity $w_t[m/s]$ calculated with the equation of Ferguson and Church [5]. Extensions for hindered settling in a riser [6] [7] yield the following formula:

$$v_s = v_f - 10^{-\frac{d}{D}} w_t(d)(1 - c_v)^{n-1} \tag{2-6}$$

Where $D[m]$ represents the riser diameter. Solving the solids velocity flux at every location ($F_i = c_{vi} \cdot v_{si}$), and spatial and temporal discretisation of the (b)1dVHT model is elaborated in [3] and leads to the following equation for the state update:

$$\begin{aligned} c_{v_i}(k+1) = c_{v_i}(k) \\ &- \chi_{i+1} \frac{\Delta t}{\Delta z} (\frac{1}{2}(F_i(k) + F_{i+1}(k)) - \frac{1}{2}(|F_{i+1}(k)| - |F_i(k)|)) \\ &+ \chi_i \frac{\Delta t}{\Delta z} (\frac{1}{2}(F_i(k) + F_{i-1}(k)) - \frac{1}{2}(|F_i(k)| - |F_{i-1}(k)|)) \\ &- \chi_{i+1} \frac{\Delta t}{2\Delta z} \psi(r_i)(sign(F_i(k)) - v_{s_i} \frac{\Delta t}{\Delta z})(F_{i+1}(k) - F_i(k)) \\ &+ \chi_i \frac{\Delta t}{2\Delta z} \psi(r_{i-1})(sign(F_{i-1}(k)) - v_{s_{i-1}} \frac{\Delta t}{\Delta z})(F_i(k) - F_{i-1}(k)) \\ &+ \epsilon_z \frac{\Delta t}{\Delta z^2}(c_{v_{i+1}}(k) - 2c_{v_i}(k) + c_{v_{i-1}}(k)) \end{aligned} \tag{2-7}$$

In order to suppress oscillations in the solution, the van Leer limiter was applied bi-directional since the velocity of the particles is possible in both directions:

$$r_i = \frac{F_{j'+1} - F_{j'}}{F_{j+1} - F_j},\ \phi(r_i) = \frac{r_i + |r_i|}{1 + |r_i|},\ i' = i - sign(v) \tag{2-8}$$

Furthermore a packing limiter was introduced, this limiter is used to make sure that cells that are completely filled with solids cannot reach a volumetric concentration larger than the maximum value. Outflow of the solids is still possible if the cell is full while inflow is blocked. The binary packing limiter has the following characteristics:

$$\chi_i = \begin{cases} 1,\ if\ 0 < c_{v,i} < c_{v,max} \\ 0,\ if\ c_{v,i} = c_{v,max} \end{cases} \tag{2-9}$$

It can be concluded that the update equations presented are non-linear, and due to terms as the *modulus*, *sign* and the packing limiter the model is non differentiable which limits the options for possible observers.

The Courant-Friedrichs-Lewy (CFL) condition is used to verify the stability of numerical schemes [8]. This fundamental stability condition of most explicit schemes for wave and convection equations expresses that the distance at covered during the time interval Δt, by the disturbances propagating with speed v_s, should be lower than the minimum distance between two mesh points. The CFL number is defined as:

$$\sigma_c = \frac{v_s \Delta t}{\Delta x} \tag{2-10}$$

For the Lax-Wendroff scheme used in the discretisation stability is ensured if the following condition holds:

$$|\sigma_c| \leq 1 \tag{2-11}$$

This means that the mesh ratio $\frac{\Delta t}{\Delta z}$ has to be chosen accordingly for the experiments.

2-2 Observability Analysis

An observability analysis is performed, the purpose of this analysis is to find a configuration of sensors that increases the observability and therefore the quality of the concentration observation. Furthermore it is verified whether the unknown input that is the particle diameter can be observed from the concentration measurements.

The b1DVHT model is non-linear which means that for an observability analysis calculating the Jacobian is needed. Due to different terms in the the equations (*modulus,sign*) the Jacobian cannot be evaluated, but under certain conditions it is possible to reduce the b1DVHT model to a form that is more convenient. Started is with $\chi_{1:m} = 1$, indicating that no plugs are present in the riser. The second assumption is that the solids are all going up which means $F_{1:m}$ is positive which removes the modulus in the formula. Third, the *van Leer*

limiter is removed, which reduces the system to the following simple upwind version of the advection-diffusion equation:

$$\begin{aligned} c_{v_i}(k+1) = c_{v_i}(k) \\ &+ \frac{\Delta t}{\Delta z} v_s(k) \cdot c_{v_{i-1}}(k) - \frac{\Delta t}{\Delta z} v_s(k) \cdot c_{v_i}(k) \\ &+ \frac{\epsilon_z}{\Delta z^2}(c_{v_{i+1}}(k) - 2c_{v_i}(k) + c_{v_{i-1}}(k)) \end{aligned} \tag{2-12}$$

Observability is analysed evaluating the rank of the observability co-distribution O_c which is derived using the observation space O_s, this matrix is shown in equation 2-13. Local observability is proved if the observability co-distribution is full rank [9].

$$O_c = dO_s,\ O_s = span \begin{bmatrix} L_f^0 h(x) \\ L_f^1 h(x) \\ L_f^2 h(x) \\ \vdots \end{bmatrix} \tag{2-13}$$

2-2-1 Sensor Configurations

The following example is analysed: a VTS is considered of which the space is divided into 8 states, it is assumed that it is possible to measure v_s. Two configurations are tested, the one proposed [2] (1) where problems were encountered, and a new configuration (2). Configuration 1 has pressure difference measurement after the booster station, this allows to determine the volumetric concentration locally at that point. Configuration 2 uses a pressure difference measurement over a long range, with this measurement the mean concentration of the covered section can be determined, covering multiple spatial states. Both configurations are shown in figure 2-2 (the riser is turned 90°):

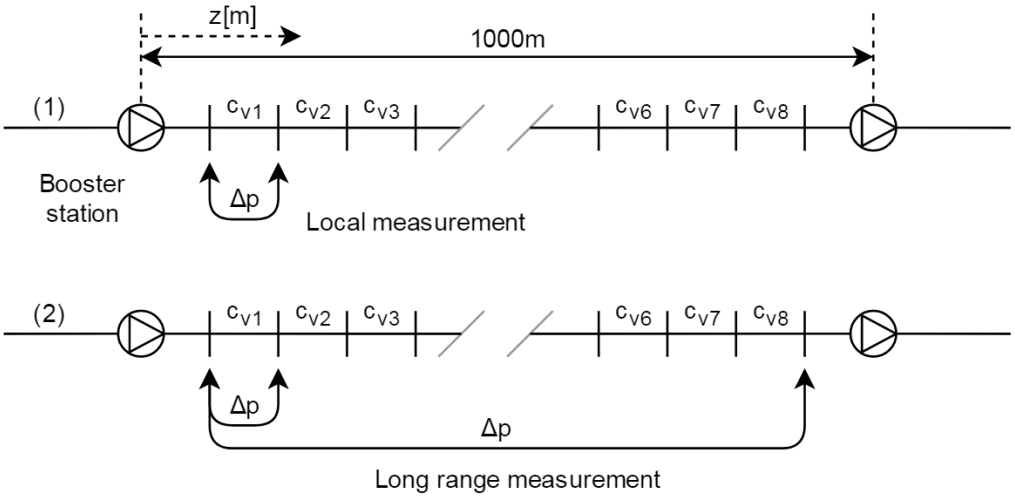

Figure 2-2: Measurement configuration 1 and 2

The reduced system leads to a state matrix that is the same for both configurations, and two different output matrices h_1 and h_2:

$$x = \begin{bmatrix} v_s \\ c_{v1} \\ c_{v2} \\ c_{v3} \\ \vdots \\ c_{v8} \end{bmatrix}, y_1 = h_1(x) = \begin{bmatrix} v_s \\ c_{v1} \end{bmatrix}, y_2 = h_2(x) = \begin{bmatrix} v_s \\ c_{v1} \\ \frac{1}{8}(c_{v1} + c_{v2} + \cdots + c_{v7} + c_{v8}) \end{bmatrix} \tag{2-14}$$

The observability analysis is performed for both configurations and the co-distributions is evaluated up to $L_f^{10}h(x)$. The smallest singular value of the observability matrix is a measure for the observability of the system [10] and is therefore compared. In figure 2-3 the singular values of the observability co-dsitrbution are plotted for configuration 1 and 2.

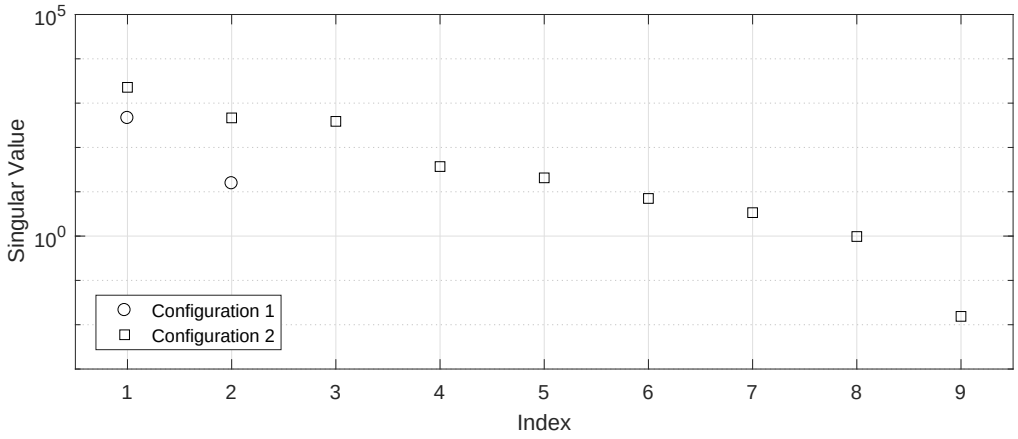

Figure 2-3: Singular values of the observability co-distribution

There is no need to compare the lowest singular values, it can be seen directly that configuration 1 yields an unobservable system since it is not full rank. This can be explained: Assuming the flow goes up causes that the states above c_{v1} will never appear in the output of c_{v1} since this state is only a affected by the states underneath is. Thus mathematically configuration 1 is unobservable, which means that the estimate of states in the riser section will only be based on the correctness of the model and not on actual measurements. Configuration 2 yields an observable system and therefore this configuration is preferred. It will be tested using measurements of the test setup whether this configuration will yield an improved observation.

What is discovered is the cause for an issue described in [2], in that thesis it was found that when configuration 1 is used it was impossible to correctly estimate the concentration of a whole riser section when the Δp measurements below that section was influenced by a static error. The reason for that is found: the states outside the booster station were actually not observable, configuration 2 will mitigate this problem.

2-2-2 Particle Diameter

The particle diameter was identified as an unknown input of the system, it is therefore analysed if this input can be estimated using configuration 2. To find out if this is true, another case is investigated, this time the solids velocity is defined as the fluid velocity minus the hindered settling velocity ($v_s = v_f - w_h$). The fluid velocity is considered to be measured instead of the solid velocity, and the hindered settling velocity (w_h) is added to the system as an extra state, this is configuration 3. The singular values of configuration 2 and 3 are compared:

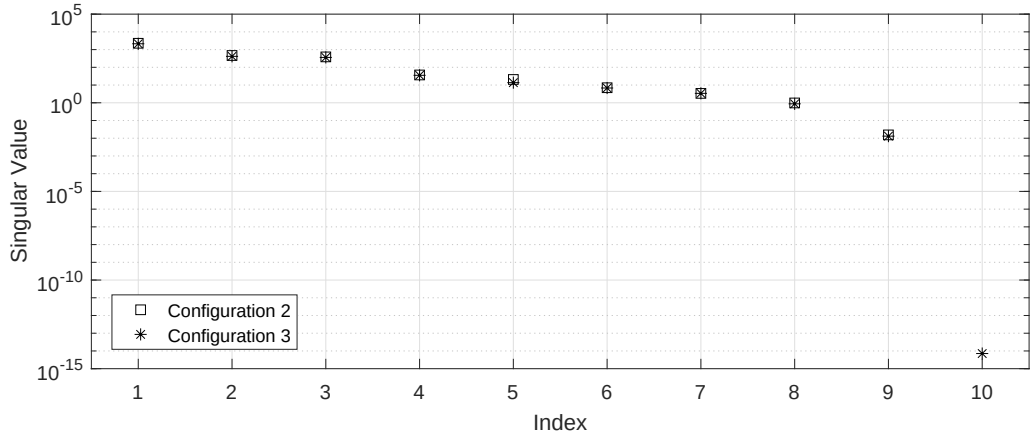

Figure 2-4: Singular values of the observability co-distribution

The singular values of configuration 3 are very similar to the singular values of configuration 2, however it has one extra state and one extra singular value in the order of 10^{-15}. This yields the observability matrix to be not full-rank and it is therefore concluded that the settling velocity and thus the particle diameter cannot be observed from this measurement configuration.

2-3 Simulation Cases

The 1DVHT model is considered to be the most accurate representation of the solid propagation inside a riser since it has been validated using sedimentation tests. In Chapter 5 an observer design will be elaborated, and in order to test this design before it is applied on the measurements, simulations of the 1DVHT model will be used. A riser is simulated with a length of $1200m$ and a diameter of $0.356m$, these values are chosen in order to simulate a section of the full scale VTS. At the bottom of this section a varying inlet concentration is simulated, this signal is shown in Figure 2-5 and represents the irregularity of collecting nodules from the sea floor:

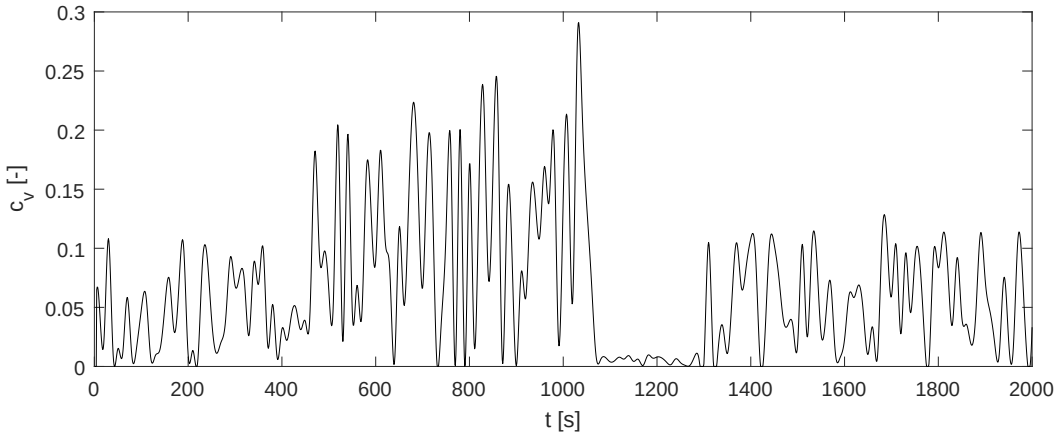

Figure 2-5: Inlet Concentration

The inlet concentration signal is used to simulate multiple cases of which an overview is provided in Table 2-1. Case A and B are designed in order to simulate slurry transport of single fractions, for a solid type with a low settling velocity (A), and for a solid type with a significantly higher settling velocity (B). Case C simulates a mixture with a mean diameter of 30mm, and a small spread in the PSD. Case D is designed to simulate a mixture that contains various fractions that can be found in a manganese nodule field, and has a mean diameter of 42mm.

Table 2-1: Simulation cases

Reference	Particle Sizes [mm]	Fractions [-]	Duration [s]	Δt	Δz
A	1	1	2000	0.1	1
B	10	1	2000	0.1	1
C	[15,25,35,45]	[0.25,0.25,0.25,0.25]	2000	0.1	1
D	[8,15,18,24,30,30,40,50,80,125]	[0.1,0.1, ... ,0.1,0.1]	2000	0.1	1

A sample of the output of simulation A and B is shown in Figure 2-6, in this image the concentration of solids in the riser can be seen discretised over 1200 states.

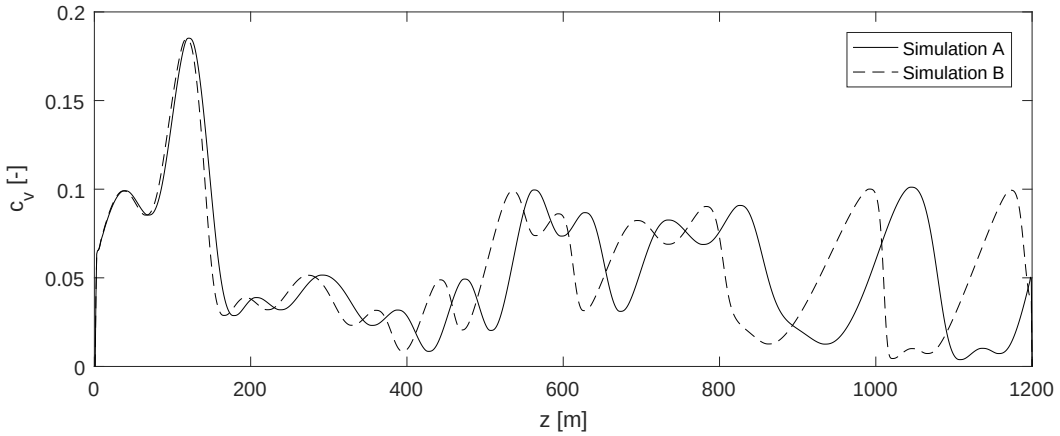

Figure 2-6: Simulated concentration in riser at $t = 500s$, case A and B

As can be seen in the figure the smaller solid fractions travel faster than the larger solid fractions. Cases C and D differ from cases A and B, the mixture cases have multiple solid fractions which means that there are also different settling velocities. This results in overtaking of solid fractions, which means that the waves of the inlet concentration are slowly transformed over the course of the riser.

Chapter 3

Experimental test setup

A test setup has been built in Halsbrücke, Germany in cooperation with the university of Freiberg (TUBAF). This setup, referred to as the *Test Setup VTS*, is a scaled version of the *full scale VTS*. In this chapter the test setup is described, along with the procedure of the experiments and findings of the flow behaviour.

3-1 Objective of IHC

Currently IHC is developing the Vertical Transport System, which will be the longest vertical hydraulic transport system ever established. Building a full scale riser with a length of 5000m is a very big leap considering that all previous vertical transport tests perfomed by IHC were in the scale of a few meters. That is why an intermediate step is made by making a test setup one order bigger than what has been done before, the result is a riser of approximately 140m. With this setup IHC aims to gain insight in flow behaviour of hydraulic transport applied to manganese nodules. One of the phenomena investigated by IHC with this setup is the occurrence of density waves, which would result in stagnating solid velocities.

For this thesis the results of the tests are very useful, which is why I have been involved with executing the experiments. The riser section of the circuit contains pressure sensors every 10m which makes this setup suitable for experiments regarding the observation of solid concentrations with Δp measurements.

3-2 Test Setup Vertical Transport System

The test program is set up to investigate the behaviour of solid particles in a vertical transport system, IHC has chosen a location in Halsbrücke for this test setup which features an empty vertical mine shaft with a depth of approximately 140m.

In this mineshaft a closed circuit is built with a riser and a downcomer: two parallel vertical pipelines $1.80m$ apart from each other. They are connected at the bottom with a U-shaped

bend and both tubes have an inner diameter of $D = 0.1452m$, the total circuit has a length of $318m$. The experimental setup is designed to simulate the conditions of the VTS, however the difference is that this circuit is a closed loop in order to establish a continuous inflow of the riser section where the majority of sensors is installed.

Above the riser (ground level) the pipeline exits the mineshaft and after a horizontal section of $20m$ it enters the injection and separation container, in this container the *hoppers* are present. These are large containers on top of the pipe, connected to the circuit. Before every slurry experiment the hoppers are filled with the right amount and type of solids and during the tests the solids are gradually added to the circuit using manually operated valves. In Figure 3-1 the pipes and components outside the mineshaft are shown: in this figure the tanks which are used to store water are marked as 1, 2 shows the separation tank which is used to store the solids after the tests. At number 3 we find the hoppers, and at number 4 the centrifugal pump is located. The above-ground pipeline is manufactured from steel, other than the underground vertical pipelines which are manufactured from High-Density Poly Ethylene (HDPE).

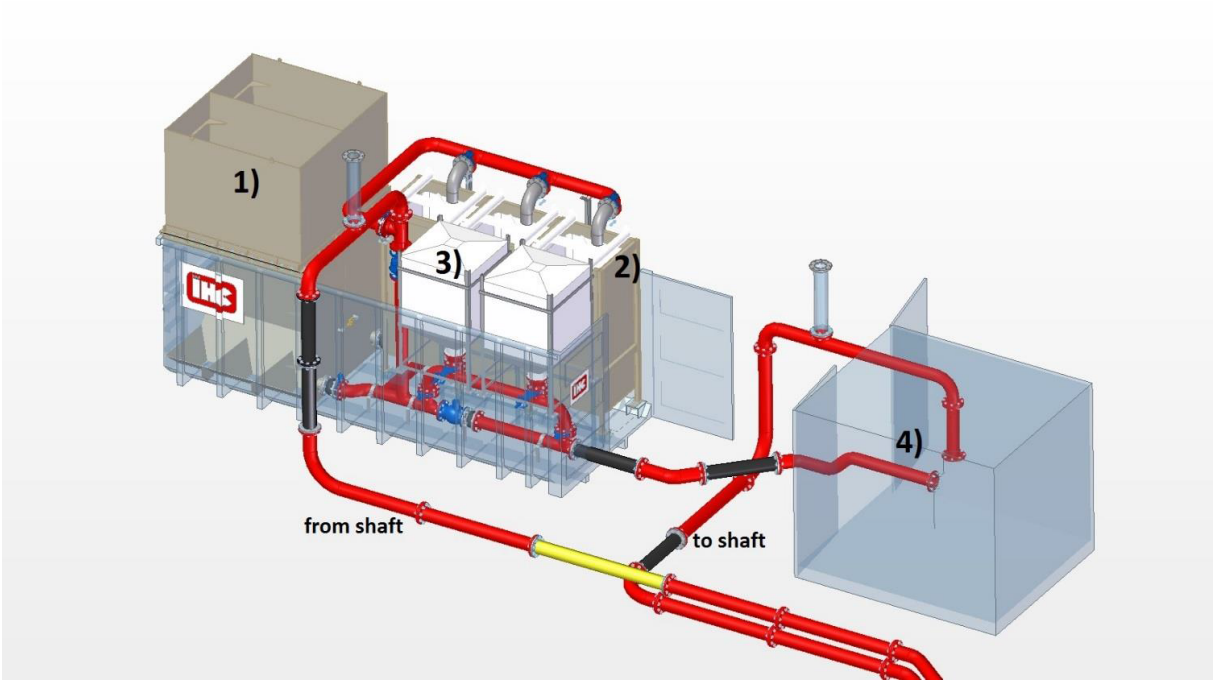

Figure 3-1: Piping and components above ground, Source: IHC

At the test site a control cabin has been placed from which the majority of valves can be controlled, and from which the rotational speed of the pump can be regulated. In the control cabin the output of sensors can be monitored as well. In Figure 3-2 a CAD drawing of the full setup is depicted in order to give an impression of the scale of this experimental setup and test site.

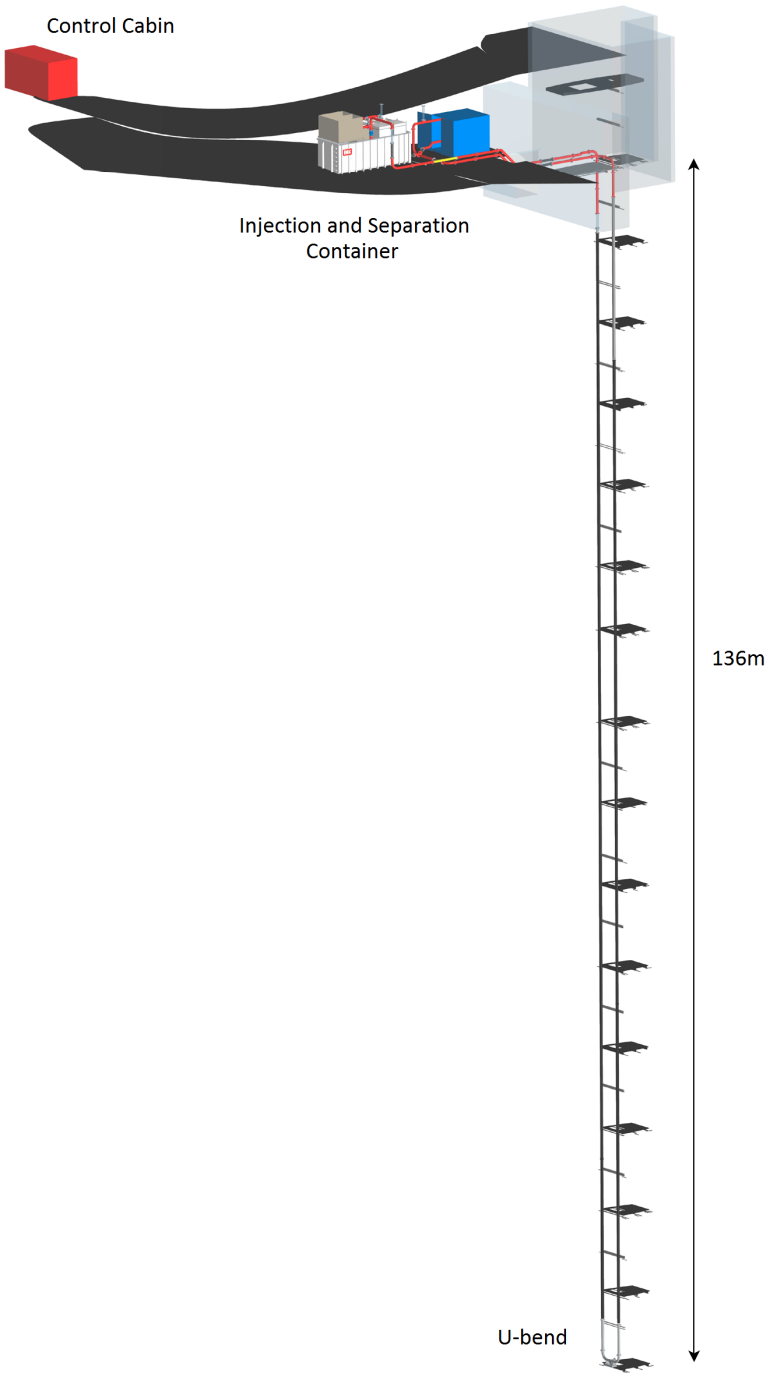

Figure 3-2: CAD-drawing of the test setup, Source: IHC

Figure 3-3 gives an impression of the worksite in Freiberg, the house above the mineshaft is visible and in the front the injection and separation container can be seen. Figure 3-4 gives an impression of the riser going up in the mineshaft. For more information about design choices of the test setup please refer to [11].

Figure 3-3: Separation and injection container, and entrance to mineshaft

Figure 3-4: Dipl.-ing. T. Mueller inspecting the riser.

3-3 Sensors

Different aspects have been monitored, this sections elaborated on the available sensor data of the test setup. The sensors available during the measurements are enlisted in Table 3-1:

Table 3-1: Available sensors

Sensor name	Measurement	Unit
$p_{01} - p_{14}$	Absolute pressure in circuit	kPa
p_{in}	Absolute pressure before pump	kPa
p_{out}	Absolute pressure after pump	kPa
p_{man}	Relative pressure over pump	kPa
T_1	Temperature at top of riser	^oC
T_2	Temperature at top of downcomer	m/s
v_f	Fluid velocity	m/s
k_{01}, k_{02}	Conductivity Concentration Meter (CCM)	μS
P_{drive}	Power supplied to electric motor	kW

A schematic representation of the setup is shown in Figure 3-5, in this image the location of all sensors has been indicated. Furthermore important parts of the circuit such as the hoppers are depicted, along with the direction of the slurry flow.

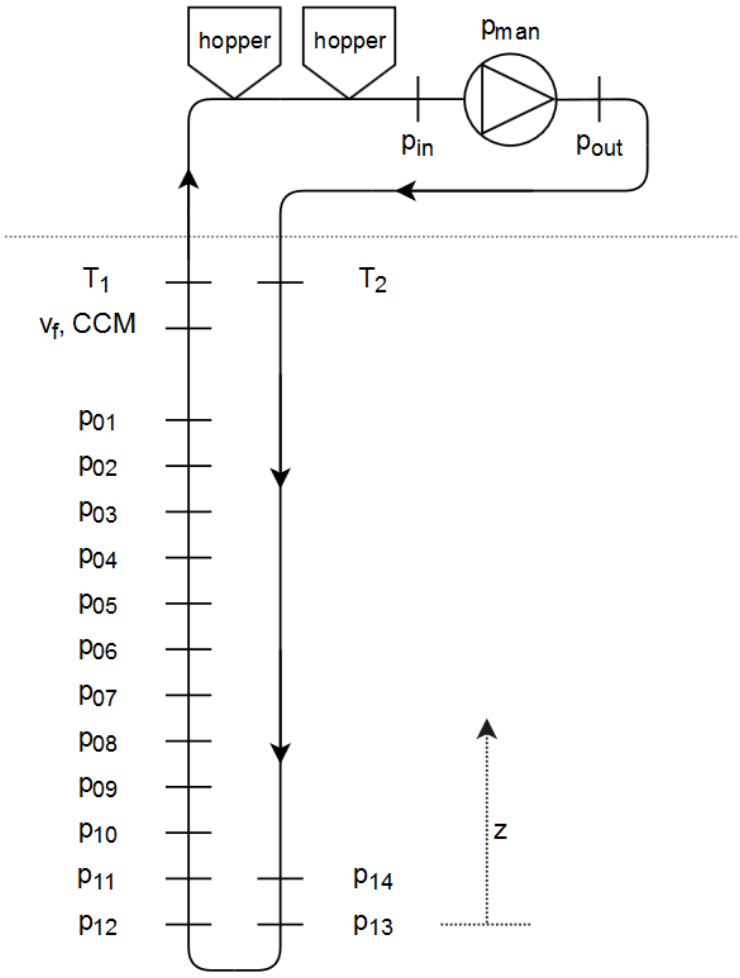

Figure 3-5: Schematic representation of the test setup

For the monitoring system it is required to know how far the sensors are placed from each other which is why in this report a reference frame is used originated in the lowest sensors (p_{12} and p_{13}), the location of the sensors is provided in Table 3-2:

Table 3-2: sensor location

sensor:	p_{12} p_{13}	p_{11} p_{14}	p_{10}	p_{09}	p_{08}	p_{07}	p_{06}	p_{05}	p_{04}	p_{03}	p_{02}	p_{01}	CCM v_f, T_1
$z[m]$	0	7.6	13.7	24.6	35.9	47.0	58.3	69.5	80.8	92.8	102.8	114.0	119.7

Pressure difference measurements will be used throughout this report and different combinations between pressure sensors will be referred to as follows: $\Delta p_{01,02}$ indicates that the pressure difference between p_{01} and p_{02} is considered.

At the bottom of the circuit the flow makes a turn, this section is referred to as the *U-bend*. In this section the sensors $p11, p12, p13$ and $p14$ are located. This combination of sensors allows calculating the delivered concentration in the U-bend while canceling out the effect of the

wall shear stress on the pressure measurements [12]. The U-bend will not be used as input for the observer since it is certain that this section will not be used in the VTS, However during the tests it has provided a rough estimate of the volumetric concentration at the bottom of the riser and furthermore it will be used to determine the effect of solids on the wall shear stress.

Originally it was planned to use the Conductivity Concentration Meter (CCM) in order to measure the concentration, and verify if this would equal the concentration determined with Δp measurements. Unfortunately large fluctuations in the the temperature of the mixture have rendered the signal of the CCM impractical to be used, in Appendix D this is explained further.

3-4 Experiment procedure

Every experiment starts with an empty circuit, before the slurry experiments start the system is filled completely with water while air is let out of the system using valves at the top of the circuit. A so called *watertest* is performed before solids are added to the circuit: At different velocities water is circulated through the system ($v_f = 0 - 6\frac{m}{s}$) and at every velocity set-point the flow is maintained for a couple of minutes. By doing so the system is checked for leakage and the performance of sensors can be evaluated, furthermore it enables determining the pipe wall roughness.

After every *watertest* the *slurrytest* takes place, these experiments are the main goal of the test program. The circuit filled with only water is brought to the right fluid velocity ($4m/s$) and using the valves beneath the hoppers an inflow of solids into the system is created. The mixture is circulated through the circuit, and at this point the presence of solids in the system can be measured from the pressure sensors, this step has the longest duration of the process. At the end of every slurrytest the separation step takes place: At ground level valves are adjusted such that the content of the circuit is directed into the separation container. Meanwhile fresh water is injected in order to prevent air from entering the circuit. All steps of the slurrytest are provided in the following list:

1. Circuit filled with water, increasing fluid velocity to $4m/s$
2. Adding solids
3. Circulating mixture
4. Seperating solids
5. Emptying circuit

Measured signals are captured through the whole process at a sample rate of $100Hz$, for the observation system data covering step 1-3 will be used.

3-5 Measurement program

Measurements have been performed with different mean concentrations, and different particle diameters, Table 3-3 provides an overview of the measurements that were executed. The measurement number will be used for reference, the effective time of the measurement has been indicated in the last column, this time represents the measurement data up to and including step 3.

Table 3-3: Measurement program

Reference	Material	Approximated $c_v[-]$	date	duration [s]
1	sand	10%	19-7-2017	1800
2	sand	10%	26-7-2017	3500
3	gravel	5%	3-8-2017	2500
4	gravel	10%	8-8-2017	1800
5	gravel	15%	10-8-2017	1300
6	sand	10%	19-8-2017	3000
7	sand/gravel (1:1)	10%	21-8-2017	1500
8	sand/gravel (1:1)	5%	22-8-2017	3000
9	sand/gravel (2:1)	10%	23-8-2017	2000
10	sand/gravel (2:1)	5%	24-8-2017	3000
11	sand/gravel (1:2)	5%	31-8-2017	1700
12	sand/gravel (1:2)	10%	5-9-2017	3000
13	sand	15%	6-9-2017	2000
14	manganese nodules	5%	19-9-2017	2800

During the tests the volume of the added solids in the system has been measured to approximate the set value, which is shown in the table. Properties of the solids that were used are depicted in Table 3-4:

Table 3-4: Solid properties of test program

Material	$d[mm]$	$\rho_s[\frac{kg}{m^3}]$
sand	1	2610
gravel	10	2620
manganese nodules	10	2150

3-6 Flow Behaviour

During the experiments an oscillating flow velocity was measured, while the pump has been controlled to run at a fixed rotational speed (RPM). Solids were not spread through the circuit homogeneously, and it is found that when the majority of solids was in the downcomer the mixture velocity increased, and the opposite was seen when the solids where in the riser section. Another effect was the settling of solids causing a lower residence time in the downcomer, and a higher residence time in the riser. This effect enforces the merging of

solids into a plug rather than spreading them homogeneously through the circuit. The effect was noticeably stronger for solids with a higher settling velocity which resulted in a limited duration for the experiments were gravel was used. The flow behaviour in the Test Setup VTS is thus different then that of the normal VTS where all slurry will be going upward, in the same direction. That is why a different model needs to be made for estimating the fluid velocity in the test setup VTS. A sample of the measured fluid velocity signal is shown in Figure 3-6. This figure represents the fluid velocity measurements for gravel measurement 4, the oscillations can clearly be observed:

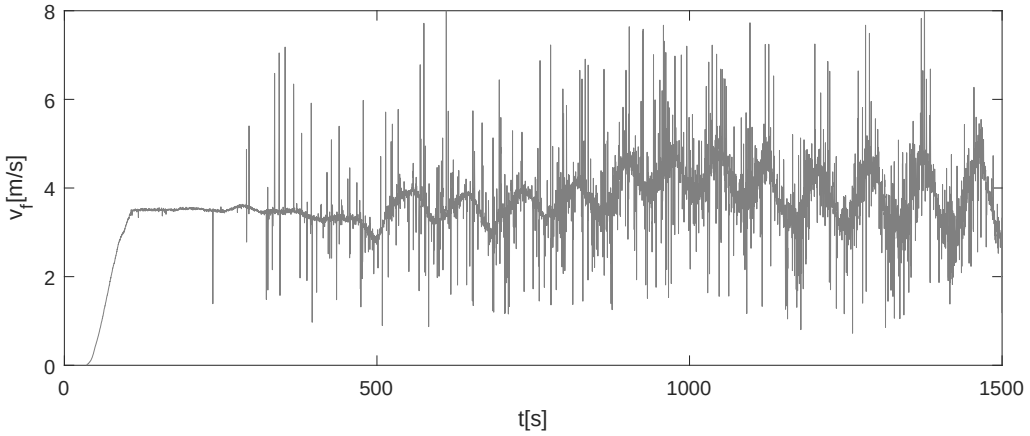

Figure 3-6: Measured v_f signal, measurement 4

It can also be seen that strong noise is present as soon as the solids are added to the system at $t \approx 300s$, this is caused by particles in the mixture colliding with the pipe wall of the Electro Magnetic Flow meter (EMF). For the measurement with the nodules this noise is even stronger due to the fact that manganese nodules conduct electricity which disturbs the measurement of the EMF even more, measurement 14 is therefore unsuitable to be used.

3-7 Difference with full scale VTS

It has been explained that the flow behaviour is different in the test setup due to the closed loop structure of the circuit. The following main differences are present between the systems as well:

Table 3-5: Differences between the test setup and the full scale riser

	Test Setup VTS	Full Scale VTS
Pipe diameter, $D[m]$	0.145	0.356
Length of riser section, $L[m]$	140	5000
Pipe inner wall material	HDPE	Steel or HDPE

It is unsure at this moment whether the full scale VTS will have an inner lining of HDPE or steel.

Chapter 4

Measurements

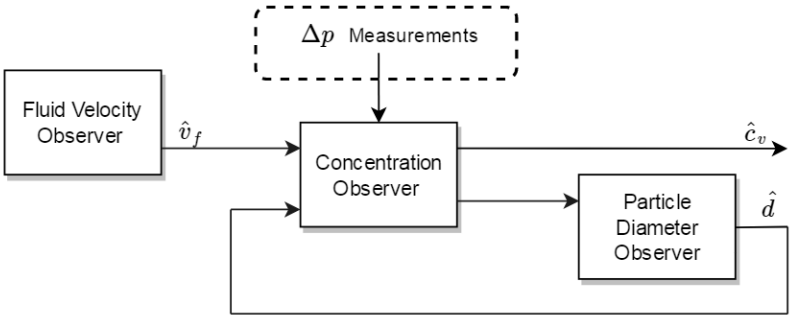

Figure 4-1: Simplified Observer Structure

In this chapter it is elaborated how pressures difference measurements (Δp measurements) will be translated into information suitable for the observer. In the riser section of the experimental setup pressure sensors are installed and furthermore the pressure created by the centrifugal pump is monitored, from these sensors two aspects will be investigated:

- The determination of the particle diameter by efficiency decrease of the centrifugal pump.
- The determination of the volumetric concentration by Δp measurements in the riser, accounting for the mixture shear stress.

4-1 Solids effect on centrifugal pumps

In this section the effect of solids on the centrifugal pump performance is evaluated. It is described in literature that the performance of a pump decreases when settling slurries are transported, and that this decrease is related to the particle diameter. Therefore it is

investigated if measuring pump performance is a suitable method for estimating the particle diameter.

4-1-1 Theory

The efficiency of a pump will decrease when a mixture containing solids is pumped. This effect is caused by the slip of solids with respect to the fluid velocity which decreases the effect of the pump compared to situation where no solids are present. If the pump efficiency is considered for a mixture (η_m) and this value is compared to the efficiency of the pump with only water (η_f), the efficiency decrease can be expressed as $\eta_m = \eta_f \cdot R_H$. Two equations were found in literature describing this relation: Equation 4-1 shows the relation between the pump efficiency under mixture conditions [13]:

$$R_H = 1 - c_v(0.8 + 0.6 \cdot log(d_{50})) \tag{4-1}$$

And an other equation was derived taking into account the impeller diameter as well [14]:

$$R_H = 1 - \frac{c_v(0.466 + 0.4 \cdot log(d_{50}))}{D_{imp}} \tag{4-2}$$

Where d_{50} is the mass-mean particle diameter.

4-1-2 Approach

The characteristics of the used pump of the experiments are shown in Table 4-1:

Table 4-1: Pump Specifications

Pump type:	Impeller diameter [mm]	Impeller width [mm]	Suction diameter [mm]
IHC 38-10-15 , 3bl	375	95	150

At the test setup the power supplied to shaft of the pump is not directly measured, which means the efficiency curve provided for the pump cannot be used. However, the power supplied to the electric motor that drives the pump is measured and will be used to determine the efficiency decrease. Using the water tests it is possible to determine the total efficiency of the pump combined with the electric motor ($\eta_{total} = \eta_{pump} \cdot \eta_{motor}$), a polynomial fit is constructed in order to match the total efficiency (η_{total}) for different mass flow rates ($Q[\frac{m^3}{s}]$). An example of one of the measurements, and created fit is shown in Figure 4-2:

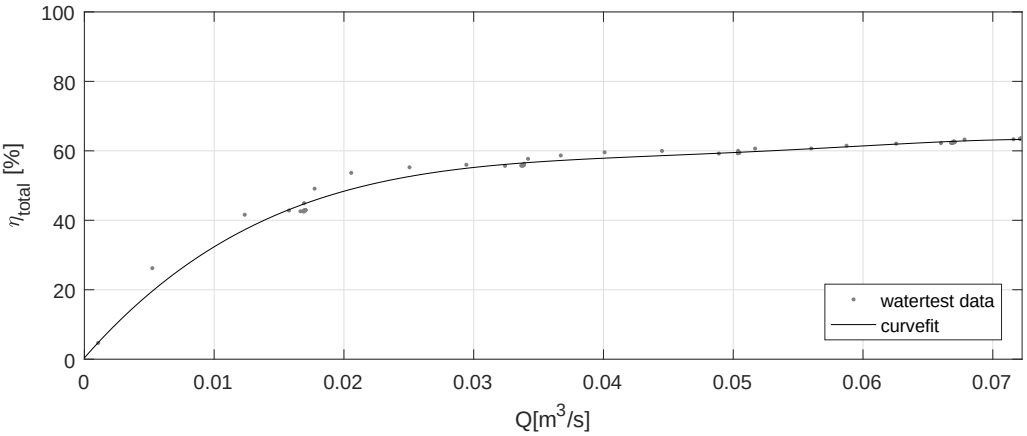

Figure 4-2: Total efficiency: measured data and curvefit

The fitted curve from the watertests is used to compare the efficiency of the pump when running a solids test, the assumption is made that the efficiency of the electric motor does not differ significant when solids are pumped, thus assuming that a decrease in total efficiency is caused by a decrease in efficiency of the pump. The following sensors are involved in order to find and compare the concentration:

Table 4-2: Sensors used for determining solids effect

p_{man}	Relative pressure over pump	kPa
p_{01}, p_{02}	Pressure in riser	kpa
v_f	Fluid velocity	m/s
P_{drive}	Power supplied to electro motor	kW

First it will be identified which of the two equations yields the best match for estimating the concentration. The volumetric concentration calculated by the pump based on Equation 4-1 and 4-2 is compared to the c_v determined using $\Delta p_{02,01}$, which is the closest concentration measurement to the pump. For this purpose the equations are rewritten to:

$$c_v = \frac{1 - R_H}{0.8 + 0.6 \cdot log(d_{50})}, \quad c_v = D_{imp} \cdot \frac{1 - R_H}{0.466 + 0.4 \cdot log(d_{50})} \tag{4-3}$$

The pipeline section between the top of the riser and the pump is horizontal and approximately $40m$ long and therefore the determined concentration in the riser will be adjusted for the settling velocity, to account for the effect that the concentration would be lower in the horizontal section. It is verified that during the tests the fluid velocity is above the Deposit Limit Velocity according to [15]. In order to remove the noise from the measurements signals have been resampled to 10Hz.

4-1-3 Results

The results of calculating the concentration with the pump are compared with the concentration determined with $\Delta p_{02,01}$, In Figure 4-3 a comparison between the two is shown for

measurment 4, using the first equation:

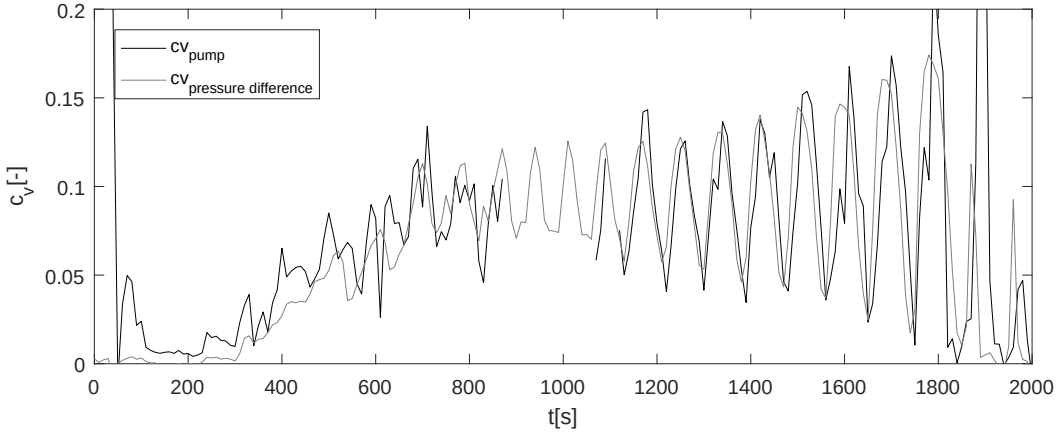

Figure 4-3: Measured concentration using pump efficiency decrease, and Δp measurement.

It can be seen that for this gravel measurement the volumetric concentration is approximated very well with the first equation. For the measurements that contain one type of solids, and wherefore the power supply was measured properly the equations 4-1 and 4-2 are compared on their ability to predict the concentration. The variance between the predicted concentration and the measured concentration is shown in Table 4-3:

Table 4-3: Comparison of solids effect measurements

	Sand		Gravel		
Measurement	6	13	3	4	5
Equation 4-1	$4.7 \cdot 10^{-4}$	$9.8 \cdot 10^{-4}$	$4.7 \cdot 10^{-4}$	$7.0 \cdot 10^{-4}$	$9.8 \cdot 10^{-4}$
Equation 4-2	$2.9 \cdot 10^{-4}$	$6.7 \cdot 10^{-4}$	$2.4 \cdot 10^{-4}$	$8.2 \cdot 10^{-4}$	$1.7 \cdot 10^{-3}$

Equation 4-2 yields the best results for the sand measurements, however when the estimated concentration is evaluated it can be seen that for both equations it is not near the measured concentration with Δp measurements. This can be explained: for small particle mixtures the efficiency decrease to measure is little and measurement error results in a larger deviation of the determined volumetric concentration. For the gravel measurements equation 4-1 yields better results, it can be seen that the estimated concentration of the pump is close to the measured concentration of the Δp measurement.

Measurements with sand show that the efficiency of the pump decreases very little when sand is present and that gravel measurements result in a larger decrease in efficiency. Efficiency decreases (R_H) of up to 30% are measured, which confirms the theory.

Since for the gravel measurements the concentration measured shows a clear similarity, it is possible to rewrite Equation 4-1 and measure the particle diameter using the efficiency decrease and the measured volumetric concentration:

$$d_{50} = 10^{\frac{(-\frac{1}{c_v})\cdot(R_H-1)-0.8}{0.6}} \tag{4-4}$$

Analysing of the gravel data with this formula did not result in a clear measurement of the particle diameter. The result found is a very noisy signal with extremely large peaks, a sensibility analysis of the formula is therefore performed to explain these results. The effect of the variance of the measured efficiency decrease (R_H) on the particle diameter measurement is analyzed, in order to do this the equation is linearised around around $d_{50} = 10mm$ and $c_v = 0.1$. The effect of measurement error on the efficiency decrease results in the following relation:

$$\sigma^2_{d_{50}} = 1.47 \cdot 10^5 \cdot \sigma^2_{R_H} \tag{4-5}$$

It is shown that uncertainties in the measurement for R_H will lead to a very large influence of uncertainties on the particle diameter, this is therefore considered infeasible.

4-1-4 Application for the measurements

Determining the particle diameter using the measured efficiency decrease of the pump has been unsuccessful, it has been concluded that measurement error in the efficiency decrease leads to large variations in the particle diameter estimation.

The volumetric concentration could be approximated well for the gravel measurements. However the estimated concentration is a result of the measurement accuracy of v_f, p_{man} and P_{drive} and it is a result of an experimental equation. Calculating the volumetric concentration is therefore considered to be less accurate than Δp measurements.

The measurements can still be considered useful: It has been proved that for settling slurries the estimated efficiency decrease can be measured, it has been used to determine the volumetric concentration which matches the Δp measurements. This means that if the concentration is known at the location of the pump the efficiency decrease of the pump (R_H) can be predicted, if the measured efficiency decrease is significantly higher it might indicate the pump failure. Based on the results it can be concluded that failure mechanisms of the pump can be monitored better.

4-2 Pressure difference measurements

It has been proposed that pressure difference measurements are a suitable way to measure the volumetric concentration in a VTS [2]. The applicability has not been tested with real measurements, and furthermore it has not been determined what will be the correct model for the wall shear stress in the regime of the test setup VTS. In this section it will be investigated how the volumetric concentration relates to the pressure drop in the conditions of the test setup, taking into account the effect of wall shear stress.

4-2-1 Theory

The mixture density of the fluid in a riser can be determined with pressure difference measurements as is described in Equation 5-18, from there the volumetric concentration can be

derived. In this equation Δp $[Pa]$ is the pressure difference measured over a vertical section with length Δz $[m]$ and diameter $D[m]$. g $[\frac{m}{s^2}]$ is the gravitational acceleration and the acceleration of the mixture in positive direction (upward) is $a[\frac{m}{s^2}]$.

$$\rho_m = \frac{\Delta p - 4 \cdot \tau_m \cdot \frac{\Delta z}{D}}{L \cdot (g + a)}, \; c_v = \frac{\rho_m - \rho_f}{\rho_s - \rho_f} \tag{4-6}$$

In the equation $\tau_m[Pa]$ represents the mixture wall shear stress, which is decomposed in a solid part (τ_s) and a fluid part (τ_f):

$$\tau_m = \tau_f + \tau_s \tag{4-7}$$

Of which the fluid wall shear stress can be determined as follows:

$$\tau_f = \frac{1}{8} \cdot f_D \cdot \rho_f \cdot v_f^2 \tag{4-8}$$

Where the Darcy-Weisbach friction factor can be approximated with the Swamee Jain equation [16]:

$$f_D = \frac{1.325}{\left(ln\left(\frac{\epsilon_{pipe}}{3.7 \cdot D} + \frac{5.75}{Re^{0.9}}\right)\right)^2} \tag{4-9}$$

In this equation ϵ_{pipe} represents the wall roughness of the pipe. Literature was found elaborating on models for the solid wall shear stress τ_s, however these models were derived using experimental data of different regimes (combinations of d,D). In the following sections measurements are elaborated which are used to find which model can best be used to calculate τ_s in the observer for the test setup.

4-2-2 Wall Shear Stress

Using the water tests the significance of the wall friction is determined for a mixture without solids, where the increase in pressure drop equals the contribution of the wall friction (since $\rho_m = \rho_f$). The relative pressure difference $\Delta p_{12,01}$ is analysed at different velocities and the increase is expressed as a percentage of the total pressure drop between the sensors in static condition. The results are found to be similar for the different tests, for measurement 4 the result is shown in Figure 4-4:

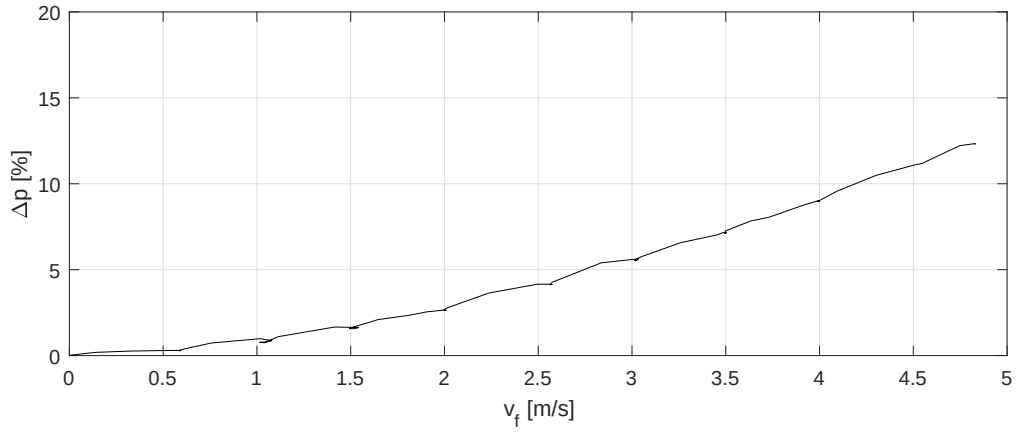

Figure 4-4: Relative pressure drop due to wall friction

It is concluded that the wall friction has a contribution of $\approx 10\%$ at $v_f = 4m/s$, for slurry which presumably adds extra wall friction this contribution is likely to be equal or higher. It is now investigated whether the contribution of the wall friction is a varying parameter. Therefore the pipe wall roughness is approximated using the following least-squares optimisation, varying ϵ_{pipe} to match the measured pressure drop over a section:

$$\min_{\epsilon} \sum_{t=0}^{t} (\Delta p - f_D \cdot \frac{\Delta z}{D} \cdot \frac{1}{2} \cdot \rho_f \cdot v_f^2 - \rho_f \cdot (g + a) \cdot \Delta z)^2, \text{ subject to: } \epsilon_{pipe} \in [1 \cdot 10^{-6}, 5 \cdot 10^{-4}] \tag{4-10}$$

In figure 4-5 the found values of the pipe wall roughness between sensor p_{13} and p_{14} are depicted for the different water tests, these values show that the contribution of wall friction of liquid only cannot be assumed to be equal for all measurements, and therefore needs to be calibrated before every slurrytest:

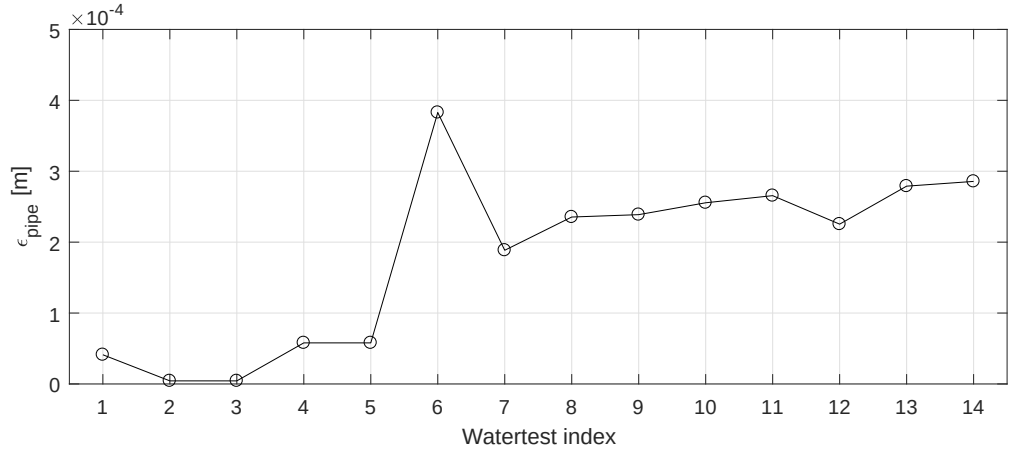

Figure 4-5: Pipe wall roughness found for different watertests

The wall friction shows an increasing trend throughout the experimental program, this indicates that the pipe wall roughness has increased due to the transport of solids. The wall roughness of measurement 6 shows a large peak, this test has been taken after a large plug was formed at the separation process after experiment 5. From this data it is derived that the plug formation has increased the pipe wall-roughness significantly, it can be seen that at watertest 7 the pipe roughness has decreased which indicates that the sand mixture of experiment 6 has polished the pipe. From these results it can be concluded that the pipe-wall roughness of the HDPE piping is significantly influenced by the transported solids and cannot be assumed constant, this value needs to be calibrated.

4-2-3 Approach

In order to find a model for the wall shear stress for solids, the pressure measurements in the U-bend are used, the approach to do this is elaborated in this subsection. Figure 4-6 shows the sensors that are used, and two introduced volumetric concentrations (c_{v1} and c_{v2}) for the downcomer and the riser section:

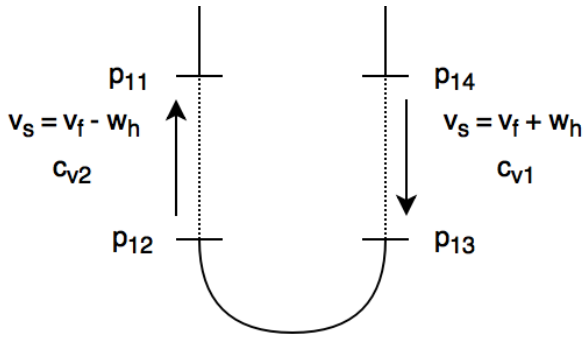

Figure 4-6: U-bend

In this configuration, the following relation is used to determine the sum of concentrations inside the U-bend [12]:

$$c_{v1} + c_{v2} = \left[\frac{(p_{12} - p_{11}) + (p_{13} - p_{14})}{L \cdot g} - 2\rho_f\right] \cdot \left(\frac{1}{\rho_s - \rho_f}\right) \tag{4-11}$$

In order to find the pressure drop due to wall shear stress it is needed to know the contribution of the mass of the solids in one of the vertical sections, it is thus needed to find the difference between c_{v1} and c_{v2} which are not equal.

The difference between c_{v1} and c_{v2} depends on the settling velocity, and the settling velocity depends on the concentration and particle diameter. In the riser the settling velocity will increase the concentration locally which lowers the settling velocity, in the downcomer this happens the other way around, which causes that both concentration and settling velocity are not equal when comparing the riser and the downcomer.

The concentration difference is found by means of iteration: using the knowledge that the same slurry passes the first section and then the second section, and that the residence time in those sections depends on the solid velocity, the following relations are found:

$$c_{v1} \propto \frac{\Delta z}{v_{f1} + w_t(1-c_{v1})^{n-1}},\ c_{v2} \propto \frac{\Delta z}{v_{f2} - w_t(1-c_{v2})^{n-1}} \tag{4-12}$$

Thus:

$$\frac{c_{v1}}{c_{v2}} = \frac{v_{f2} - w_t(1-c_{v2})^{n-1}}{v_{f1} + w_t(1-c_{v1})^{n-1}} \tag{4-13}$$

Using the mixture bulk velocity that is constant through the circuit, the fluid velocity is solved at both sections:

$$v_f = \bar{v}_m + c_v \cdot w_t \cdot (1-c_{v1})^{n-1} \tag{4-14}$$

Both concentrations are unknown from the start, however using equation 4-11 the summation of these two values can be calculated. The iteration is started with the assumption that $c_{v1} = c_{v2}$, from there the ratio between the concentrations is calculated, resulting in two concentrations which are then filled in equation 4-13 and 4-14 again. This iteration is repeated 5 times since it was found that after 5 iterations the result does no longer changes.

In figure 4-7 the result of this procedure is shown for two different particle sizes. The ratio between the concentration of the riser and the downcomer is shown for different mean concentrations. As expected the ratio is larger for the bigger particles which have a higher settling velocity:

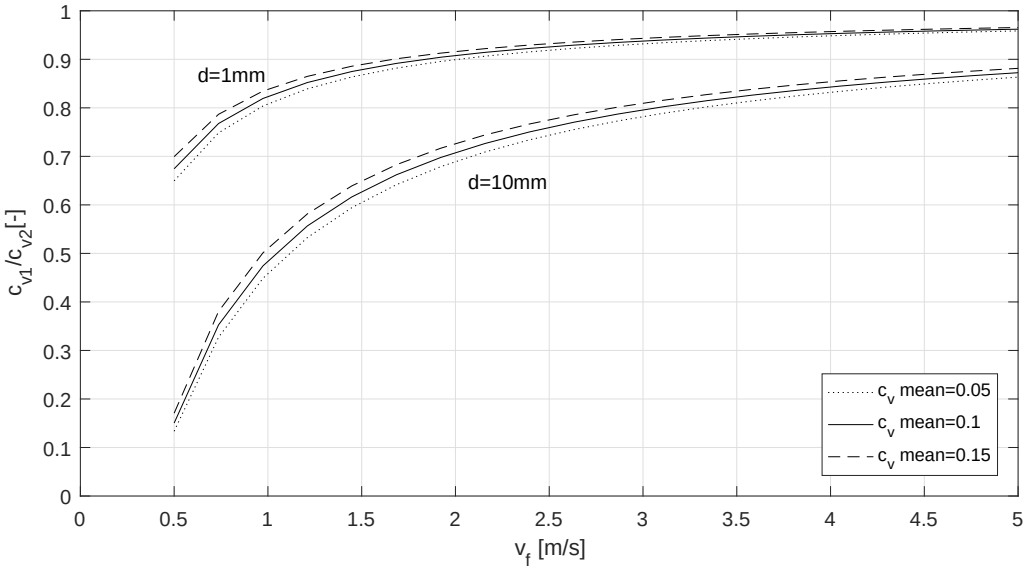

Figure 4-7: Ratio between the concentration in a riser and the downcomer, for different particle diameters

From the figure it can be read that at $4m/s$ the density of the gravel in the riser is about 85% of the density in the downcomer which confirms that the concentrations cannot be assumed

equal. These iteration measurements performed in the downcomer will be used to determine the contribution of the wall shear stress, the downcomer section is chosen since it comes before the bend and is therefore considered a better reference than the section that comes after the bend where solids will likely be bouncing in between the walls. The following relation is derived in order to express the mixture shear stress to the measured pressure drop in the downcomer:

$$\frac{p13 - p14 - \Delta z \cdot (g - a) \cdot (c_{v1} \cdot (\rho_s - \rho_f) + \rho_f)}{4 \cdot \Delta z / D} = \tau_m \tag{4-15}$$

With the mixture wall shear stress (τ_m) measured, and the fluid wall shear stress (τ_f) calculated using 4-8, it is possible to find the solid wall shear stress (τ_s). The different models for this value of Shook & Bartosik [17], Ferre & Shook [18], Bartosik [19] and Xia [20] are compared.

4-2-4 Results

The settling velocity is important for determining the concentration inside the vertical section as was shown, for single fraction mixtures this values can be predicted best which is why first only the measurements where one type of solids is used are analysed. These measurements are 2,6 and 13 (sand) and measurements 3,4 and 5 (gravel). The results for measurements of τ_f and τ_m at different fluid velocities are displayed in figure 4-8 till 4-13, the different volumetric concentration ranges have been given a grey-scale indication. In the figures the fluid wall shear stress is depicted based on the watertest that was taken before and after the slurry test (τ_f (next)), this gives an indication of the evolution of the pipe wall roughness.

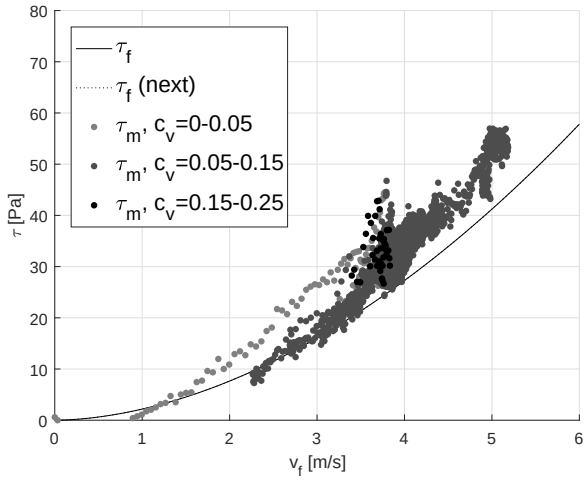

Figure 4-8: Measured wall shear stress, measurement 2 (sand, $c_v = 0.05$)

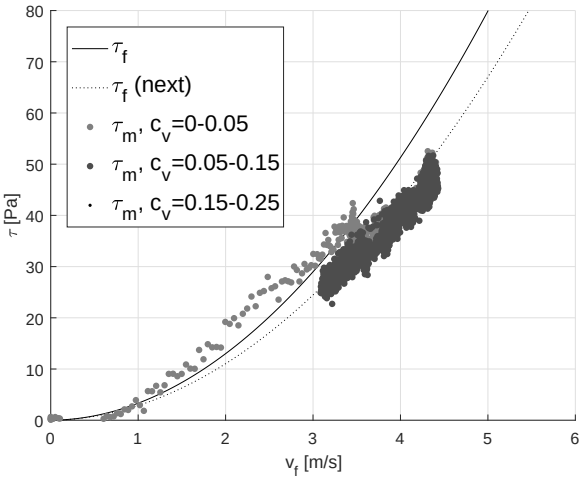

Figure 4-9: Measured wall shear stress, measurement 6 (sand, $c_v = 0.10$)

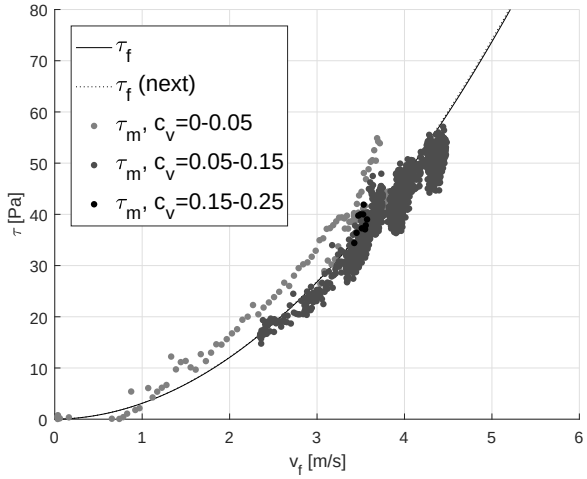

Figure 4-10: Measured wall shear stress, measurement 13 (sand, $c_v = 0.15$)

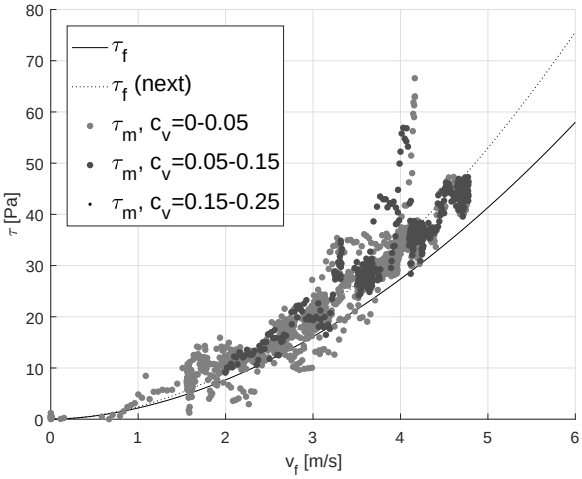

Figure 4-11: Measured wall shear stress, measurement 3 (gravel, $c_v = 0.05$)

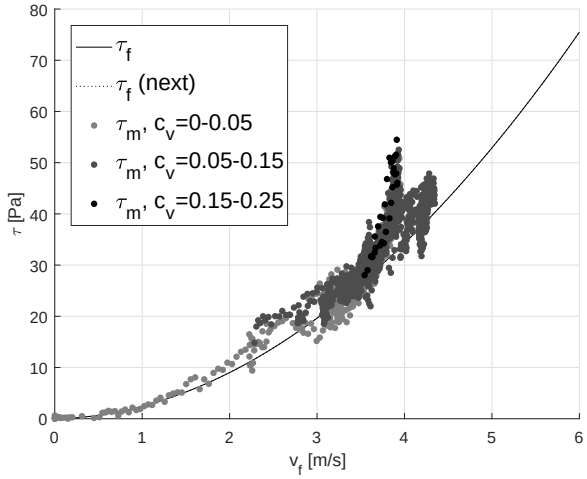

Figure 4-12: Measured wall shear stress, measurement 4 (gravel, $c_v = 0.10$)

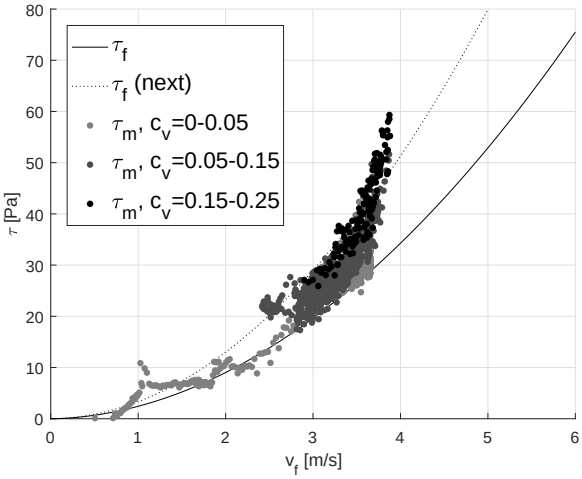

Figure 4-13: Measured wall shear stress, measurement 5 (gravel, $c_v = 0.15$)

From the data it can be seen that the mixture wall shear stress remains close to the fluid wall shear stress ($\tau_m \approx \tau_f$), this indicates that the contribution of solids to the wall friction is little. This result can be attributed to the off-wall lift that causes the solids to move to the center of the pipe. The graphs show that for some of the measurements the watertest before and after the slurrytest yields a different result for τ_f, this shows the effect of the changing pipe wall roughness throughout the experiment, this negatively influences the possibility to find a correct model.

For gravel mixtures with a high volumetric concentration ($c_v = 0.15 - 0.25$) the wall shear stress increases significantly, which indicates that under high concentrations the effect of off-wall lift is less effective. Unfortunately this effect is hard to measure since this simultaneously effects the pipe-wall roughness as can be seen in measurement 3 and 5.

The aim is to find a model that matches τ_s closely using the fluid velocity, the volumetric

concentration and the particle diameter as input. The case where there is no influence of the solids ($\tau_m = \tau_f$), the model of Shook & Bartosik, Ferre & Shook the model of Bartosik and the model of Xia are compared in Table 4-4, the variance of the error between the measured τ_s and the calculated τ_s from the models is compared:

Table 4-4: Variance of the error between measured wall shear stress and models from literature

	Sand			Gravel		
Model/Measurement #	2	6	13	3	4	5
$\tau_m = \tau_f$	9.8	16.0	9.7	10.5	13.5	22.5
Shook & Bartosik	9.8	16.0	9.7	10.5	13.5	22.5
Ferre & Shook	9.6	16.6	10.2	9.7	10.9	14.5
Bartosik	9.8	16.1	9.8	9.4	9.8	7.0
Xia	17.2	26.3	30.1	10.2	12.0	18.6

The variance is very high on all comparisons. The model of Xia appears to differ most from the measurements and other models provide a slightly better estimate, however the result is still not close. The closest match is found for the model of Bartosik and measurement 5:

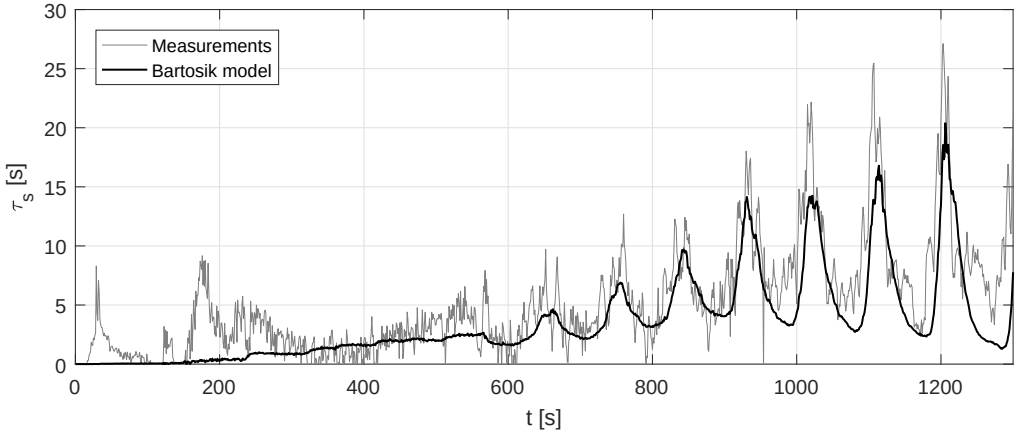

Figure 4-14: Validation of measured mixture shear stress with the model proposed by Bartosik

But unfortunately this model did not yield equally good results for the other measurements. Since the results do differ significantly from the models it is chosen that for the observation of solids in the test setup the relation $\tau_m = \tau_f$ will be used: this assumption yields an estimate that equals the quality of the calculations found from the models.

4-2-5 Sensitivity

It is chosen to assume $\tau_m = \tau_f$, the results of this assumption are important and it is therefore analysed what the effect of this assumption is on the measurements of the volumetric concentration. First it is determined what the error is when this assumption is made, figure 4-15 shows the measured τ_m with respect to the determined τ_f for measurements [2,6,13,3,4,5] (sand and gravel):

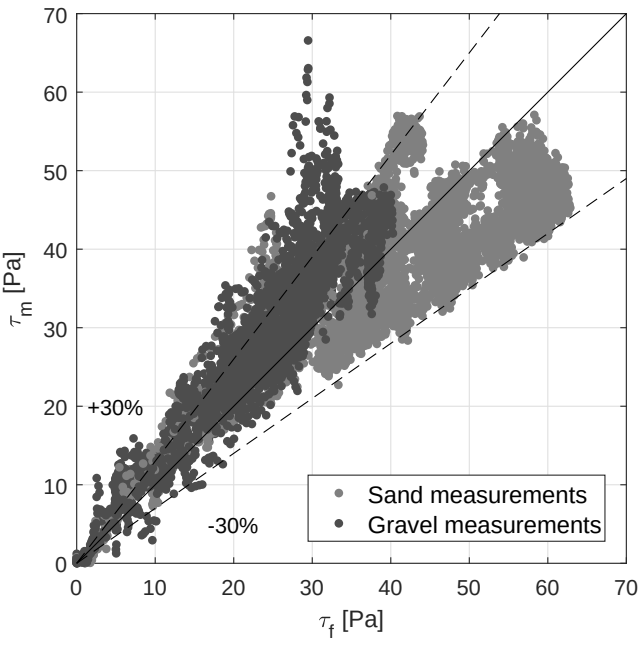

Figure 4-15: Validation of mixture shear stress

It can be seen that the majority of the measurement points stay within a 30% bound of the fluid wall shear stress, there is a large spread but this can be explained due to the change in pipe wall roughness at the beginning of the experiment series when these experiments were made. The same plot is made for the mixture measurements [7,9,11,8,10,12], for these sets the assumption is made that the hindered settling velocity depends on the mass-mean particle diameter in order to find the concentration in the downcomer by means of iteration. The result is shown in Figure 4-16:

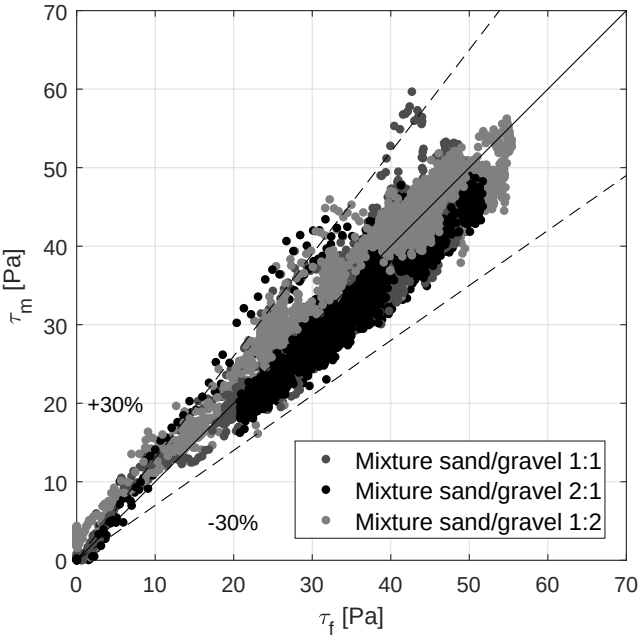

Figure 4-16: Validation of mixture shear stress

The spread is lower for this set of measurements, and the majority of τ_m measurements is within a 30% interval of the τ_f. From both plots it is concludes that sand measurement are over-estimated, and mixtures containing gravel are underestimated, furthermore results were $\tau_f < \tau_m$ can be found in the data and usually is found with the sand measurements. This is considered to be measurement error, what can be concluded is that for sand mixtures the concentration in the downcomer is overestimated yielding a lower estimate for the pressure drop due to wall friction. Therefore it can be concluded that the settling velocity for sand is underestimated. This shows a weakness of the measurements performed: the results are very dependent on an accurate definition of the settling velocity which is not available. Another aspect influencing the measurements is the change in pipe wall roughness: since the pipe wall roughness has the tendency to decrease for sand-mixtures, the mixture shear stress measured is lower than the fluid shear stress determined by the watertest.

The effect of assuming $\tau_m = \tau_f$ is evaluated by determining the variance of the error of τ_m, and by calculating how this results in a measurement error for the density. Measurement 6 is considered and outlier and is excluded, using the rest of the data it is found that:

$$\sigma^2_{\tau_m} = 16.9 \tag{4-16}$$

Excluding the effect of uncertainties on the other parameters $(\Delta p, \Delta z, D, g, a)$ this would have the following effect on the density measurements:

$$\sigma^2_{\rho_m} = \sigma^2_{\tau_m} \cdot \frac{(4 \cdot \Delta z/D)^2}{(g \cdot \Delta z)^2} = 133.0,\ \sigma_{\rho_m} = 11.5 \tag{4-17}$$

For a volumetric concentration of $c_v = 0.2$ the mixture density would be $\rho_m = 1330\ [kg/m^3]$, the standard deviation that was calculated is within an 1% error margin of this density. The effect of the assumption $\tau_m = \tau_f$ is therefore considered to be low and acceptable.

The acceleration term of the mixture reaches values within a range of $\pm 0.05 m/s^2$, it has been found that the effect of not incorporating this parameter is roughly $\pm 0.5\%$ on the error of the mixture density measurement. Since acceleration measurements are usually very noise, especially for the system considered, and since the effect is negligible this parameter is therefore not included.

4-2-6 Measurement Covariance

In order to tune the observer it is needed to know the covariance between the measurements and the volumetric concentration. An approximation is derived using sensor pair $\Delta p_{02,01}$, the mixture density is then calculated as follows:

$$\rho_m = \frac{(p_{02} - p_{01}) - \frac{1}{2} \cdot f_D \cdot \frac{\Delta z}{D} \cdot \rho_f \cdot v_f^2}{g \cdot \Delta z} \tag{4-18}$$

It is found that p_{01} and p_{02} are affected by the same noise and are thus correlated, parameters $g, \Delta z, D, \rho_f$ and ρ_s are assumed to be known and non-varying. For this sensor pair $\Delta z = 11.2m$, which is also a good reference for the distances between other pressure sensors, the variance of the density ρ_m is then defined as:

$$\begin{aligned} \mathrm{Var}(\rho_m) = [&\mathrm{Var}(p_{01}) + \mathrm{Var}(p_{02}) - 2 \cdot \mathrm{Cov}(p_{01}, p_{02}) + \\ &\mathrm{Var}\left(\frac{1}{2} \cdot f_D \cdot \frac{\Delta z}{D} \cdot \rho_f \cdot v_f^2\right)] \cdot \frac{1}{(g \cdot \Delta z)^2} \end{aligned} \tag{4-19}$$

The term $\mathrm{Var}(\frac{1}{2} \cdot f_D \cdot \frac{\Delta z}{D} \cdot \rho_f \cdot v_f^2)$ is evaluated using the watertests: the pressuredrop of $\Delta p_{02,01}$ is calculated using the formula, and is compared with the measured pressure drop. After evaluating equation 4-19, the covariance for the volumetric concentration is defined as:

$$\mathrm{Var}(c_v) = \mathrm{Var}(\rho_m) \cdot \frac{1}{(\rho_s - \rho_f)^2} \tag{4-20}$$

Filling in the equations yields a value of:

$$\mathrm{Cov}(c_v) = \sigma_{c_v}^2 \approx 2 \cdot 10^{-7} \tag{4-21}$$

This parameter will be the initial guess when tuning the observer.

4-2-7 Application for the measurements

Pressure difference measurements have been analyzed for the purpose of measuring mixture density and volumetric concentration. The unknown parameter for this purpose was the mixture shear stress, and it is concluded that the mixture shear stress can be approximated with the fluid wall shear stress. This assumption results in an error of approximately 1% which is considered acceptable. Omitting the incorporation of the acceleration term yields a maximum error of 0.5%, this is considered acceptable as well.

4-3 Conclusion

Two aspects have been investigated, the determination of the particle diameter by efficiency decrease of the centrifugal pump and the determination of the volumetric concentration by Δp measurements in the riser. It was found that centrifugal pumps are not a suitable way to measure the particle diameter since that parameter is very sensitive to error in the measured efficiency decrease. It is however possible to notice the efficiency decrease that was described in literature, based on that result it can be valuable to monitor the efficiency decrease of the pump in order to measure deviations which can indicate pump failure.

Pressure difference measurements were analysed in order to find the contribution of the mixture wall shear stress, it was concluded that under the conditions of the experiments this parameter contributes to 10% of the pressure drop. Based on measurements in the u-tube of the circuit it is decided that the mixture wall shear stress can be approximated with the fluid wall shear stress. Models for the mixture wall shear stress were evaluated but the data from the test setup did not a clear match with a model that can be used for all measurements. It has been investigated what the effect is of assuming the mixture wall shear stress equal to the fluid wall shear stress, it has been found that this assumption has only little effect on the determination of the mixture density just as omitting the acceleration of the mixture in the equation.

Chapter 5

Observer Design

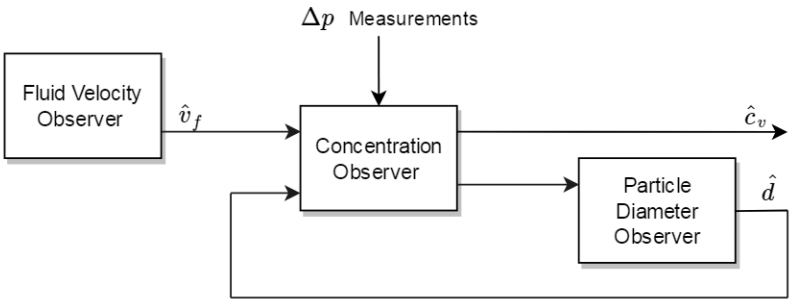

Figure 5-1: Simplified Observer Structure

In this chapter the design of the observer is elaborated, the different components presented in Figure 5-1 will be addressed. The aim is to design an observer suitable for both the real size VTS and the test setup VTS, simulations will be used to help with the design. The observer is be compared with a previous proposed design, and benchmarks are defined which will be used to evaluate the performance improvements of the observer when it is applied to the measurement data of the test setup.

5-1 Cascade Observer

The observer designed for observing solid concentrations will be a result of multiple observer algorithms. It was concluded that the performance of the cascaded Kalman filters is comparable to the siltation were the observer was built as one Kalman filter [21], an advantage of the decoupling of observers is that modularity is increased and parameters are tuned more easily. For this observer the advantage that is gained is that observers for models of which the Jacobian can be evaluated (a model for the fluid velocity) can be separated from observers

of which the Jacobian cannot me evaluated (b1DVHT model), thus using the strength of different observer types. The parts of the cascade observer are elaborated in the following sections.

5-2 Fluid velocity Observer

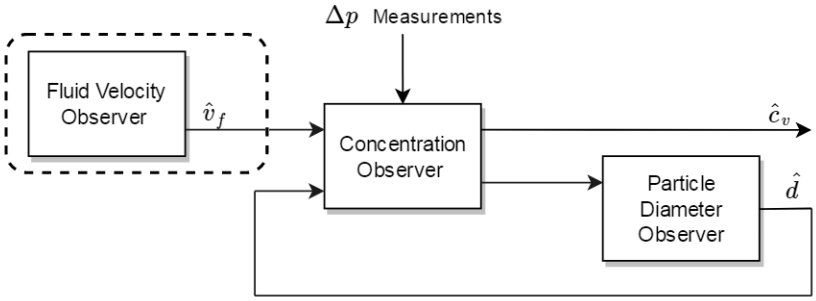

Figure 5-2: Simplified Observer Structure

In order to observe the propagation of solid concentrations inside the test setup VTS it is needed to measure the fluid velocity, this parameter is also needed for estimating the contribution of wall shear stress. Two filters for observing the fluid velocity are designed and compared: a low-pass filter and an Extended Kalman Filter (EKF).

5-2-1 Low-pass filter

If the noise on the v_f signal has a higher frequency than the bandwidth of the system, a low-pass filter can be used, a frequency analysis is therefore performed to verify this. Using the fast Fourier transform the frequency spectrum (P) of the signals is calculated, and it is found that both the system and noise have a bandwidth ranging from 0-10Hz. In figure 5-3 the frequency spectrum of measurement 8 is shown:

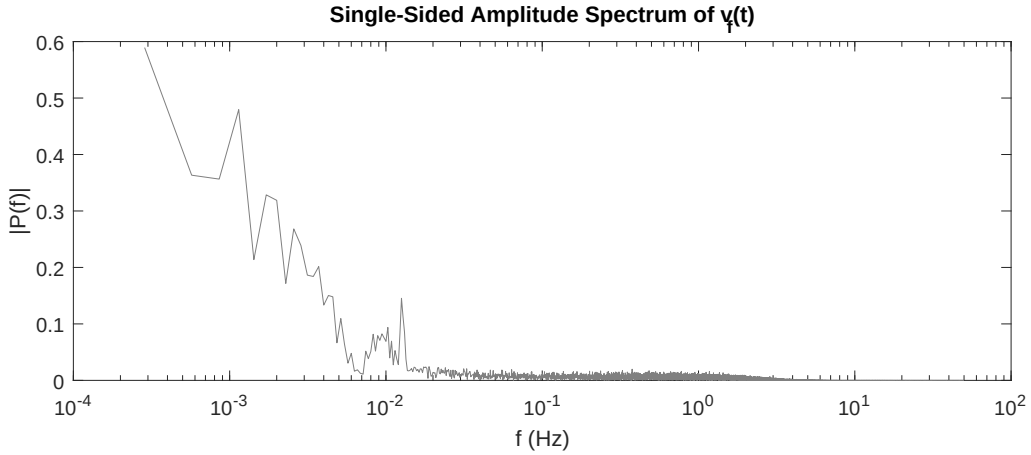

Figure 5-3: Single-Sided Amplitude Spectrum of $v_f(t)$, measurement 8

The bandwidth of the system is approximated to examine the availability of a low-pass filter: the fluid velocity shows an sinusoidal osculation when solids are transported and the period of this wave corresponds to time of a full circuit run. The full length of the circuit is approximately $300m$ and with an average velocity of $4m/s$ this means a period of $75s$ $[0.013Hz]$. Another characteristic property of the system is the rise time (t_r): at the water tests steering the velocity from one set point to another takes $\approx 10s$, a rule of thumb is that the bandwidth of a signal is approximately equal to $0.34/t_r = 0.034Hz$ [22]. This frequency is found to be the highest in the bandwidth of the system and therefore a first order low pass filter is designed with a cut-off frequency (f_c) of $0.1Hz$. The filter is converted to a discrete time model using the zero order hold method.

5-2-2 Extended Kalman Filter

The second approach to observe the fluid velocity is by means of an Extended Kalman Filter (EKF), for this method a model is created under the assumption that $\dot{v}_f(t) \approx \dot{\bar{v}}_m(t)$. The acceleration of the mixture is the summation of forces working on the mixture, divided by the total mass of the mixture (m_m). The driving force is the pressure generated by the centrifugal pump (manometric pressure, p_{man}) divided by the cross sectional area of the pipe (A_p), and the pressure drop due to wall shear stress is expressed as the non-linear function $f_v(v_f)$. The acceleration of the fluid velocity is influenced by the balance between mass going up and down in the system, this effect is present since during the tests the slurry was not spread through the circuit homogeneously. A term is brought in ($m_{diff}[kg]$) which represents the amount of mass going down minus the amount of mass going up. This parameter is approximated with measurements using p_{14} with p_{out}, and p_{12} with p_{in} to approximate the mass difference between respectively the downcomer and the riser. The term m_{diff} could be introduced as an input but due to the horizontal sections in between the pressure difference measurements it cannot me measured properly, it is therefore chosen to change this input into a state in order to observer the input as well [23]. An approximation of the mass difference dynamics is made too, the mass difference increases as mass flows from the riser into the downcomer and decreases when this happens the other way around. These mass fluxes in and out are approximated using the density calculated with $\Delta p_{02,01}$ (ρ_{m1}), and the density calculated using the U-bend (ρ_{m2}). The state space model is then written as follows:

$$\begin{aligned} \dot{\hat{v}}_f(t) &= (p_{man}(t) - f_v(v_f(t)) \cdot \frac{A_p}{m_m} + m_{diff}(t) \cdot \frac{g}{m_m} \\ \dot{\hat{m}}_{diff}(t) &= -\rho_{m2}(t) \cdot v_f(t) \cdot A_p + \rho_{m1}(t) \cdot v_f(t) \cdot A_p \end{aligned} \tag{5-1}$$

The inputs are calculated using the unfiltered pressure and velocity measurements. The state vector, the inputs ($u(t)$) and outputs ($y(t)$) are defined as:

$$\hat{x}(t) = \begin{bmatrix} v_f(t) \\ m_{diff}(t) \end{bmatrix}, u(t) = \begin{bmatrix} p_{man}(t) \\ \rho_{m1}(t) \cdot v_f(t) \\ \rho_{m2}(t) \cdot v_f(t) \end{bmatrix}, y(t) = \begin{bmatrix} v_f(t) \\ m_{diff}(t) \end{bmatrix} \tag{5-2}$$

The model is discretised using the Euler-Forward method, the Extende Kalman filter is used to observe v_f, this observer is chosen because of the non-linear contribution of the wall-friction

in the system. It is found that using the v_f signal to correct the fluid velocity estimate makes the estimate more noisy, therefore the EKF is tuned in a way that corrections regarding v_f are made on the mass difference state resulting in the following measurement covariance matrix (R) and (non-symmetric) state covariance matrix (Q):

$$R = \begin{bmatrix} 100 & 0 \\ 0 & 1000 \end{bmatrix}, Q = \begin{bmatrix} 0.001 & 0 \\ 50 & 0.1 \end{bmatrix} \tag{5-3}$$

5-2-3 Comparison

The low-pass filter and Extended Kalman filter are compared in order to select the best approach for the observer. First the results are analysed visually: it is verified whether the observers are able to capture the fastest motion which is the increase of velocity at the start of the test program. In Figure 5-4 it is shown that when the velocity increases rapidly the low-pass filter lags behind the measured signal:

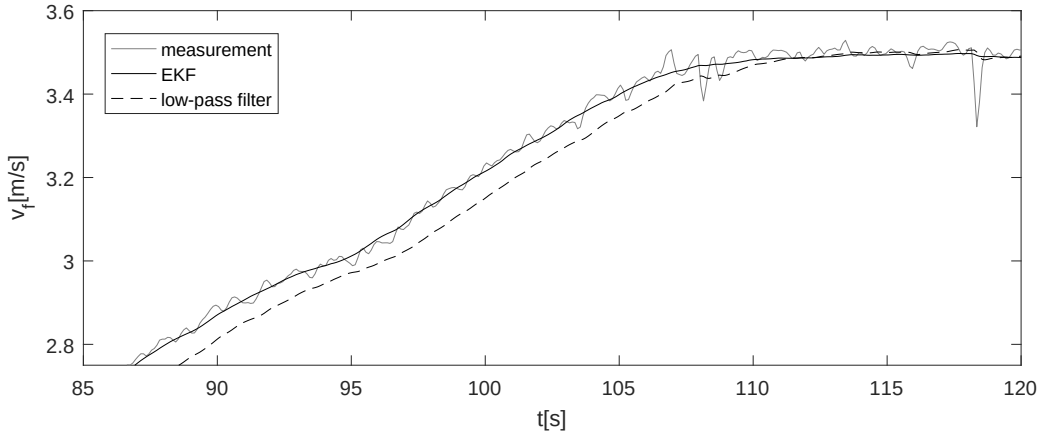

Figure 5-4: Comparison of EKF and low-pass filter applied on measurement 4

The second comparison is for the time range were solids are added and strong noise is present, it is observed that the high peaks of the measured signal have more effect on the low-pass filter than on the EKF which can be seen in Figure 5-5. Both filters generally follow the same path.

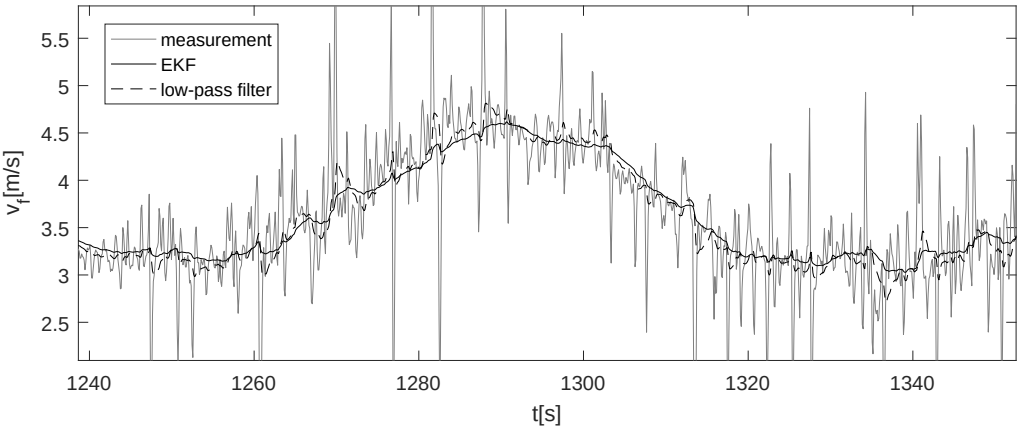

Figure 5-5: comparison of EKF and low-pass filter applied on measurement 4

A benchmark performed to compare the signals is the calculation of the Variance Accounted For (VAF) [23]: The signal of v_f is treated with a moving average filter, and is compared to the results of the low-pass filter and the EKF. It is found that for all measurements both values for the VAF are in the range 95-99%. The VAF for the EKF is found to be always higher by 0.5-2% and it is therefore concluded that the performance of the EKF is slightly better than that of the low-pass filter.

Interesting to see is a comparison of the filters in the in the frequency domain, a magnitude plot is shown in Figure 5-6. It can be seen that both observers are effectively a low-pass filter, the EKF has a higher cutoff frequency but the output of the EKF was found to be less affected by noise. The way the EKF is tuned has proven to yield an advantage with respect to the low-pass filter.

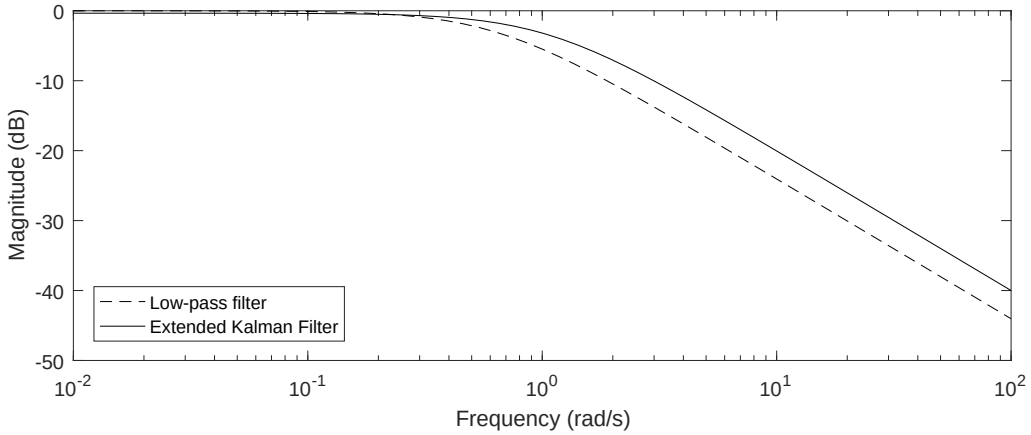

Figure 5-6: Magnitude plot of of EKF and low-pass filter

5-2-4 Conclusion

An Extended Kalman Filter is designed to estimate the fluid velocity at the place of the flow sensor, and the performance is considered better than the performance of the low-pass filter. To get these results a lot of tuning of the model error co-variance matrix Q was needed. Estimating the fluid velocity of a mixture in the test setup VTS is different than it is in the real VTS, it is more complex. Since it is different it could have been omitted from the research and an off-line moving average filter could be used to process the signals. However since it it is uncertain that in the VTS the velocity measurements will be improved it is valuable to know that noise can be greatly reduced by constructing and tuning an appropriate model.

Using the fluid velocity and information about the concentration in the EMF, the bulk mixture velocity can be determined. This parameter is equal through the whole riser and is determined as:

$$\bar{v}_m = c_v \cdot v_s + (1 - c_v) \cdot v_f \tag{5-4}$$

5-3 Concentration Observer

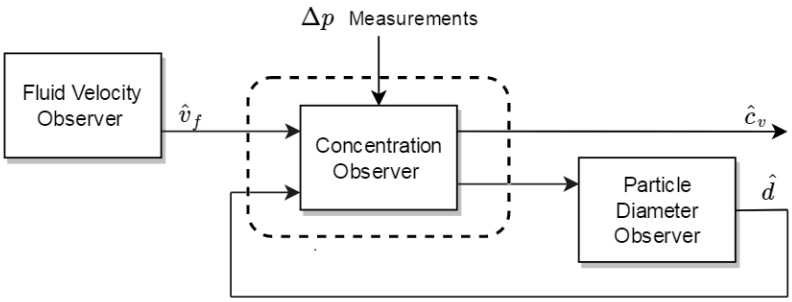

Figure 5-7: Simplified Observer Structure

The next part of the observer is elaborated: the observation of the volumetric concentration. For this part the Ensemble Kalman Filter (Enkf) is used. In this section problems encountered with the Ensemble Kalman Filter (Enkf) are addressed and improvements of the Enkf are elaborated.

5-3-1 Ensemble Kalman Filter

The Ensemble Kalman filter is an observer type suitable for online observing of large-dimensional systems for models whereof the Jacobian cannot be evaluated. It was decided that for estimating the concentration the b1dVHT model will be used, and for this model the Jacobaian cannot be evaluated. Furthermore the full scale VTS will be spatially discretised which will result in an amount of states in the vicinity of 500 which is considered large dimensional. The Ensemble Kalman filter will therefore be used to observe the concentration propagation in the observer. The theoretical formulation of [24] is used to implement the Enkf.

Simulations that were created are depicted in table 2-1, the Enkf will be applied to these simulations in order to simulate the observation of solids over the course of $1000m$ (one riser section). Applying the observer is started by using a local measurement first, the fluid velocity observation and the conversion to and from a pressure difference are omitted in this section. A measurement at $z = 100$ is applied, such that:

$$y = h(x) = [c_{v_{100}}] \tag{5-5}$$

Tuning the Enkf will be elaborated for the test setup VTS, but for the simulations this process is omitted from the report. For the simulations a number of ensembles of 30 is chosen, and furthermore: $\sigma_w = 0.0001$,$\sigma_w = 0.0001$ and $R = 10^{-8}$. To give an idea of the output of the observer, figure 5-8 shows the output of the Enkf alongside the results of simulation A at $t = 400s$.

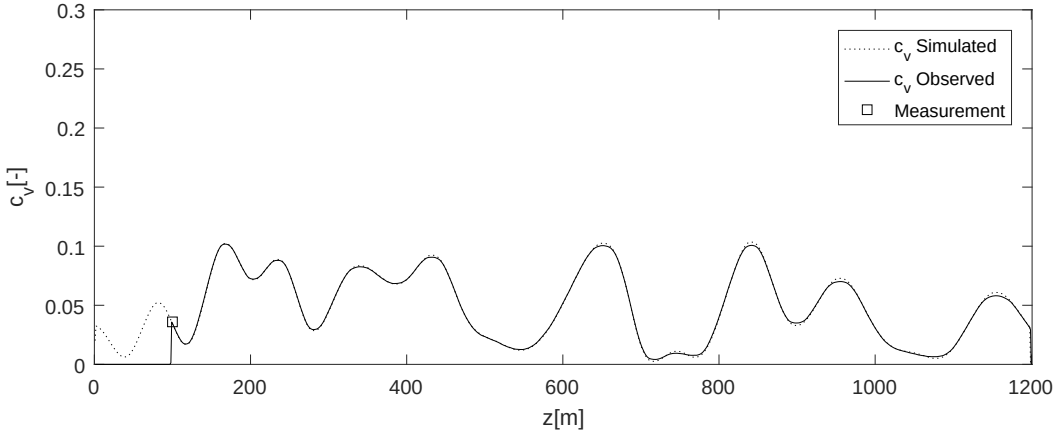

Figure 5-8: Observer output and simulation output

For this observation the same particle diameter was used for both the observer and the simulation, the results are very similar which confirms that the b1DVHT model used in the observer and the 1DVHT model provide equal results under the same conditions.

An adjustment is made in the definition of the model error co-variance since all states below sensor 1 cannot be measured properly as long as the solids move up. Not observing the section below is not a problem, but it affects the functionality of measurement 1 and thereby the section above measurement 1. Since the inflow is unknown to the observer the model covariance of states below the first sensor is increased by adding a predefined state model error co-variance matrix Q to the co-variance determined by the Ensemble Kalman filter.

5-3-2 Long Range Pressure Measurements

Interesting is to investigate the effect of long-range pressure difference measurements added to the observer. This configuration was proven to increase the observability in Chapter 1, and will be investigated by means of simulation. Besides the measurement at $z = 100$, a long-range measurement over $z = 100 - 1100m$ is added, such that:

$$y = h(x) = \begin{bmatrix} c_{v_{100}} \\ \frac{1}{1000} \cdot (c_{v_{100}} + c_{v_{101}} + c_{v_{102}} + \cdots + c_{v_{998}} + c_{v_{999}} + c_{v_{1000}}) \end{bmatrix} \tag{5-6}$$

Measurements are validated at $z = 1100$, at this location the variance of the error between the simulated concentration and the observed concentration is investigated over time ($\text{Var}(c_{v1000}(1:t)$-$\hat{c}_{v1000}(1:t))$). The results of the long range measurements on the observation for simulation A,B,C and D are depicted in table 5-1:

Table 5-1: Effect of long range measurements on the observation

Simulation	$\text{var}(c_v(1:k) - \hat{c}_v(1:k))$	$\text{var}(c_v(1:k) - \hat{c}_v(1:k))$ Long Range Measurement
A	$7.17 \cdot 10^{-6}$	$7.11 \cdot 10^{-6}$
B	$1.48 \cdot 10^{-6}$	$1.40 \cdot 10^{-6}$
C	$2.58 \cdot 10^{-4}$	$2.33 \cdot 10^{-4}$
D	$3.87 \cdot 10^{-4}$	$3.62 \cdot 10^{-4}$

For all simulations an improvement of the observation has been witnessed, especially for simulations C and D which are mixtures with multiple fractions an advantage is gained. It is concluded that the added measurements have a positive effect on the observation.

5-3-3 Localization

The Ensemble Kalman filter calculates the state covariance which is defined as $P_f(k)$. This is not a deterministic approach, and by doing so covariance relations can be found between states that are physically not close to each other, a method to avoid this problem is called *localization*: A field ($\rho\ \mathbb{R}^{m \times m}$) is created indicating which states can be affected by other states, in the case of the VTS these are the neighbouring states defined by a cutoff length l. The localisation field is multiplied with the covariance matrix using the Hadamard product and the kalman gain then becomes:

$$K(k) = (\rho \circ P_f(k))H^T(H(\rho \circ P_f(k))H^T + R)^{-1} \tag{5-7}$$

Gaspari-Cohn's fifth-order polynomial function [25] is used to create the localisation field ρ. The state covariance matrix $P_f \in \mathbb{R}^{m \times m}$ gains large proportions if the amount of states increases. Since localization is used only parts of the covariance matrix are evaluated. In order to save memory it is possible to save the term $\rho \circ P_f$ as a sparse matrix.

It is verified whether localisation increases the quality of the observation by means of the variance of the error at $z = 1100m$, furthermore it is verified whether the computational time is reduced. The results for two different cut-off lengths are depicted in Table 5-2:

Table 5-2: Effect of localisation on the computational time, and state observation

Simulation	$t_c[s]$	$t_c[s]$ Loc. $(l = 2)$	$t_c[s]$ Loc. $(l = 0.25)$	$\text{Var}(c_v - \hat{c}_v)$	$\text{Var}(c_v - \hat{c}_v)$ Loc. $(l = 2)$	$\text{Var}(c_v - \hat{c}_v)$ Loc. $(l = 0.25)$
A	663	923	925	$7.09 \cdot 10^{-6}$	$7.11 \cdot 10^{-6}$	$7.11 \cdot 10^{-6}$
B	671	929	928	$1.39 \cdot 10^{-6}$	$1.40 \cdot 10^{-6}$	$1.40 \cdot 10^{-6}$

The error of the observation is increased but this effect is not considered to be significant. What is most surprising is that the computational time is not decreased, while solving the Kalman gain is easier. Due to the fact that the number of measurements is small the Kalman gain is already easy to solve, multiplying with the very large localization field therefore increased the computational effort rather than decreasing it.

From the simulation results it can be seen that localisation will not yield an advantage in the computation time nor observation and it is therefore chosen to not use this method in the observer.

5-3-4 Inflation

An other extension often applied to the Ensemble Kalman filter is *inflation*. This method can be applied if the covariance matrix is underestimated as as result of the limited ensemble size. The following step is added to the measurement update step of the filter.

$$x_f = \bar{x}_f + r \cdot (x_f - \bar{x}_f) \tag{5-8}$$

It is found that the ensembles are blown up faster than that they can be adjusted by the measurements. This has an effect on the states that are far from the measurements. Even for low values $r = 1.01$ it the observation diverges too quickly, therefore inflation is not applied.

5-3-5 Negative Concentrations

The b1DVHT cannot cope with negative c_v values, besides the fact that this is physically not feasible the simulation will also become unstable. After every propagation of the forecast step artificial noise $(w(k))$ is added to the ensembles to simulate model error, this creates the problem that artificial noise may cause a certain state to be: $c_v < 0$. This problem can be omitted by setting al negative c_v values to zero, however this pushes up the ensembles. To demonstrate this issue Figure 5-9 shows not only the ensemble mean but also the highest and lowest value in the set of ensembles. The effect of removing negative values on the ensemble mean is shown after the initial ensemble $(t = 0)$, which is done for $\sigma_w = 0.01$. It is found that the ensemble observation is pushed up which results in the effect that concentrations close to zero will be overestimated:

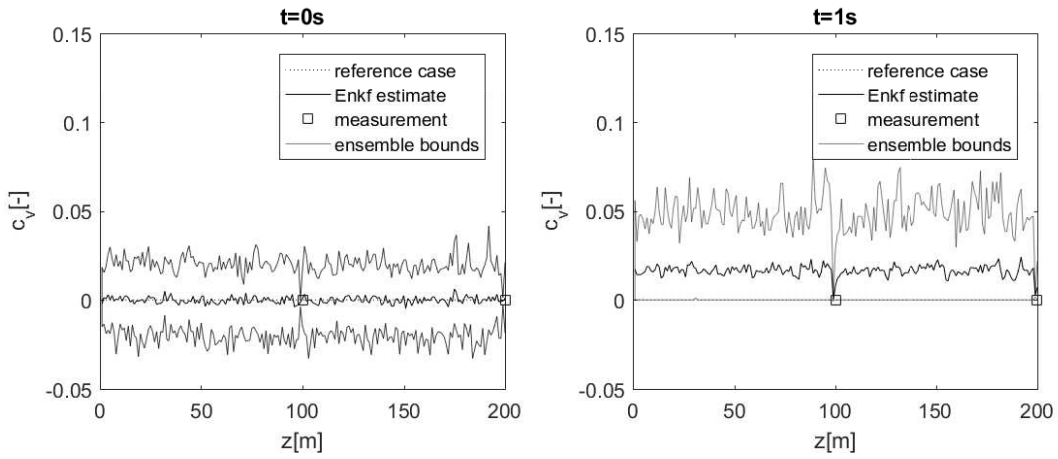

Figure 5-9: Effect of saturating negative states

A mitigation is found making the standard deviation of the added noise relative to the ensemble mean as is shown in equation 5-9.

$$\sigma_w = \begin{cases} \sigma_w, \, if \;\; \bar{x}_f \geq 5 \cdot \sigma_w \\ \dfrac{\bar{x}_f}{5}, \, if \;\; \bar{x}_f < 5 \cdot \sigma_w \end{cases} \tag{5-9}$$

For $\sigma_w = 1 \cdot 10^{-4}$ the results of this addition are evaluated, the effect on the observation is shown in Table 5-3:

Table 5-3: Effect of relative noise on the observation

Simulation	$\text{var}(c_v(1:k) - \hat{c}_v(1:k))$	$\text{var}(c_v(1:k) - \hat{c}_v(1:k))$ Long Range Measurement
A	$7.22 \cdot 10^{-6}$	$7.17 \cdot 10^{-6}$
B	$1.68 \cdot 10^{-6}$	$1.48 \cdot 10^{-6}$

An increase in performance is achieved using this method. A side effect is that the covariance of low value states decreases with respect to high value states, this effect is mitigated by adding a minimum covariance to all states by adjusting Q.

5-3-6 Conclusion

The Ensemble Kalman filter has been applied using the b1DVHT model and has been tested on simulations of a riser section. It was found that long range pressure measurements can be added to the Ensemble Kalman filter in order to improve the estimation of states. The addition of localisation and inflation did not result in an improvement of the observation. A method to cope with artificial noise around states that are close to $c_v = 0$ has been presented and it has been proven to yield an improved observation.

5-4 Particle Diameter Observer

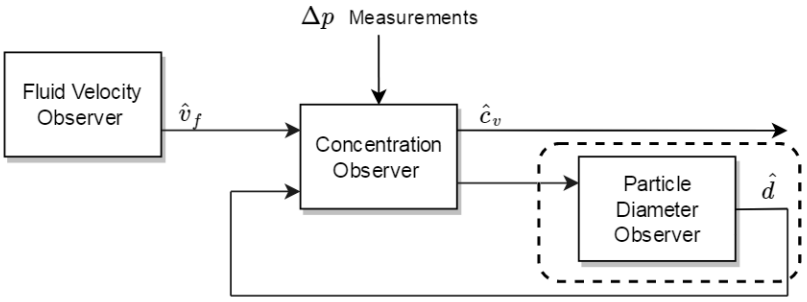

Figure 5-10: Simplified Observer Structure

The particle diameter was identified as the unknown input of the system, estimating this parameter is needed in order to predict the velocity of solids through the system. In Chapter 2 it was found that this parameter is not observable from the outputs that were defined, in this chapter it is elaborated what the effect is of different particles diameters on the solids velocity in the VTS and two methods are presented which can be used to measure the particle diameter in a slurry. One of these methods will be selected for the final design of the observer.

Slurry flows may contain multiple fractions of solids with different velocities, the aim of the particle diameter observer is to find one particle diameter that can be used in the observer to find the best results for the concentration measurements.

5-4-1 Sensibility

The significance of particle diameter variation is analysed in order to determine the effect on the observation. The particle diameter determines directly the hindered settling velocity in the flow which results in the velocity of solids in the riser. The effect of this parameter is determined using basic calculations on a simple case: the time to travel through a riser section is compared for different particle sizes. A riser section of 1000m is considered with a diameter of $0.356m$, the mixture velocity inside the riser is $4m/s$ and the volumetric concentration is 10%. The hindered settling velocity along with the time to travel through the riser for different particle sizes is shown in Table 5-4:

Table 5-4: Travel time through riser section of 1000m

Material	d_m [mm]	w_h [m/s]	t[s]
Sand	1	0.08	255
Gravel/Small manganese nodule	10	0.35	274
Average manganese nodules	30	0.55	289
Largest manganes nodules	100	0.63	297

It is shown that within a section of 1000m different types of solids will result in significantly different residence times. The most interesting difference can be seen between the residence

time of sand and average sized manganese nodules, this difference is $45s$. From an operator perspective it is valuable information to distinguish whether sand or nodules are lifted, estimating the particle diameter will thus be valuable in two ways: it will improve the observer, but will also provide information about the solids that are lifted. Two approaches to measure the particle diameter will be considered:

- A separate observer is constructed based on a model where the particle diameter is observable, using the Extended Kalman Filter.
- By creating an extra output an extension of the Enkf is created, based on the Proportional Adaptive Observer.

5-4-2 Extended Kalman Filter

It is possible to measure the volumetric concentration at different locations in the system, in this section it is explained how an observer for the particle diameter is constructed using this information.

Observability analysis

Since the particle diameter is directly related to the settling velocity, it is verified if the particle diameter can be observed if the settling velocity is measured. In order to determine the observability the hindered settling velocity for different particle diameters and concentrations is analysed for a pipe diameter of $D = 0.356m$:

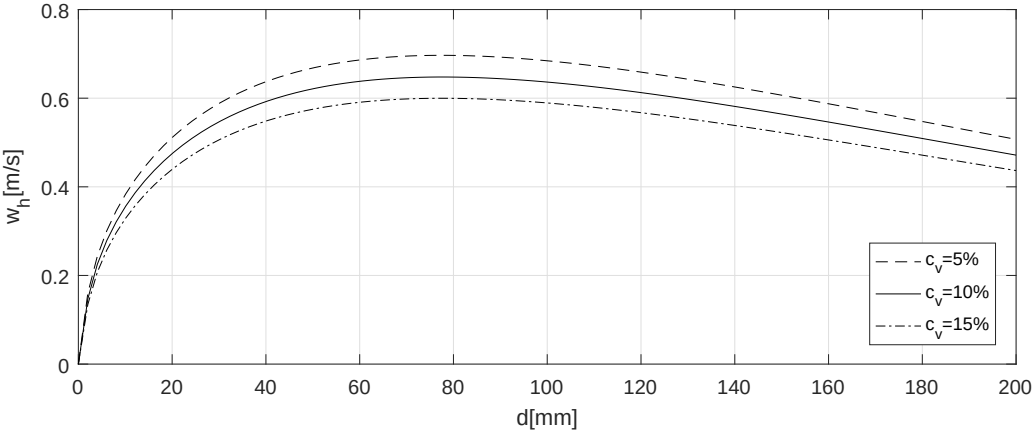

Figure 5-11: Hindered settling velocity.

In the figure it can be seen that for every combination of w_h and c_v there are two possible solutions for d. However it is known that 90% of the nodules are below 80mm [26], and it is thus certain that the mean diameter is always below this value. This assumption makes the mean particle diameter locally observable if c_v and w_h are measured.

Observer Structure

A strategy to measure the settling velocity and particle diameter is presented in this paragraph: A section of the riser is selected, as shown in figure 5-12. The riser section is marked with the dotted lines, and in between the section there is a known sum of concentrations representing the total mass. This sum of concentrations can only change if mass flows in or out of the boundaries that are marked with the dotted lines, the variation of the mass will therefore be used to estimate the mass fluxes in and out of the section in order to reconstruct the solid velocity.

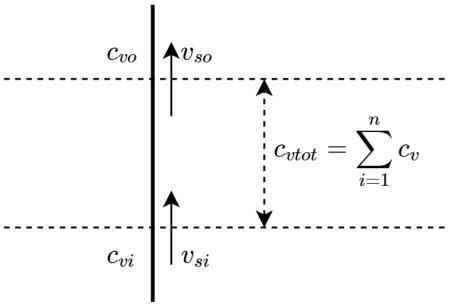

Figure 5-12: Selected riser section with ingoing and outgoing flux.

If the concentration at the inflow (bottom) is named c_{vi} and the concentration at the outflow is named c_{vo} an equation can be set up which relates the total concentration to the in- and outflow, in this formula the effect of axial dispersion is neglected:

$$c_{v_{tot}}(t) = c_{v_{tot}}(0) + \int_0^t c_{vi}(t) \cdot v_{so}(t) - c_{vo}(t) \cdot v_{so}(t)\ dt \tag{5-10}$$

Which translates to:

$$\dot{c}_{v_{tot}}(t) = c_{vi}(t) \cdot v_{so}(t) - c_{vo}(t) \cdot v_{so}(t) \tag{5-11}$$

For now the assumption is made that the fluid velocity is known at both points, the solids velocity (v_s) is rewritten as a combination of the fluid velocity (v_f) and the hindered settling velocity (w_h) which yields the following equation for the mass fluxes:

$$c_v \cdot v_s = c_v \cdot (v_f - \overbrace{w_t 10^{-\frac{d}{D}} (1 - c_v)^{n-1}}^{w_h}) \tag{5-12}$$

Combining equation 5-10 and 5-12 the following 2-state model is constructed:

$$\begin{aligned} \dot{c}_{v_{tot}}(t) =& (v_{fi}(t) - w_h(d, t, c_{vi})) \cdot c_{v_i}(t) - (v_{fo}(t) - w_h(d, t, c_{vo})) \cdot c_{v_o}(t) \\ \dot{d}(t) =& 0 \end{aligned} \tag{5-13}$$

An uncertain parameter without a model can be described as a random walk model [27], which is done for the particle diameter. The equations are then discretised as:

$$\begin{aligned}\hat{c}_{v_{tot}}(k+1) =& \frac{\Delta t}{\Delta z} \cdot (v_{fi}(k) - w_t(k) \cdot (1 - c_{vi}(k))^{n_{rz}}) \cdot (c_{vi}) - \\ & \frac{\Delta t}{\Delta z} \cdot (v_{fo}(k) - w_t(k) \cdot (1 - c_{vo}(k))^{n_{rz}}) \cdot (c_{vo}) + c_{v_{tot}}(k) \\ \hat{d}(k+1) =& d(k) + e(k)\end{aligned} \tag{5-14}$$

In this equation $e(k)$ represents the Wiener process. The observer model is applied using an Extended Kalman Filter (EKF) which is chosen because of the suitability for non-linear systems, a jacobian of the states is modeled accordingly. The model has the following state, input and output vectors:

$$\hat{x}(k) = \begin{bmatrix} c_{v_{tot}}(k) \\ d(k) \end{bmatrix}, u(k) = \begin{bmatrix} c_{vi}(k) \\ c_{vo}(k) \\ v_{fi}(k) \\ v_{fo}(k) \end{bmatrix}, y(k) = \begin{bmatrix} c_{v_{tot}}(k) \end{bmatrix} \tag{5-15}$$

Covariance matrices are tuned as is shown in 5-16. The covariance of the second state $\hat{d}$ is set low compared to the first state in order to prevent fast fluctuation of the particle diameter.

$$R = \begin{bmatrix} 1 \end{bmatrix}, \; Q = \begin{bmatrix} 1 & 0 \\ 0 & 10^{-5} \end{bmatrix} \tag{5-16}$$

Simulation Tests

The observer is tested on simulation cases A and B, the observation is started with an initial guess of $d = 5mm$. For simulation A and B the results are depicted in figure 5-13.

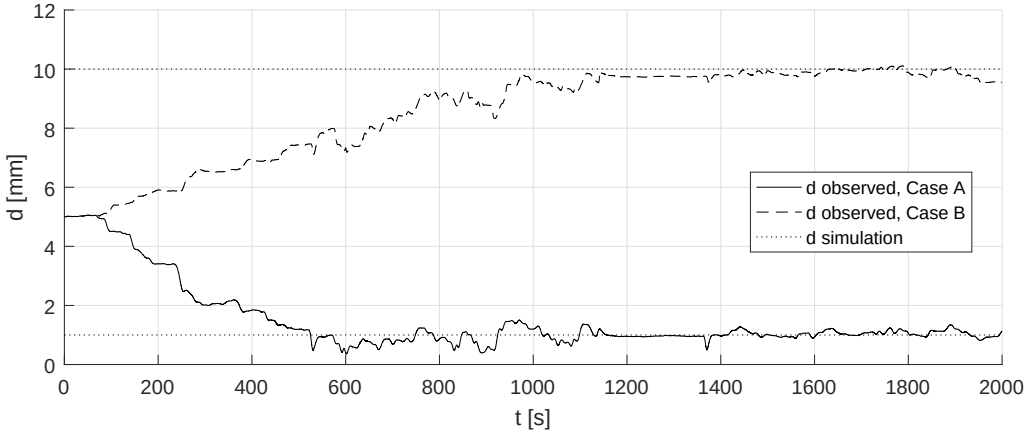

Figure 5-13: d observed for simulation cases A and B.

The observations converge to the particle diameter that was used in the simulations with no steady state error, due to the low model covariance the estimate of the particle diameter is

adjusted slowly but this has the advantage that there are no strong oscillations. The non-linearity of the settling velocity cannot entirely be captured by the EKF which can only handle 1st order non-linear systems, that is why small peaks are still present in the result.

For the case with multiple solids fractions C and D the observation is initiated with $d = 0.15mm$, the results are shown in figure 5-14.

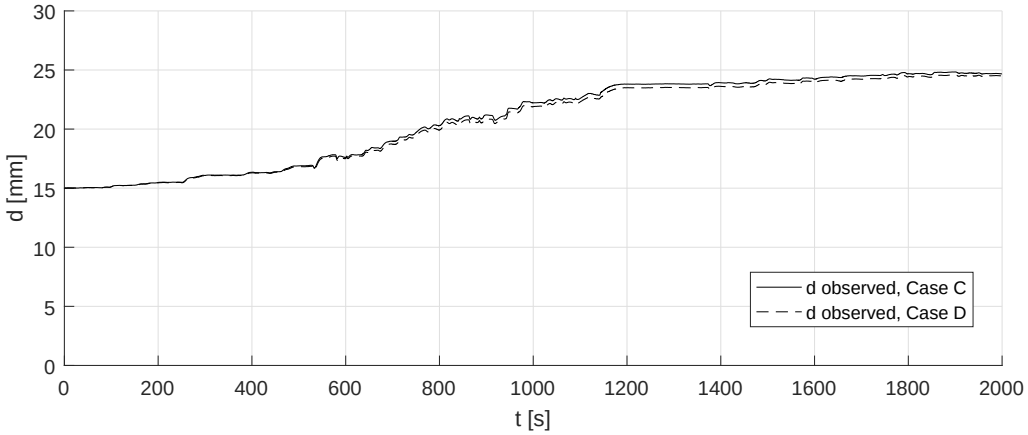

Figure 5-14: d observed for simulation cases D and D.

Both observations generally follow the same path, and for both cases a value is observed which is lower than the mean value of the mixture (For case C: $30mm$, for case D: $42mm$). The mean particle diameter of Case D is higher but the observation ends up lower than C, this result is attributed to the fact that the slurry in Case D also contains a lot of smaller solids fractions. In a slurry with multiple particle sizes the smaller particles will take over the larger particles which increases the volumetric concentration, this effect will decrease the settling velocity which results in a lower observed particle diameter.

When the mean solid velocity is evaluated from the 1DVHT model, it is found that this corresponds close to a particle diameter of $20 - 25mm$ for case C and D, which confirms that the results are correct.

Remarks and Conclusion

An observer for the mean particle diameter is presented. Using characteristics of the concentration propagation it is possible to approach the mean particle diameter using an Extended Kalman Filter. Small peaks are present in the observations, and the reason for this is that the Jacobian of the EKF does not capture the non-linearity of the hindered settling velocity completely. Use of a particle filter will likely improve the results.

It is found that the estimation of the particle diameter is very sensitive to the fluid velocity. In the simulation observations it was assumed this value could be directly measured at multiple locations, as well as the concentration at different points. Attempts have been made to apply this observer on the Δp measurements of the test setup but unfortunately no clear results were obtained, please refer to Appendix D to see these results.

It has been shown that this observer is not feasible for the test setup, however the most important conclusion from this section is that the observation of multiple fraction solids will not necessarily result in an observation of the mean particle diameter, this is a result that will be compared with the other approach.

5-4-3 Proportional-Integral-Observer

The second approach for estimating the particle diameter is based on correcting the results of Enkf: In order to measure the influence of the particle diameter an extra output of the observer is created. This output is the cross correlation between the observation at a certain location, and the measured concentration at that location. Between these signals a time-lag can then be determined indicating that the estimated concentration arrives earlier or later at a certain location than is measured. From Table 5-4 it can be seen that the residence time in the riser depends on the particle diameter which means that if a difference of residence time is witnessed, the particle diameter needs a correction.

This principle is demonstrated in figure 5-15, here we have a slurry with particles of $d = 1mm$, but the guess of the observer is a diameter of $d = 10mm$ which has a larger settling velocity. What is seen is a lag between the observation and the real concentration in the riser:

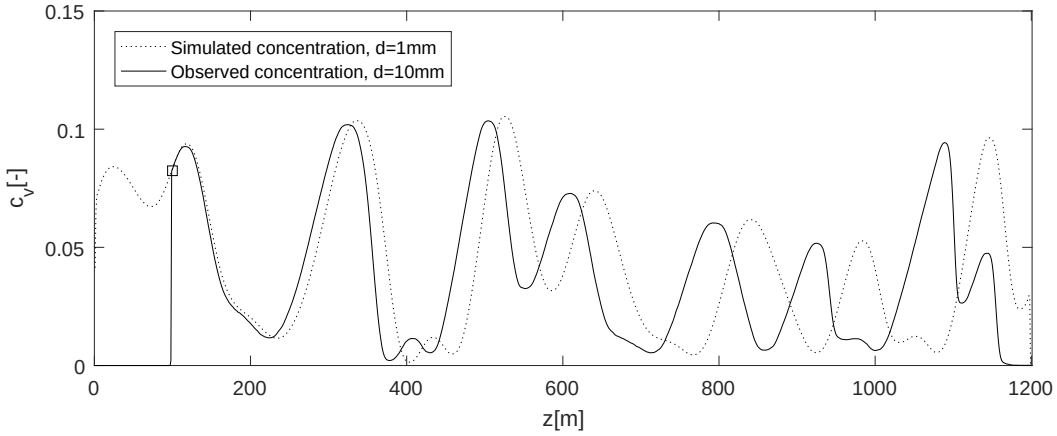

Figure 5-15: c_v observed, and c_v from simulation

When the observation and the measured concentration are compared at $z = 1100m$ it can be seen that the observed concentration lags behind the measured concentration, this effect is shown in Figure 5-16.

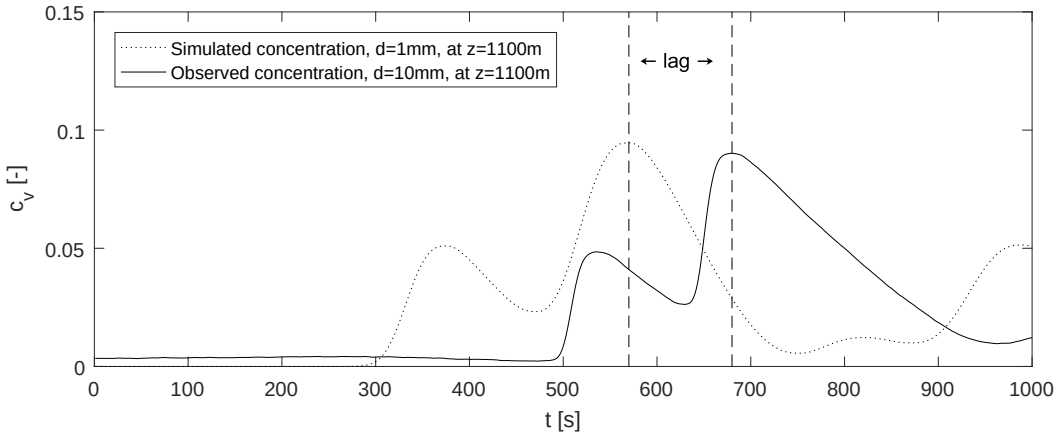

Figure 5-16: c_v observed at $z = 1100m$

A Proportional-Integral-Observer is designed in order to observe the particle diameter: the particle diameter is integrated with a proportional gain, multiplied with the time-lag that is measured:

$$\hat{d}(k+1) = \hat{d}(k) - P \cdot (y(k) - \hat{y}(k)) \tag{5-17}$$

In this equation $y(k)$ is the time lag that is aimed for: this value is always zero since that occurs when the particle diameter of the observer and the mixture are the same. The value $\hat{y}(k)$ is the measured time lag of the observer of which the meaning is demonstrated in Figure 5-16. This simple additions results in a Proportional-Integral-Observer extension of the Enkf. Using simulations it will be verified whether this structure is able to find the right particle diameter and whether it will provide an improvement of the observation.

Simulation Tests

Case A and B are used to verify whether the particle diameter of single fraction solids can be observed:

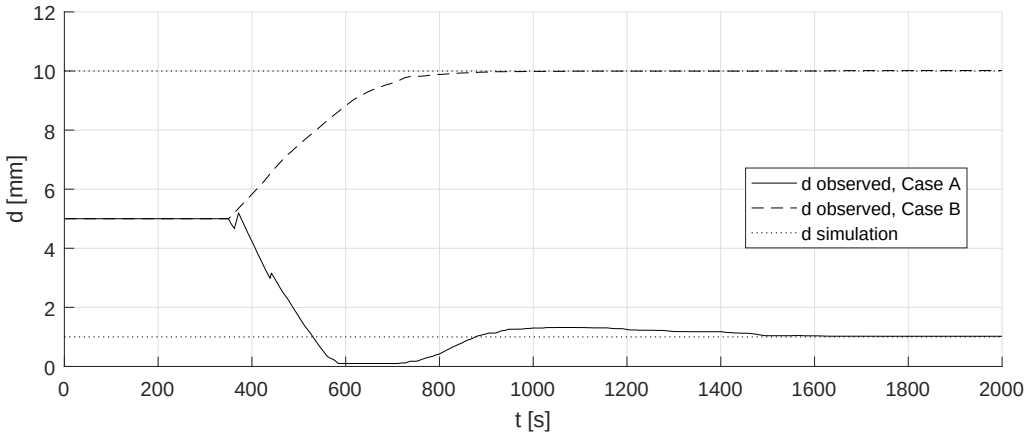

Figure 5-17: d observed for simulation cases A and B.

From figure 5-17 it can be seen that the particle diameter is estimated correctly for case A and B, it can be noticed that the settling velocity has a steep curve for low particle diameters which explains the overshoot for the estimation of sand. Mixture simulations C and D are evaluated too:

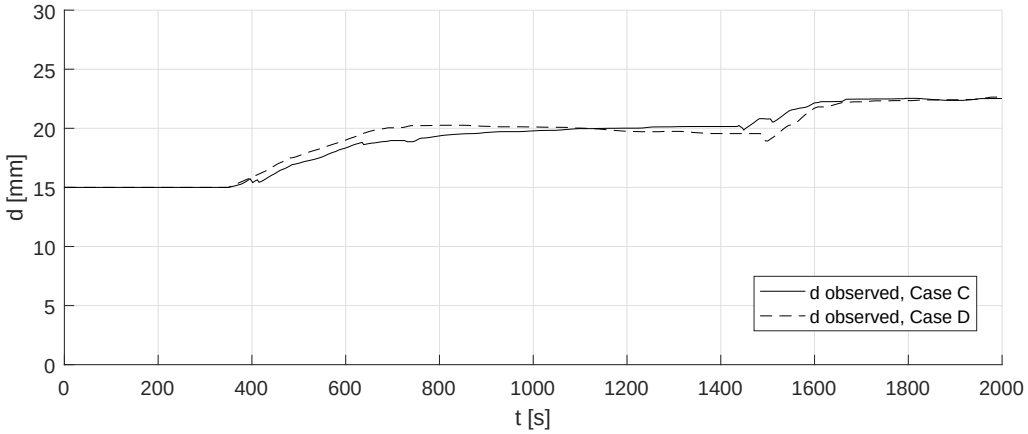

Figure 5-18: d observed for simulation cases C and D.

Again a particle diameter is found between $20 - 25mm$ which confirms that that would be a good estimate for the particle diameter. The observation is corrected in multiple phases which shows that the correction depends on finding a good cross-correlation for the concentration, which is not always directly found for multiple fraction mixtures.

Important to measure is the performance of the observer when the particle diameter is adjusted, compared to the performance of the observer when the mean particle diameter is considered without adjustment. The observer is applied to case C and D in order to find if the performance increases, the initial guess is the mean particle diameter. The result is shown in Table 5-5:

Table 5-5: Effect of long range measurements on the observation

Simulation	$\text{var}(c_v\text{-}\hat{c}_v)$, $d = \bar{d}$	$\text{var}(c_v\text{-}\hat{c}_v)$ Proportional Adjusted d
C	$2.33 \cdot 10^{-4}$	$1.92 \cdot 10^{-4}$
D	$3.62 \cdot 10^{-4}$	$3.22 \cdot 10^{-4}$

With these results it is proven that the observer is able to find a solution that reduces the variance of the concentration observation significantly.

Remarks and conclusion

The Proportional-Integral-Observer extension to the Ensemble Kalman Filter has proven to find the right particle diameter in the simulation cases were one fraction of solids is present. For the cases were a mixture of multiple fractions is simulated it has proven to find a solution which reduces the observation error, compared to the situation where the mean particle diameter would be used.

The main advantage of this observer structure is that it it possible to adapt the observer to variations of the particle diameter that are only visible and significant after propagation over a large distance. Enabling boundary conditions $0.1 \leq \hat{d} \leq 80$ will furthermore ensure that the estimated value will never result in an unfeasible estimate. A disadvantage is that the adoption depends on the cross correlation between two signal: the observation at a certain point compared with the measurement at that point. In order to correctly adjust the particle diameter it is therefore crucial to correctly estimate the volumetric concentration over a large distance and it is uncertain if this is possible over the course of $1000m$.

5-4-4 Comparison and Conclusion

Two observers for the particle diameter have been presented, both observers are able to find an equivalent particle diameter for single- and multiple-fraction mixtures. The 1st method based on the EKF has been applied on the measurements from the test setup but no clear observation of the particle diameter was observed.

The 2nd approach is therefore preferred, This method has been proven to find an equivalent diameter for the slurry that reduces the error of the concentration observation. In simulations this has been proven, but applicability in reality will depend on finding a good cross-correlation between the observed and the measured concentration over a distance.

5-5 Combined observer structure

The observers that were elaborated are combined, in Figure 5-19 a complete scheme of all signals involved is shown. This scheme is what lies underneath the simple structure that was shown throughout this report, the observer shown is a design for both the full scale VTS and the scaled test setup VTS.

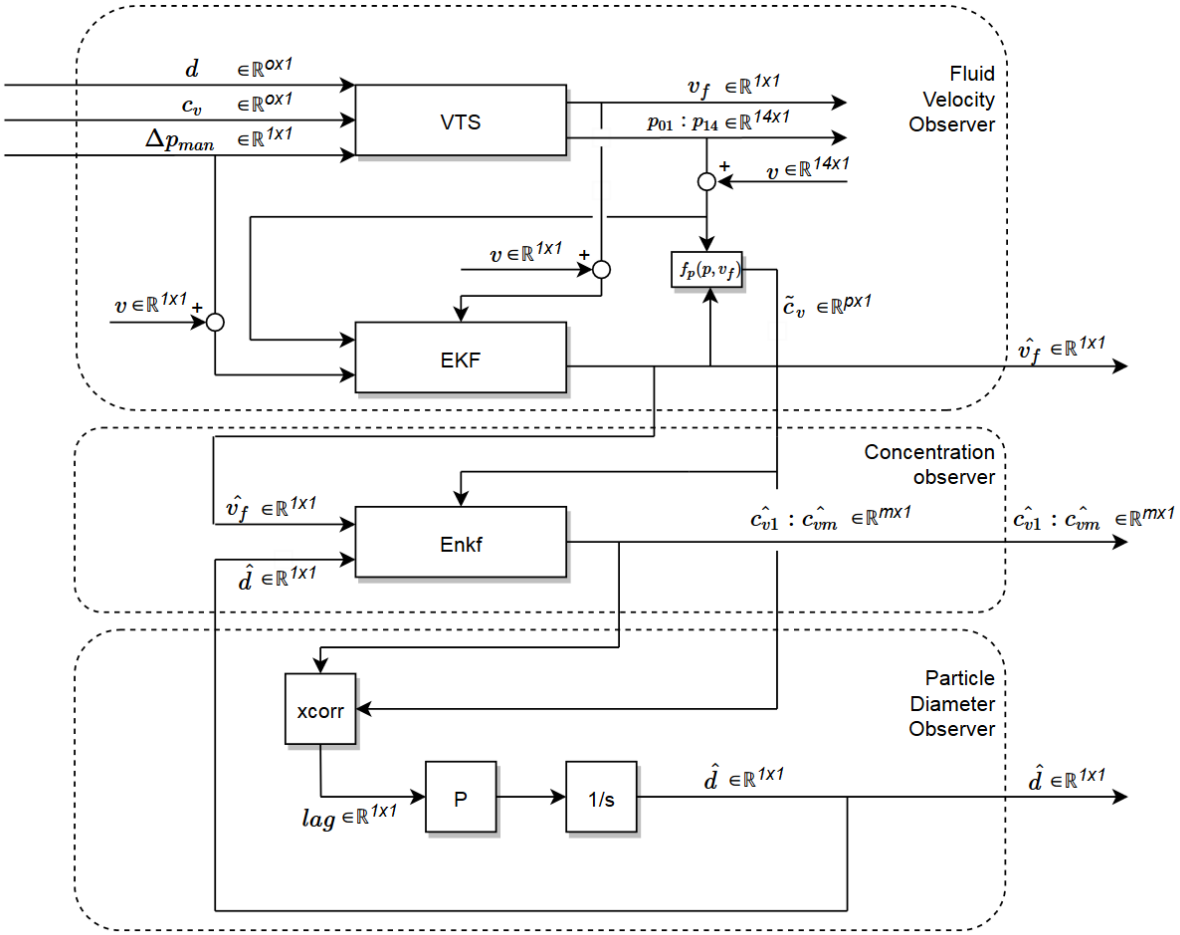

Figure 5-19: Observer Design

Inputs to the VTS are the pressure delivered by one pump ($p_{man} \in \mathbb{R}^{1\times1}$) and the solid fractions added to the system ($c_v \in \mathbb{R}^{o\times1}, d \in \mathbb{R}^{o\times1}$). As a result of the propagating of solids through the system we measure a pressure distribution ($p_{01} : p_{14} \in \mathbb{R}^{14\times1}$), and a fluid velocity ($v_f \in \mathbb{R}^{1\times1}$) in the riser. Measured parameters are affected by measurement noise (v).

The pump pressure (p_{man}) is used for the observation of $\hat{v}_f$ in the EKF and furthermore the pressure sensors are used in order to estimate the difference between mass going up and down (m_{diff}). The estimated $\hat{v}_f$ is used in combination with the pressure differences to determine the measured volumetric concentration between the pressure sensors ($\tilde{c}_v$) by accounting for the wall shear stress, this equation is shown in the scheme as $f_p(p, v_f)$:

$$f_p(p, v_f) = \tilde{c}_v = \left(\frac{\Delta p - 4 \cdot \tau_m \cdot \frac{L}{D}}{\Delta z \cdot g} - \rho_f \right) \cdot \left(\frac{1}{\rho_s - \rho_f} \right) \tag{5-18}$$

The observed fluid velocity is an input of the Enkf, but due to the different concentrations this value is not equal through the whole riser. At the location of the electromagnetic flow meter the *mixture* bulk velocity which is equal through the riser is determined based on the

fluid velocity, the local volumetric concentration, and an estimation of the hindered settling velocity:

$$\bar{v}_m = (\hat{v}_f - \hat{w}_h(\hat{d}, \hat{c}_v)) \cdot \hat{c}_v + (1 - \hat{c}_v) \cdot \hat{v}_f \tag{5-19}$$

Using the mixture velocity and the concentration the solids velocity is solved at every location, the output of the Enkf is a concentration distribution discretised into m states. This field is adjusted by the Enkf at certain locations using the measured concentration $\tilde{c}_v$.

The output of the Enkf is compared with the measured concentration at a chosen validation point. At this point the cross correlation between the observation $\hat{c}_v$ and the measurement $\tilde{c}_v$ is calculated resulting in a time delay between the signals, this time delay is used to correct the particle diameter using a proportional integration. As a result an observer is made which provides an estimation of the volumetric concentration of solids over the whole length of the riser while simultaneously correcting the particle diameter, this is called the Proportional -Adaptive Enkf. The cascade structure of this observer enables that the Jacobian of the fluid velocity model can be used for the observation which is an advantage compared to the heuristics approach of the Enkf, furthermore this has enabled tuning the model error covariance which was needed to filter the very noisy measurements for this parameter.

The following state space matrices lie underneath the blocks shown in Figure 5-19:

$$\overbrace{\hat{x}(k) = \begin{bmatrix} v_f(k) \\ m_{diff}(k) \end{bmatrix},\ \hat{y}(k) = \begin{bmatrix} v_f(k) \\ m_{diff}(k) \end{bmatrix},\ u(k) = \begin{bmatrix} p_{man}(k) \\ \rho_{m1}(k) \cdot v_f(k) \\ \rho_{m2}(k) \cdot v_f(k) \end{bmatrix}}^{\text{EKF}} \tag{5-20}$$

$$\overbrace{\hat{x}(k) = \begin{bmatrix} c_{v1}(k) \\ c_{v2}(k) \\ c_{v3}(k) \\ \vdots \\ c_{vm}(k) \end{bmatrix},\ \hat{y}(k) = \begin{bmatrix} \vdots \end{bmatrix},\ u(k) = \begin{bmatrix} v_f(k) \end{bmatrix}}^{\text{Enkf}} \tag{5-21}$$

Where the output of the Enkf depends on the chosen measurement configuration. For the experiments the observer is discretised using spatial and temporal discretization defined as: $\Delta t = 0.1$ and $\Delta z = 1$. These values are small compared to a real VTS, but for the test setup they are chosen in order to accurately measure the performance improvements. The test setup VTS is discretised into $m = 160$ states.

5-6 Difference between the test setup and the full scale VTS

The main part of the observer is designed for application on the full scale VTS, however there is only possibility to apply it to the test setup that is available. The following differences need to be considered:

5-6-1 Fluid Velocity Observation

A model for the fluid velocity has been elaborated for the test setup VTS, in the test setup estimating v_f is complex due to the difference in mass flows going up and down in the closed circuit. In the full scale VTS the volume flow will be going in one direction which makes that it is easier to model, a model is presented in [2] and can be used for this purpose. This does not change the structure of the observer as designed, but only the model that lies underneath the fluid velocity observer.

5-6-2 Particle Diameter observation

Using simulations of a full scale riser section it has been shown that the particle diameter can be corrected using the Proportional-Adaptive Enkf, for the test setup this will unfortunately be more complicated. The pipe diameter of the test setup is about half the the diameter of the full scale VTS which means that the settling velocity (which scales with $10^{-\frac{d}{D}}$) will be significantly lower for all particles. Furthermore the total length of the test setup riser is approximately $100m$ which is 10 times shorter than a section of the full scale VTS, the residence times of the particle diameters will therefore be closer to each other. These two differences will cause that the effect of the different particle diameters will be less significant in the test setup and therefore harder to measure as can be seen in the next table:

Table 5-6: Travel time through scaled riser section of 1000m

Material	d_m [mm]	w_h [m/s]	t[s]
Sand	1	0.08	25.5
Gravel	10	0.32	27.2

5-7 Difference with proposed observer

An observer design was elaborated before [2], this design was based on the Enkf algorithm only, using measurement configuration (1) which was elaborated in Chapter 2. In this observer the mixture velocity observation was incorporated in the Enkf structure. It was found that for the measurements of the test setup the velocity measurements were very noise which have required a lot of tuning of the model error co-variance matrix of the EKF, the Enkf has a heuristic approach to determine this and it is argued that this would yield less accurate results. An other difference is that the observer designed for this research incorporates an estimation of the pressure drop due to wall shear stress, where the proposed observer assumes a static contribution. The most important difference is that the proposed observer is applied with a static estimate of the particle diameter, the designed observer provides a correction of the particle diameter simultaneously while estimating the concentration states.

5-8 Benchmark

The performance of the observer will be evaluated based on the quality of the volumetric concentration observation at a selected verification point, at this point the concentration is measured using Δp measurements. Two benchmarks will be performed in order to compare the performance: the variance between the observed concentration and the measured concentration will be calculated at the chosen verification point:

$$\mathrm{Var}(\hat{c}_v(1:k_{end}) - \tilde{c}_v(k_{end})) = \frac{1}{k_{end}} \cdot \sum_{k=0}^{k_{end}} [\hat{c}_v(k) - \tilde{c}_v(k)]^2 \tag{5-22}$$

The first benchmark will show precisely any increase or decrease in the observation error, the second benchmark shows the similarity of the signals expressed as a percentage. For this measure the Variance Accounted For (VAF) [23] is used:

$$\mathrm{VAF}(\hat{c}_v(1:k_{end}), \tilde{c}_v(k_{end})) = \left(1 - \frac{\mathrm{Var}(\hat{c}_v(1:k_{end}) - \tilde{c}_v(1:k_{end}))}{\mathrm{Var}(\tilde{c}_v(1:k_{end}))}\right) \cdot 100\% \tag{5-23}$$

For the second benchmark, a score of 100% means that two signals are exactly equal which is aimed for.

Chapter 6

Results

In this chapter the performance of the observer is evaluated. Two cases will be treated, first the observer is tested on the ability to measure concentrations over a long distance where the effect of long range pressure measurements is investigated. Second, the effect of proportionally adapting the particle diameter on the concentration observation is tested. It is investigated how these results relate to what can physically be explained.

6-1 Long distance observation

In the full scale riser there is $1000m$ between the locations where the volumetric concentration can be measured. It is logical that close to the measurements the concentration will be predicted right, what is needed to known is how well the observation is far away from the measurements. With other words: It is tested how well the concentration is observed over a large distance. This will be tested with the test setup VTS.

6-1-1 Sensor Configuration

A sensor configuration is made that mimics the design constraints of the VTS where pressure sensors can only be placed at the booster stations, the sensor configuration that will be used is shown in Figure 6-7:

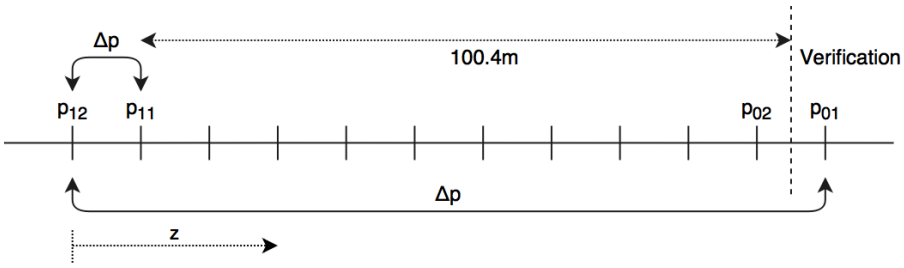

Figure 6-1: Sensor Configuration for Long Distance Observation

For this scenario the concentration is measured using the lowest pressure sensor pair $\Delta p_{12,11}$ and the observation is bench-marked using the highest pressure sensor pair $\Delta p_{02,01}$ at the top of the riser, this verification measurement is not added as an observation to the observer. The effect of using a long range measurement between sensor $\Delta p_{12,01}$ is tested, this measurement does not provide information locally at the location of the verification, but only measures the mean concentration in between the pressure measurements.

For the evaluation of this case the particle diameter observation is not yet tested, but the observer is implemented using the known particle diameter. With the configuration that is shown it will be tested whether the volumetric concentration can be estimated over the course of $100m$, and it will be tested whether long range measurements improve the observation.

6-1-2 Tuning the Enkf

The fluid velocity observer has already been tuned using the data of the test setup and is considered to be optimal, this section adresses tuning of parameters of the concentration observer (Enkf). In order to give an idea of the observations an output of the observer is depicted in Figure 6-2:

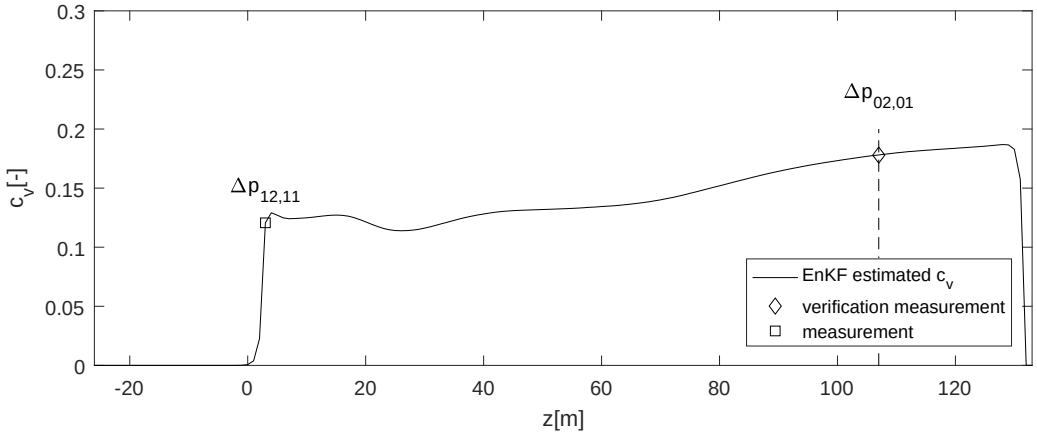

Figure 6-2: Enkf output, measurement 5, $t = 1000s$

It can be seen how the bottom measurement is added to the concentration observation, and how this observation is benchmarked using the verification measurement at the top of the riser. The local Δp measurements are applied on the concentration state that is located in the center between the pressure sensors.

A few parameters of the Ensemble Kalman Filter are left to be chosen and they are tuned using the data of experiment 5. The tuning parameters are varied over a certain range in order to find the best performance, the parameters that are tuned and the range that is considered a shown in Table 6-1:

Table 6-1: Tuning Parameters

Parameter	Meaning	min.	max.
σ_w	Standard deviation of model perturbation	$5 \cdot 10^{-5}$	$5 \cdot 10^{-3}$
q	Number of ensembles	2	150
R	Measurement covariance matrix	$1 \cdot 10^{-7}$	100

Varying the model perturbation did not yield significant difference in the performance of the observer, just like the different values for the ensemble size. It is chosen to use $\sigma_w = 0.0001$, the ensemble size is chosen to be $q = 25$ to be on the safe side in order to prevent undersampling.

The output matrix and measurement covariance matrix are tuned for the local and the long measurement, the following values were found to yield optimal results:

$$y = \begin{bmatrix} c_{v3} \\ \frac{1}{111}(c_{v3} + c_{v4} + c_{v5} + \cdots + c_{v113}) \end{bmatrix}, R = \begin{bmatrix} 10^{-7} & 0 \\ 0 & 10^{-6} \end{bmatrix} \tag{6-1}$$

The index of the concentration states (c_{vi}) indicates the height in $z[m]$ where the state is located in the test setup.

6-1-3 Results

The estimation of the observer is compared with the measurement at the verification point, the benchmarks are evaluated and it is verified whether the long range measurement of $\Delta p_{12,01}$ has a positive effect on the observation. The results are shown in Table 6-2:

Table 6-2: Effect of long range measurements on observer performance

#	$\mathrm{Var}(\tilde{c}_v - \hat{c}_v)$	$\mathrm{VAF}(\tilde{c}_v, \hat{c}_v)$ [%]	$\mathrm{Var}(\tilde{c}_v - \hat{c}_v)$ longrange	$\mathrm{VAF}(\tilde{c}_v, \hat{c}_v)$ [%] longrange
1	$4.00 \cdot 10^{-4}$	93.2	$2.30 \cdot 10^{-4}$	96.1
2	$4.04 \cdot 10^{-5}$	96.8	$2.02 \cdot 10^{-5}$	98.4
3	$5.06 \cdot 10^{-5}$	87.0	$9.88 \cdot 10^{-5}$	74.5
4	$8.30 \cdot 10^{-5}$	97.0	$3.40 \cdot 10^{-5}$	98.8
5	$1.42 \cdot 10^{-4}$	97.4	$4.04 \cdot 10^{-5}$	99.3
6	$2.52 \cdot 10^{-5}$	93.7	$7.46 \cdot 10^{-6}$	98.1
7	$6.21 \cdot 10^{-5}$	95.1	$1.15 \cdot 10^{-5}$	99.1
8	$3.42 \cdot 10^{-5}$	88.1	$8.53 \cdot 10^{-6}$	97.0
9	$4.46 \cdot 10^{-5}$	95.4	$8.89 \cdot 10^{-6}$	99.1
10	$1.79 \cdot 10^{-5}$	86.5	$4.12 \cdot 10^{-6}$	96.9
11	$3.20 \cdot 10^{-5}$	95.7	$1.38 \cdot 10^{-5}$	98.1
12	$2.23 \cdot 10^{-5}$	97.8	$6.02 \cdot 10^{-6}$	99.4
13	$5.26 \cdot 10^{-5}$	95.8	$7.91 \cdot 10^{-6}$	99.4
14	$3.00 \cdot 10^{-4}$	0.7	$5.69 \cdot 10^{-5}$	81.2

Again it is shown that the long range measurements increase the quality of the observation, just as was proven with the observability analysis and the simulations. It can be seen that the

Variance Accounted For yields values that are larger than 95% for most of the measurement sets, this indicates a very good state estimation.

A high value for the VAF was found for measurement 8 of which the result is shown below. At this measurement it can very well be seen that the solids are not spread through the system homogeneously, and that batches of settling solids have the tendency to cluster rather than spread out. It can be clearly seen that the system starts with a circuit that only contains water ($c_v = 0$) and that gradually the mean concentration increases as the solids are added during the test:

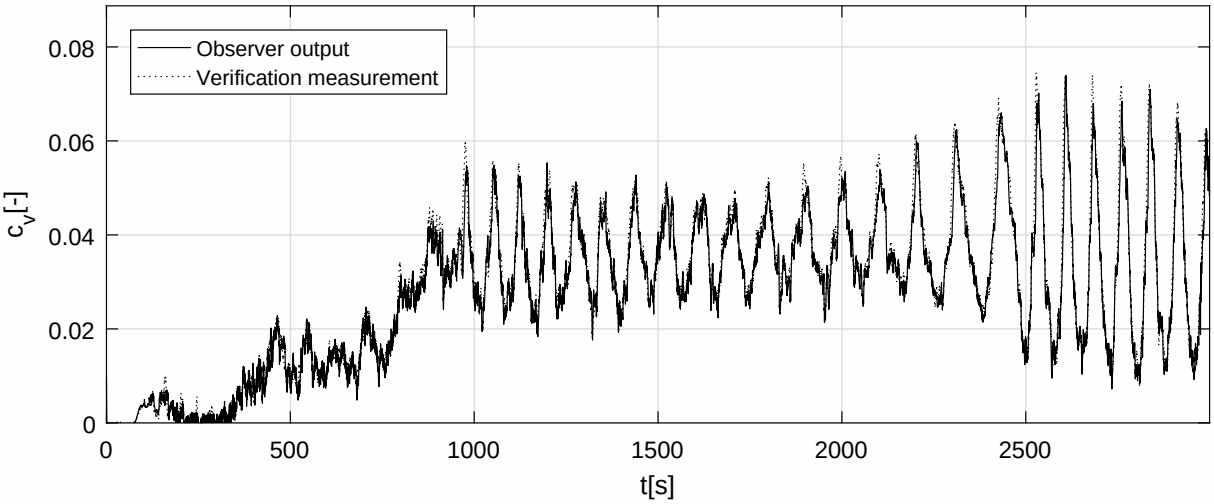

Figure 6-3: Estimated concentration ($c_v[-]$), measurement 8

Usually during the measurement procedure the solids were stored in to two hoppers, which were added to the circuit serially. In measurement 2 (sand) this can be seen very good: two batches of solids were added to the circuit each contributing to a mean volumetric concentration of 5%. Just as can be seen in the other measurements the mean value of the measured concentrations represents the concentration of the solids that are added to the circuit:

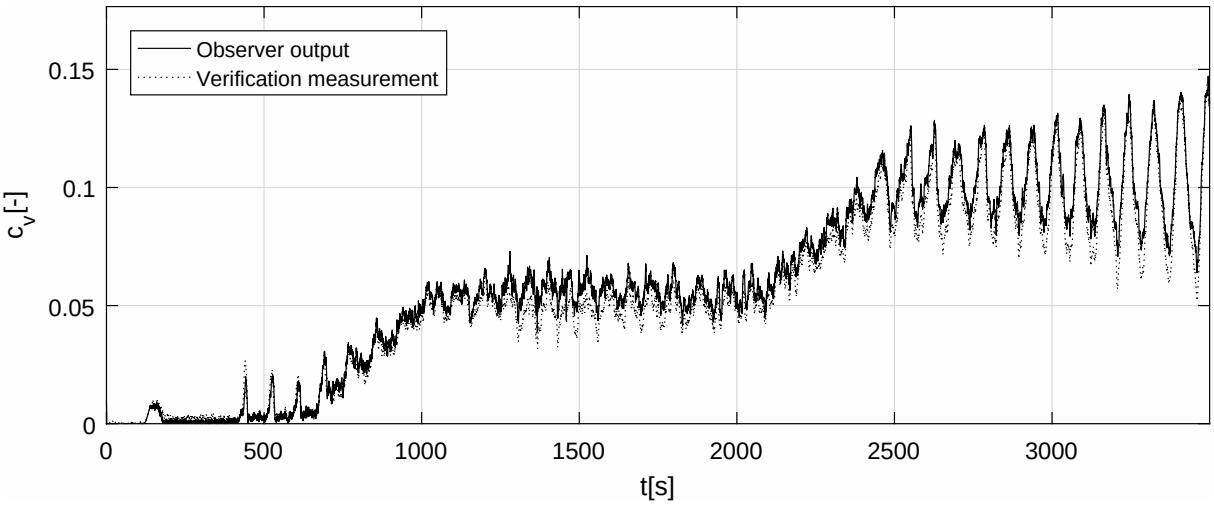

Figure 6-4: Estimated concentration ($c_v[-]$), measurement 2

For measurement 3 a relatively low VAF is found between the signals, also this is the only measurement where a performance decrease was witnessed when adding the long range-measurements. The discrepancy can visually be confirmed when looking at the results:

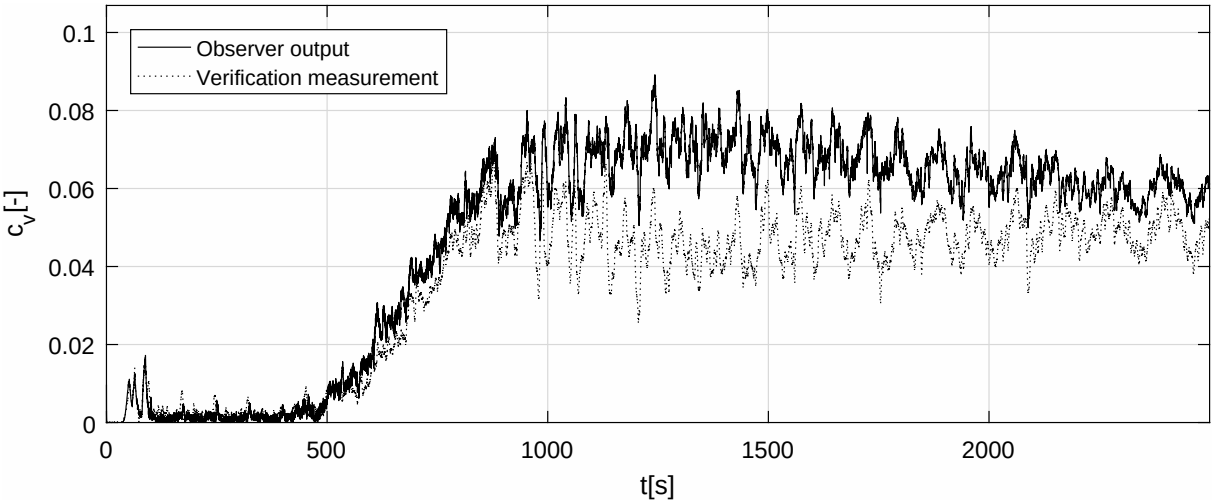

Figure 6-5: Estimated concentration ($c_v[-]$), measurement 3

This result can be explained since measurement 3 was the first experiment where gravel was used instead of sand. Using the watertest before the experiment the pip wall roughness (ϵ_{pipe}) was approximated, the solids added to the circuit grind along the pipe wall and increase the roughness of the pipe which creates a larger pressure drop than is estimated based on the watertests. The increased pressure drop due to wall friction results in a larger measured concentration than actually is present. This result has shown the dependency of the results on a good estimate of the pipe wall roughness.

Interesting to see is how the inputs of the observer relate to the outputs, for measurement 5 these signals are shown:

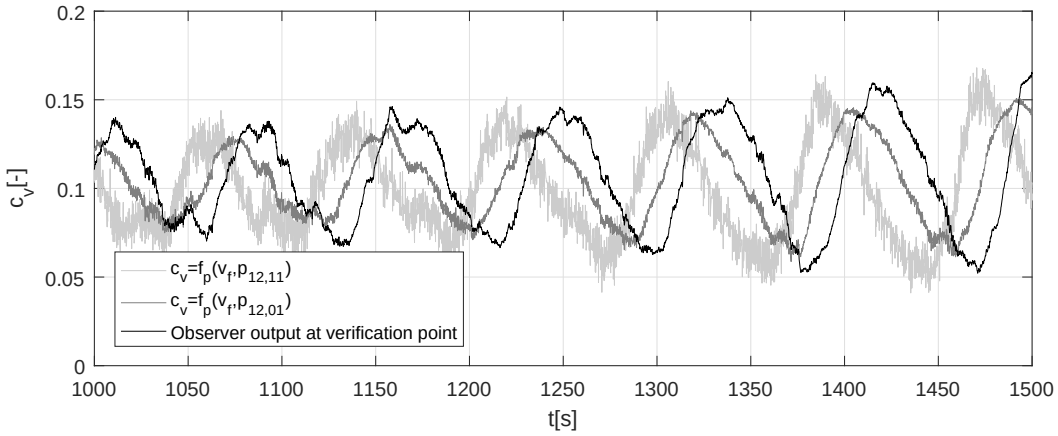

Figure 6-6: Input and output of the observer, measurement 5

What can be seen is a very noise measurement from the bottom of the riser ($f_p(v_f, p_{12,11})$), this

noise is caused by the fact that there is only a small distance between the lowest sensors ($7.6m$) and thus the noise to signal ratio is relatively larger than that of the long-rang measurement ($f_p(v_f, p_{12,01})$) which covers a distance of $113.7m$. It is furthermore witnessed that the output of the observer contains less noise than the inputs, and that the output signal is even smoother when the long-rang measurement is not applied. This effect is attributed to the diffusion term of the advection-diffusion model, this term causes that large concentration gradients are smoothed out. This feature makes the observer resistant against large noise on the measurement input, as long as it is not on the long-range measurements.

In Figure 6-6 it can also be seen that the long range measurement is out of phase with the output of the observer. With that result it is shown that the improved quality of the output is therefore not something that could be assumed in the first place.

The results of all measurements (1-14) can be found in Appendix E. It is shown visually and statistically that the observer yields very accurate results over the course of $100m$ and that observations have been improved significantly by using long range pressure difference measurements. Discrepancy of the observer output with the verification measurements has been found to be caused by the pipe wall roughness that was altered by the solids during the tests, this has influenced the Δp measurements.

6-2 Particle Diameter

The observer is tested on the capability of estimating the particle diameter. A different configuration for the sensors is elaborated, and it is verified whether the performance of the concentration observation is improved.

6-2-1 Sensor Configuration

The configuration of sensors is chosen different than the configuration for the long-range observation, this is because of the pressure sensors that are not equally distributed (Table 3-2). The unequal distances between the pressure sensors results in the effect that propagating density waves are not measured equally at different locations. Therefore two sensors pairs that have an equal distance between them are used resulting in the following configuration:

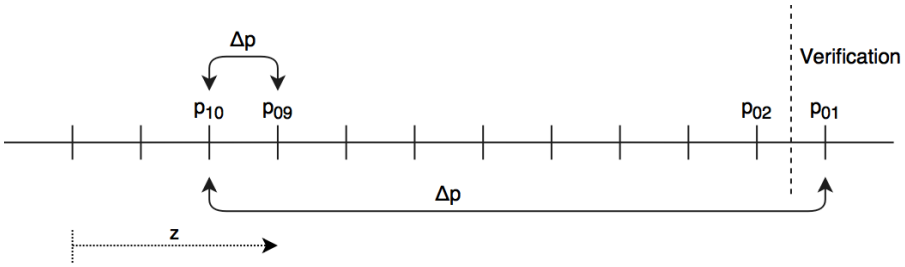

Figure 6-7: Sensor Configuration for Particle Diameter Observation

6-2-2 Results

First of all the results are analysed visually, it is found that reasonable observations are found by shifting the location of verification point virtually by $6m$. This choice is justified by the fact that there is approximately $11m$ between the pressure sensors which makes that the real location of the measured concentration is uncertain.

The extension for the proportional integral adaption is configured: a gain of $P = 2 \cdot 10^{-6}$ is used, and for the determination of the cross correlation the signals are evaluated $200s$ back in time. Comparing sand and gravel measurements then yields the following results for the particle diameter observation over time:

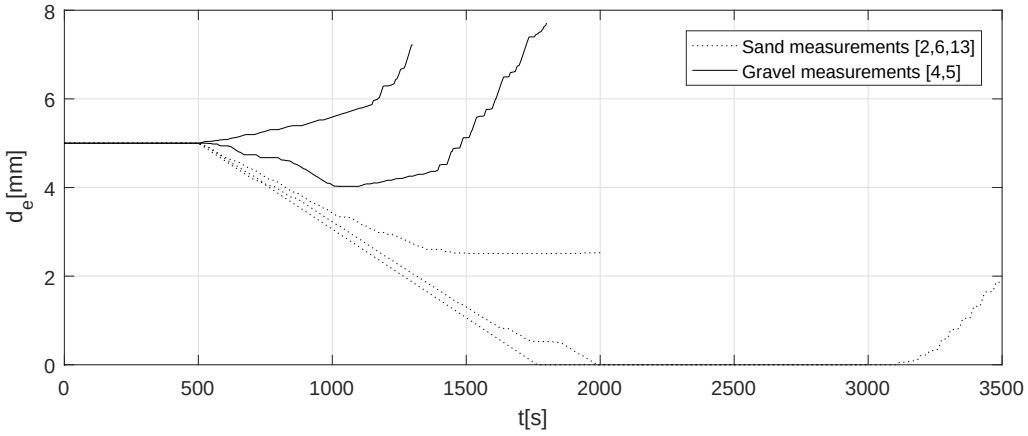

Figure 6-8: Particle Diameter Observation

It can be seen that the different solid types (sand and gravel) are distinguished. However, due to the only subtle effect of the particle diameter, and due to the very noisy fluid velocity measurements on the scaled setup it is hard to precisely measure the particle diameter. This can be seen in the result of the sand measurements, the observations do not all end at the same estimate and the results lay somewhere in between the range $d = 1 - 3mm$.

Mixtures have been evaluated as well, of which the 5% mixtures yield the best results:

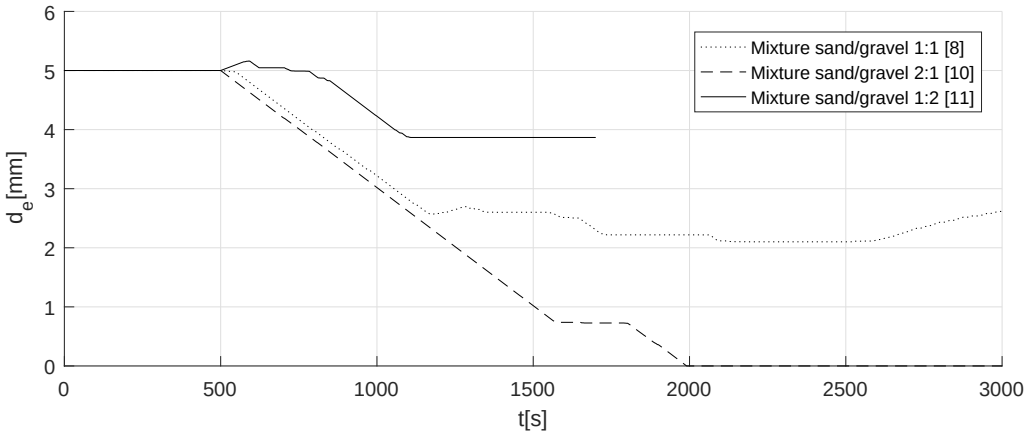

Figure 6-9: Particle Diameter Observation

This set of results shows a difference between the different mixtures that were testes. The mixture that contains the largest fraction of sand yields the lowest particle diameter, and the mixture that contains the largest fraction of solids yields the highest particle diameter. Furthermore the mixture that contains sand and gravel on a 1:1 ratio yields an estimate of the particle diameter that lies in between the other estimate. That shows a good correlation with what would be physically expected.

Similar results were found when tests with larger concentrations of 10% were performed, except for measurement 12 which is expected to be higher the mixtures can be distinguished:

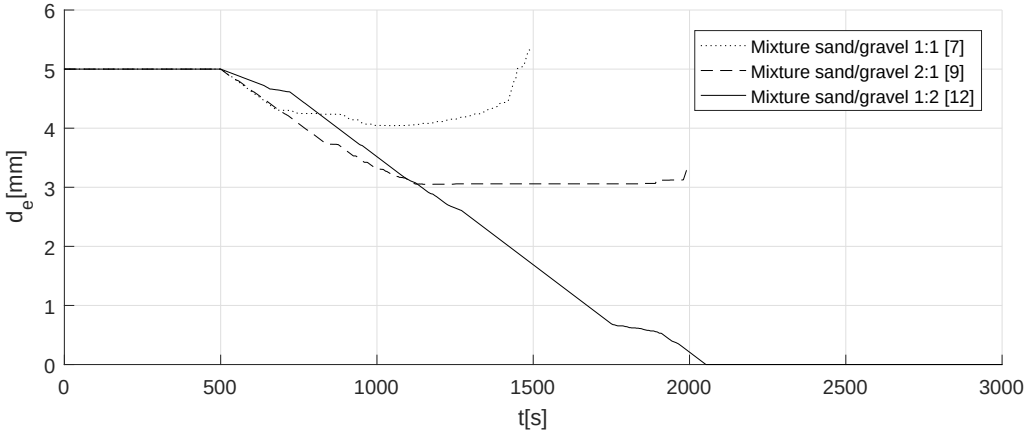

Figure 6-10: Particle Diameter Observation

For measurement 12 there were barely density waves noticed, under these conditions the observer is found to be less effective. As was shown with the simulations the observer depends on finding a good cross correlation between the observer output and the measurements.

Using the benchmarks that were defined, it is verified whether the observation of the particle diameter yields better results compared to the situation where the particle diameter is not

known and assumed constant, the initial guess for the particle diameter observation is $d = 5mm$. The results are found in Table 6-3:

Table 6-3: Effect of particle diameter adaptation on observer performance

#	$\text{Var}(\tilde{c}_v - \hat{c}_v)$ $d = 5mm$	$\text{VAF}(\tilde{c}_v, \hat{c}_v)$ [%] $d = 5mm$	$\text{Var}(\tilde{c}_v - \hat{c}_v)$ d adapted	$\text{VAF}(\tilde{c}_v, \hat{c}_v)$ [%] d adapted
1	$1.22 \cdot 10^{-4}$	97.96	$1.18 \cdot 10^{-4}$	98.00
2	$7.41 \cdot 10^{-6}$	99.41	$7.09 \cdot 10^{-6}$	99.44
3	$3.03 \cdot 10^{-5}$	92.18	$3.02 \cdot 10^{-5}$	92.20
4	$1.81 \cdot 10^{-5}$	99.35	$1.80 \cdot 10^{-5}$	99.35
5	$2.32 \cdot 10^{-5}$	99.58	$2.31 \cdot 10^{-5}$	99.58
6	$3.84 \cdot 10^{-6}$	99.03	$3.58 \cdot 10^{-6}$	99.10
7	$1.69 \cdot 10^{-5}$	98.67	$1.68 \cdot 10^{-5}$	98.67
8	$3.29 \cdot 10^{-6}$	98.86	$3.11 \cdot 10^{-6}$	98.92
9	$3.95 \cdot 10^{-6}$	99.59	$3.87 \cdot 10^{-6}$	99.60
10	$2.15 \cdot 10^{-6}$	98.38	$2.17 \cdot 10^{-6}$	98.37
11	$4.32 \cdot 10^{-6}$	99.42	$4.23 \cdot 10^{-6}$	99.43
12	$2.49 \cdot 10^{-6}$	99.76	$2.33 \cdot 10^{-6}$	99.77
13	$4.77 \cdot 10^{-6}$	99.61	$4.59 \cdot 10^{-6}$	99.63
14	$5.32 \cdot 10^{-5}$	82.38	$5.32 \cdot 10^{-5}$	82.40

A subtle performance increase is measured for all performed measurements. With Table 6-3 it is shown that by proportionally integrating the particle diameter based on the lag that is measured, it is possible to get an improved observation of the solid concentration. It has therefore been shown that the proposed observer structure can lead to an improved observation of the concentration.

6-3 Conclusion

It is shown visually and statistically that the observer yields accurate concentration observations over a course of $100m$, it was found that long range pressure difference measurements improve the observation significantly. At every test a defined amount of solids was added to the circuit and from the results it can be seen that after the solids are added the mean value of the measured concentration corresponds to this amount. A sensitivity of the observer is found to be the pipe wall roughness. There are tests where this parameter is altered throughout the experiments and at these results it can be seen that there is a discrepancy between the observer output and the verification measurement.

It has been shown that using the designed observer structure the difference between two different solid sizes (gravel and sand) could be distinguished as well as different mixtures. A clear observation was not achieved as could be seen for the sand tests, of which the observation lies between $0 - 3mm$. Aspects as the very noisy fluid velocity signal and the fact that the settling velocities of different solids is close to each other in the test setup have resulted in a non-optimal situation for observing the particle diameter. It is likely that over a longer riser section the effect of different particle diameters will be more significant and thus easier

to measure. However, with the experiments performed it has been shown that adjusting the particle diameter proportional to the time-lag measured will result in an improved measurement of the concentration, and with that result combined with the simulations that were performed a proof of concept of the observer structure is provided.

Chapter 7

Conclusion and Recommendations

An observability analysis has been performed resulting in an improved configuration for pressure difference measurements. Experiments were performed with a scaled VTS and it has been investigated how the pressure drop relates to the volumetric concentration, the efficiency decrease of centrifugal pumps has been investigated as well. Based on these findings an observer design was created which is suitable for both the full scale VTS and the test setup VTS. The observer design has been applied to measurements of the test setup VTS in order to evaluate improvements for the observation of the volumetric concentration of solids, this final chapter contains an answer to the research questions of this thesis and it ends with recommendations for further research.

7-1 Sub-Questions

An answer is provided for the sub-questions that were formulated for this thesis:

How significant is the contribution of the solids to the pressure drop created by wall friction in a vertical pipe?

It has been investigated what the contribution is of the solids on the wall shear stress of the mixture; in the test setup the wall friction of water contributes to approximately 10% of the pressure drop. Using pressure measurements in the u-bend it has been possible to make an approximation of the contribution of the mixture wall shear stress, multiple models were compared but there was not a model which gave a very good match with the experimental data. One of the difficulties encountered was that the pipe wall roughness of the test setup was altered throughout the experiments which made it hard to find a clear measure for the contribution of the solids to the wall shear stress. However using measurement data from all experiments it was found that the mixture wall shear stress does not deviate significantly from the fluid wall shear stress under the conditions of the test setup; for the calculation of the mixture density it would yield an error of less than 1% if the mixture wall shear stress is assumed to be equal to the fluid wall shear stress.

It is found that pipe roughness of the material used in the test setup (HDPE) is influenced by the transport of solids, and that the change in pipe roughness has a large effect on the measurement of the volumetric concentration with pressure difference measurements. Therefore determining the wall roughness of the VTS is needed periodically in order to account for this effect. Since the pressure drop due to wall friction scales with $\frac{1}{D}$ it is expected that the contribution of the mixture shear stress will be less significant in the full scale VTS.

Is the particle diameter of the solids measurable in the performance of a centrifugal pump?

A clear decrease in efficiency of the centrifugal pump could be noticed, related to the particle diameter. Using the efficiency decrease of the pump it was proven to be possible to approximate the volumetric concentration of the solids when gravel was used. It was attempted to measure the particle diameter based on the efficiency decrease but this did not yield satisfying results. The conclusion for this sub-question is: no, but if we know the concentration we can approximate what the efficiency decrease should be. Using this knowledge a deviation of the efficiency decrease can be monitored, which can be used to indicate failure mechanisms of the pumps.

What are the problems previously encountered with the Ensemble Kalman filter? How are they mitigated?

An observer was proposed before, for this observer it was proposed to measure the volumetric concentration locally in the booster stations and predict the concentration in the riser sections based on these measurements. This configuration would make the observation of all concentration states outside the booster station not observable. A new configuration is proposed where the pressure difference over a whole riser section is used as a measurement too, this has proven to increase the observability of the system theoretically. Furthermore, using simulations and experiments with the test setup VTS it has been proven that it increases the quality of the concentration observation in reality. A different issue found when implementing the Enkf is the artificial noise that is added to simulate model error, for states in the vicinity of zero this would result in negative concentrations. A mitigation is found which also improves the quality of the observation; added perturbation noise can be modelled relative to the ensemble mean preventing states to become below zero.

Is it possible to measure the particle diameter in a vertical flow using pressure difference measurements, combined with fluid velocity measurements?

Two methods were proposed for estimating the particle diameter based on a measured fluid velocity and concentration at multiple locations, using simulations of a validated model it was found that both methods yield good estimates of the particle diameter which means that theoretically it is feasible under the right conditions. The method that was selected for the observer design is an extension to the Ensemble Kalman Filter: proportionally the particle diameter is integrated using the lag that is measured between the estimate of the concentration and the measured concentration. This method has been tested using the experiments of the test setup VTS, it is found that using this method it has been made possible to distinguish different mixtures. Mixtures with a lower mean particle diameter were found to have a smaller settling velocity than mixtures with a larger mean particle diameter. There is a spread in the

found results indicating that the measurements are not very accurate, however it is argued that at the test setup particle diameters are harder to be measured due to the smaller pipe diameter and the shorter distance that is traveled in the riser. Using the designed structure it has been proven that an increase in the quality of the concentration observation can be achieved by adapting the particle diameter.

How do results of scaled experiments translate into a conclusion for a full scale vertical transport system?

An observer design is created and this design is valid for both the full scale and the test setup VTS, the only difference will be the fluid velocity model that has to be used. The pressure drop due to wall friction was determined to be approximately 10% of the static pressure drop, this contribution will likely be lower in the full scale VTS due to the larger riser diameter. It was shown that the wall roughness of the pipe has changed during the experiment program, this was found for the material HDPE. Whether this will occur in the full scale VTS will depend on the material choice for the inner pipe. It has been proven that the concentration can be measured very accurately over the course of $100m$ which is one tenth of the section of a riser. Likely the quality of this estimation will decrease when this distance is larger, however the summation of the concentrations can be corrected using long-range measurements which ensures that the mean concentration over the $1000m$ section will be approximated. The effect of the particle diameter was hard to measure in the test setup and the effect of this parameter will be more significant in the full scale VTS. Whether the particle diameter can be correctly adjusted depends on the correlation found between the measurements and the estimate at the end of the riser section.

7-2 Research Question

An answer to the main research question of this thesis is provided:

How can the observation of solid concentrations inside a riser be improved?

The answer to this question consists out of recommendations, and findings of the experiments. The following recommendations related to the research question were found during this research:

1. It was found that under the conditions of the measurements the wall shear stress induced by the mixture is very close to the wall shear stress of fluid only. Incorporating an estimate of the mixture wall shear stress in the observer is an improvement of what has been proposed. This feature has been important under the conditions of the test setup VTS due to the varying mixture velocity.
2. It is found that the efficiency decrease of the centrifugal pump can be predicted when the volumetric concentration and the particle diameter are known. Since an estimation of these parameters will be included in the observer the efficiency decrease of the pump can be monitored, this enables to find deviations from the predicted efficiency decrease which would indicate failure mechanisms.

3. A cascade observer structure has been designed, this structure has enabled that parameters could be observed with different algorithms. The fluid velocity observer needed a lot of tuning in the model error covariance matrix and this was enabled due to the cascade structure.

The following was proven using the measurement data of the test setup VTS:

1. By performing an observability analysis it has been proven that long range pressure difference measurements increase the observability of the concentration observation inside the riser. It has been proven using both simulations and experiments that using these measurements increase the quality of the concentration measurements in the Vertical Transport System when an Ensemble Kalman filter is used for the observation.

2. A method to measure the particle diameter in a Vertical Transport System did not exist and has now been designed: A proportional integral observer extension is added to the Enemble Kalman Filter. With this construction an estimate of the particle diameter is adjusted based on the lag that is measured between the observer output and the measured concentration at a chosen point. Using simulations it was proven that when the particle diameter of a slurry flow is not known, this algorithm can significantly increase the performance of the concentration observation. The method has been applied on the test setup VTS and using the measurements it was proven that the particle diameter estimation can increase the quality of the concentration observation. Due to the scaling of the test setup the conditions were not ideal to measure the particle diameter which was seen in the results, however it has been shown that mixtures containing different fractions of solids sizes could be distinguished.

7-3 Recommendations

It is found that the wall roughness of the pipes is changed due to the tests. Estimating the wall friction is important for the pressure difference measurements and therefore re-calibrating the pipe-wall roughness needs to be done periodically in order to remain good estimates of the solid concentration.

A flow meter was used which appears to provide a very noisy signal when solids are transported, and an unusable signal when manganese nodules were transported. It is recommended to investigate methods to improve this device, or switch to another method. An improvement of this device will also improve observation of the particle diameter, of which the velocity is determined with respect to the fluid velocity.

In the test setup VTS a conductivity concentration meter was installed of which the results unfortunately were not useful for this research, this was due to an inability to compensate the measurements for the quickly varying temperature of the mixture. It is recommended that it is investigated how this can be prevented at the full scale VTS.

Bibliography

[1] "Polymetallic Nodules," *International seabed authority*, pp. 1–8, 2006.

[2] M. van Dort, *Monitoring of the slurry density along the length of the VTS*. MSc Thesis, Tu Delft.

[3] J. van Wijk, *Vertical Hydraulic Transport for deep sea mining*. PhD thesis, Tu Delft.

[4] J. van Stappen, *Observing Solid Concentrations in a Vertical Hydraulic Transport System: Literature Survey*. 2018.

[5] R. I. Ferguson and M. Church, "A simple universal equation for grain settling velocity," *Journal of Sedimentary Research*, vol. 74, no. 6, pp. 933–937, 2000.

[6] J. Richardson and W. Zaki, "Sedimentation and fluidisation: Part I," *Chemical Engineering Research and Design*, vol. 75, no. 3, pp. S82–S100, 1997.

[7] P. N. Rowe, "A convenient empirical equation for estimation of the Richardson-Zaki exponent," *Chemical Engineering Science*, 1987.

[8] C. Hirsch, *Numerical Computation of Internal & External Flows*. Butterworth-Heinemann, 2nd ed., 2007.

[9] D. Jeltsema, *Modeling & Nonlinear Systems Theory*. 2nd ed., 2013.

[10] S. Hong, H.-h. Chun, S.-h. Kwon, M. H. Lee, and S. Member, "Observability Measures and Their Application to GPS / INS," *IEEE Transactions on Vehicular Technology*, vol. 57, no. 1, pp. 97–106, 2008.

[11] S. Dasselaar, E. de Hoog, S. de Jong, J. van Stappen, T. Mueller, and J. van Wijk, "Development and demonstration of a test setup for large scale slurry transport tests," tech. rep., European Commission Seventh Framework Programme NMP-2013.4.1-2 GA No. 604500, 2017.

[12] R. Clift and D. H. Manning Clift, "Continuous measurement of the density of flowing slurries," *International Journal of Multiphase Flow*, vol. 7, no. 5, pp. 555–561, 1981.

[13] A. Stepanoff, *Pumps and Blowers, Two-Phase Flow: Selected Advanced Topics.* J. Wiley, 1965.

[14] S. A. Miedema, "Considerations on limits of dredging processes," 1994.

[15] C. van den Berg, *Pipelines as Transportation Systems.* European Mining Course Proceedings, MTI, 1998.

[16] P. K. Swamee and A. K. Jain, "Explicit equations for pipe-flow problems," *Journal of Hydraulic Division, ASCE*, vol. 102, no. 5, pp. 657–664, 1976.

[17] C. A. Shook and A. S. Bartosik, "Particle-wall stresses in vertical slurry flows," vol. 81, pp. 117–124, 1994.

[18] A. L. Ferre and C. A. Shook, "Course partical Wall Friction in Vertical Slurry Flows," *Particulate Science and Technology*, vol. 16, no. 2, pp. 125–133, 1998.

[19] A. Bartosik, "Influence of Coarse-Dispersive Solid Phase on the "Particles-Wall" Shear Stress in Turbulent Slurry Flow with High Solid Concentration," *The Archive of Mechanical Engineering*, vol. LVII, no. 1, 2010.

[20] J. X. Xia, J. R. Ni, and C. Mendoza, "Hydraulic Lifting of Manganese Nodules Through a Riser," *Journal of Offshore Mechanics and Arctic Engineering*, vol. 126, no. 1, p. 72, 2004.

[21] Z. Lendek, R. Babuška, and B. de Schutter, "Distributed Kalman filtering for cascaded systems," *Engineering Applications of Artificial Intelligence*, vol. 21, no. 3, pp. 457–469, 2008.

[22] B. Owiller, "Oscilloscope Vertical Amplifier," 1969.

[23] M. Verhaegen and V. Verdult, *Filtering and system identification: A least squares approach.* 2007.

[24] G. Evensen, "The Ensemble Kalman Filter: Theoretical formulation and practical implementation," *Ocean Dynamics*, vol. 53, no. 4, pp. 343–367, 2003.

[25] G. Gaspari and S. E. Cohn, "Construction of Correlation Functions in Two and Three Dimensions," *Quarterly Journal of the Royal Meteorological Society*, vol. 125, no. 554, pp. 723–757, 1999.

[26] W. Boomsma, N. Ostergaard, P. Vercruijsse, A. Mitzlaff, L. Rattmann, G. Nicholson, K. Green, and J. Warnaars, "Terms of Reference for VTS design Confidential," tech. rep., European Commission Seventh Framework Programme NMP-2013.4.1-2 GA, 2014.

[27] G. Kitagawa, "A Self-Organizing State-Space Model," *Taylor & Francis*, vol. 93, no. 443, pp. 1203–1215, 2017.

[28] J. M. van Wijk and B. W. G. Blok, "The influence of grain size on the performance of conductivity concentration meters," *Flow Measurement and Instrumentation*, vol. 45, pp. 384–390, 2015.

[29] G. Archie, "The electrical resistivity Log as an aid in determining some reservoir characteristics," *Pet.Technol.*, vol. 1422, pp. 54–62, 1942.

[30] J. A. Sorensen and G. E. Glass, "Ion and temperature dependence of electrical conductance for natural waters," *Analytical Chemistry*, vol. 59, pp. 1594–1597, jul 1987.

Glossary

List of Symbols

Abbreviations

1DVHT	1-Dimensional Vertical Hydraulic Transport
b1DVHT	Basic 1-Dimensional Vertical Hydraulic Transport
CCM	Conductivity Concentration Meter
EKF	Extended Kalman Filter
EMF	Electromagnetic Flow Meter
EnKF	Ensemble Kalman Filter
PSD	Particle Size Distribution
VTS	Vertical Transport System

Greek Symbol

α	Empirical parameter	$[-]$
χ	Packing limiter	$[-]$
Δp	Pressure difference	$[kPa]$
Δt	Temporal discretization	$[t]$
Δz	Spatial discretization	$[m]$
ϵ_z	Axial dispersion coefficient	m^2/s
ϵ_{pipe}	Pipe-wall roughness	$[-]$
ϵ_{Taylor}	Taylor dispersion coefficient	m^2/s
μ_f	Dynamic viscosity of carrier fluid	$[Pa \cdot s]$
ψ	Flux limiter	$[-]$
ρ	Localization field	$[-]$

ρ_f	Fluid density	$[kg/m^3]$
ρ_m	Mixture density	$[kg/m^3]$
ρ_s	Solid density	$[kg/m^3]$
σ_c	Courant number	$[-]$
τ_f	Fluid wall shear stress	$[Pa]$
τ_m	Mixture wall shear stress	$[Pa]$
τ_s	Solid wall shear stress	$[Pa]$
d_m	Mean particle diameter	$[m]$
k	Time step indication	$[-]$

Roman symbol

$\bar{v}_m$	Bulk mixture velocity	$[m/s]$
a	Acceleration of mixture	$[m/s^2]$
A_p	Cross sectional area of riser	$[m^2]$
c_v	Volumetric concentration	$[-]$
$c_{v_{tot}}$	Total concentration in a section	$[m/s]$
D	Riser diameter	$[m]$
d	Particle diameter	$[mm]$
d_{50}	Mass mean particle diameter	$[mm]$
F	Mass flux	$[m/s]$
f_D	Darcy-Weisbach friction factor	$[-]$
g	Gravitational Constant	$[m/s^2]$
H	Output Matrix	$[-]$
i	Cell indication	$[-]$
K	Kalman gain	$[-]$
k_f	Fluid conductivity	$[-]$
k_m	Mixture conductivity	$[-]$
k_{01}, k_{02}	Conductivity measurements	$[\mu S]$
L	Riser length	m
m	Mass of slurry in test circuit	$[-]$
m_{diff}	Mass difference between riser and downcomer	$[kg]$
n_{rz}	Richardson and Zaki exponent	$[-]$
P	Integrator gain	$[-]$
p	Pressure	$[kPa]$
P_f	Estimated state covariance matrix	$[\sigma^2]$
$p_{01} - p_{14}$	Pressure measurements	$[kPa]$
P_{drive}	Power supplied to electro motor	$[kW]$
p_{in}	Absolute pressure before pump	$[kPa]$
p_{man}	Manometric pressure of pump	$[kPa]$
p_{out}	absolute pressure after pump	$[kPa]$

Q	State covariance matrix	$[\sigma^2]$
q	Number of ensembles	$[-]$
R	Measurement covariance matrix	$[\sigma^2]$
r	Ratio of gradients in flux limiter	$[-]$
Re	Reynolds number	$[-]$
Re_p	Particle Reynolds number	$[-]$
Stk	Stokes number	$[-]$
t	Time	$[s]$
T_0	Mixture temperature at $t = 0$	$[^oC]$
T_1, T_2	Temperature measurements	$[^oC]$
u	Input vector	$[-]$
v_f	Fluid velocity	$[m/s]$
v_m	Mixture velocity	$[m/s]$
v_s	Solid velocity	$[m/s]$
w	Settling velocity	$[m/s]$
w_h	Hindered settling velocity	$[m/s]$
w_t	Terminal settling velocity	$[m/s]$
x	State vector	$[m]$
y	Output vector	$[m]$
z	Height	$[m]$

Appendix A

Conductivity Concentration Meter

In this section the measurements of the conductivity concentration meter CCM are evaluated. It is tested if this device will be suitable for validating the observer.

A-1 Theory

A conductivity concentration meter was used in the test setup, in [28] the calibration of this device is elaborated. The measured volumetric concentration is derived from the ratio between the mixture conductivity k_m and the conductivity of water k_f. For sand the equation relating conductivity can be approximated with the Maxwell model:

$$\frac{k_m}{k_f} = \frac{2 - 2 \cdot c_v}{2 + c_v} \tag{A-1}$$

A different relation that can be used is the Archie Equation [29]:

$$\frac{k_m}{k_f} = (1 - c_v)^{\zeta} \tag{A-2}$$

During the slurry tests only k_m can be measured. It is needed to estimate what k_f would be under the same conditions in order to use equation A-1 or A-2. During the tests the fluid conductivity is measured at $t = 0$ when no solids are present yet, after that k_f is determined based on the change in temperature:

$$\frac{k_{f,t}}{k_{f,t=0}} = 1 + \alpha \cdot (T - T_0) \tag{A-3}$$

In this equation α represents an empirical relation between the temperature change and the fluid conductivity [30].

A-2 Approach and Results

Sand measurements [2,6,13] and gravel measurements [3,4,5] are used to test the measurements. The calculated concentration is compared with the concentration determined with pressure difference measurement $\Delta p_{02,01}$ which is close to the CCM. Measurements are investigated up to $t = 1300s$. Again the VAF is calculated between the signals. The results are shown in table A-1.

Table A-1: VAF between $\Delta p_{02,01}$ and CCM

	Sand			gravel		
Measurement	2	6	13	3	4	5
VAF	84.34	79.56	68.58	17.52	67.44	86.48

Both signals show relatively good agreement for most of the measurements. However one of the flaws of the measurements is discovered. The results of the conductivity meter need to be corrected for the temperature. It is found that during the experiments the temperature in the system is not homogeneous. When filling the circuit the water that is below the mineshaft is cooler than the water higher in the system. When circulating the flow the temperature differences are transported, the differences diffuse but it takes time. It is found that the temperature sensor was not able to accurately measure the quickly varying temperature which causes that compensating the conductivity meter for the temperature properly was not possible. In figure A-1 and A-2 the influence of the temperature on the concentration measurement is visible. Oscilations are present in the outcome.

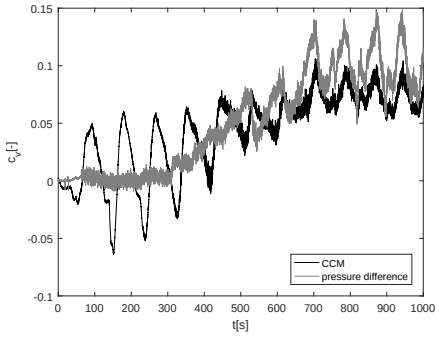

Figure A-1: Measured $c_v[-]$, Measurement 4

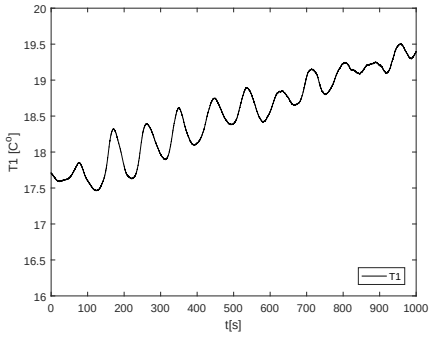

Figure A-2: Measured temperature, Measurement 4

It can be seen that for the first 600s in the measurement the CCM is strongly affected by the temperature variation, the relationship to the temperature can be observed when looking at the figure. As a 2nd test the measurements have been applied to the watertests, the outcome of the measurements should yield $c_v = 0$ under the conditions. It was concluded that it was not possible to correctly adjust the measurements for the temperature. The cause of this problem is that the temperature sensor did not adjust fast enough to measure the varying temperature.

Appendix B

Solids effect

B-1 Solid effect on centrifugal pumps

Results of the concentration measurements using pump efficiency for the different measurements are depicted in the figures below:

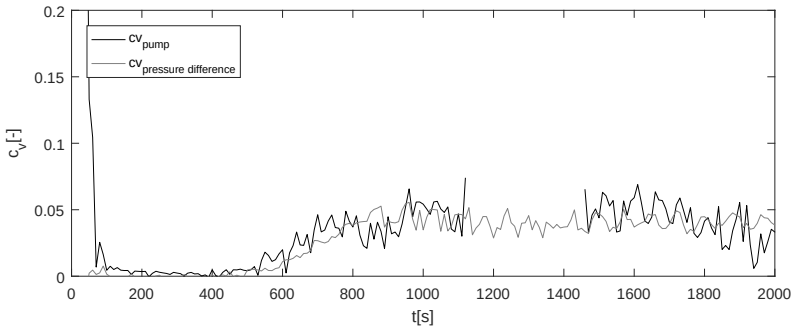

Figure B-1: Measured ($c_v[-]$), measurement 3

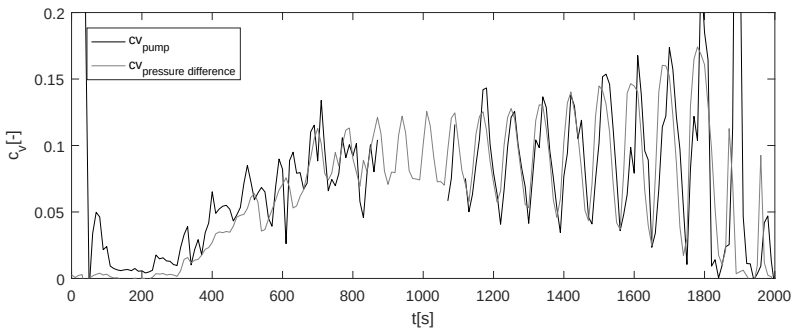

Figure B-2: Measured ($c_v[-]$), measurement 4

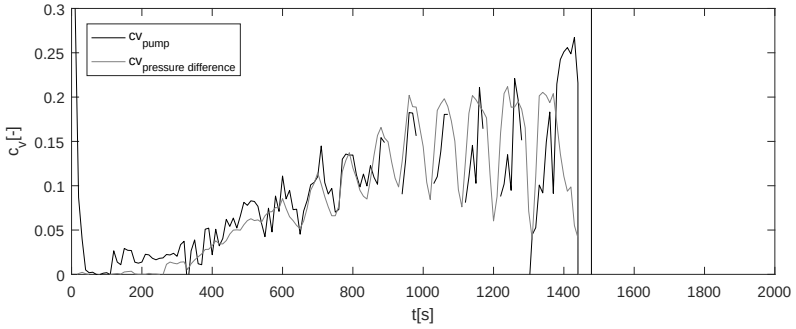

Figure B-3: Measured ($c_v[-]$), measurement 5

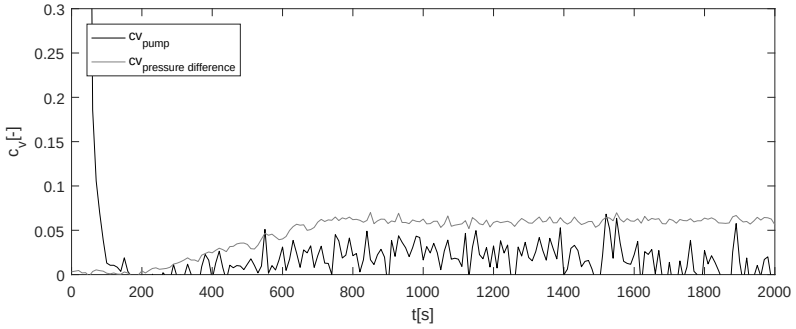

Figure B-4: Measured ($c_v[-]$), measurement 6

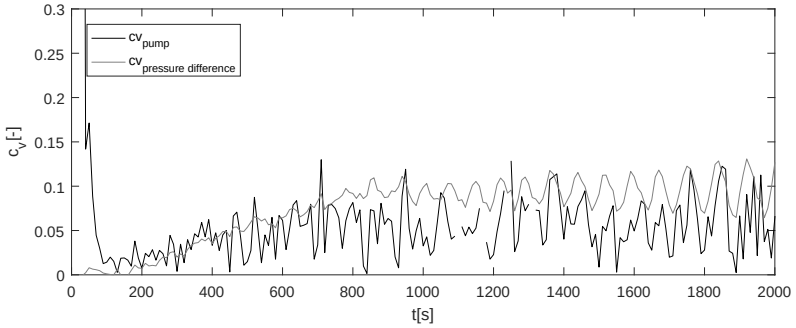

Figure B-5: Measured ($c_v[-]$), measurement 13

Appendix C

Fluid velocity Observation

Results of the fluid velocity observer for the different measurements are depicted in the figures below:

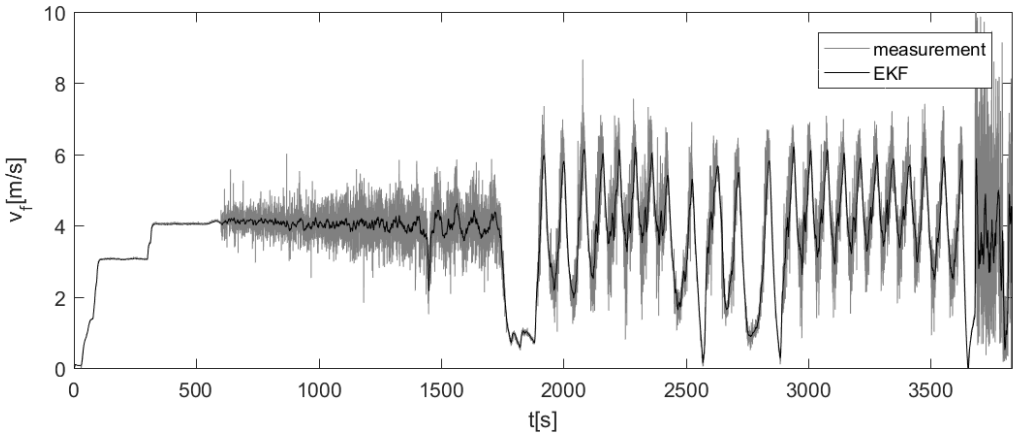

Figure C-1: Estimated fluid velocity $(v_f[m/s])$, measurement 1

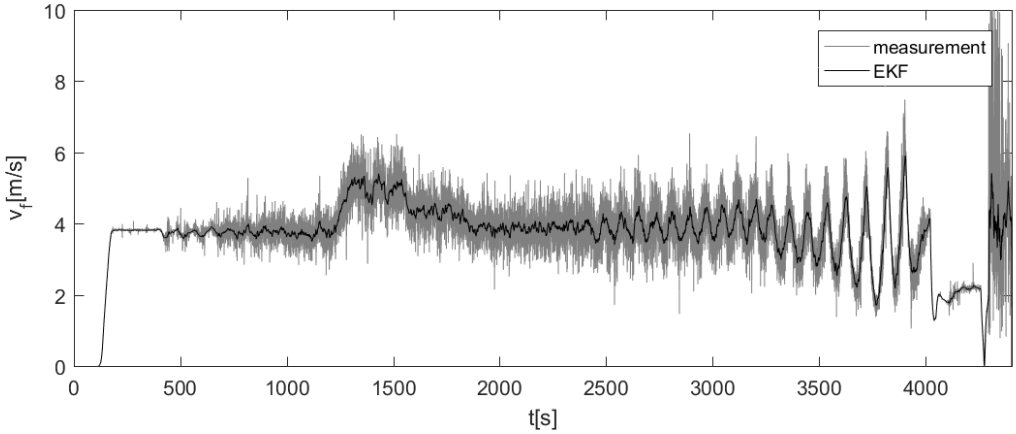

Figure C-2: Estimated fluid velocity $(v_f[m/s])$, measurement 2

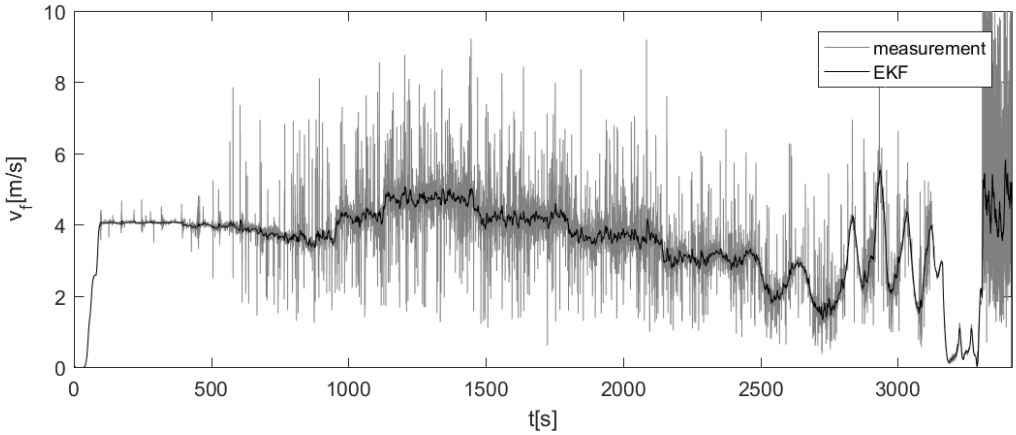

Figure C-3: Estimated fluid velocity $(v_f[m/s])$, measurement 3

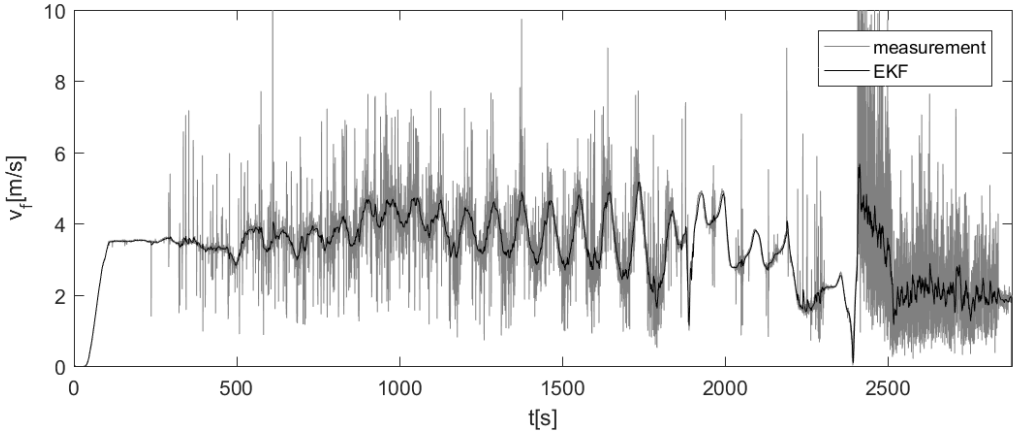

Figure C-4: Estimated fluid velocity $(v_f[m/s])$, measurement 4

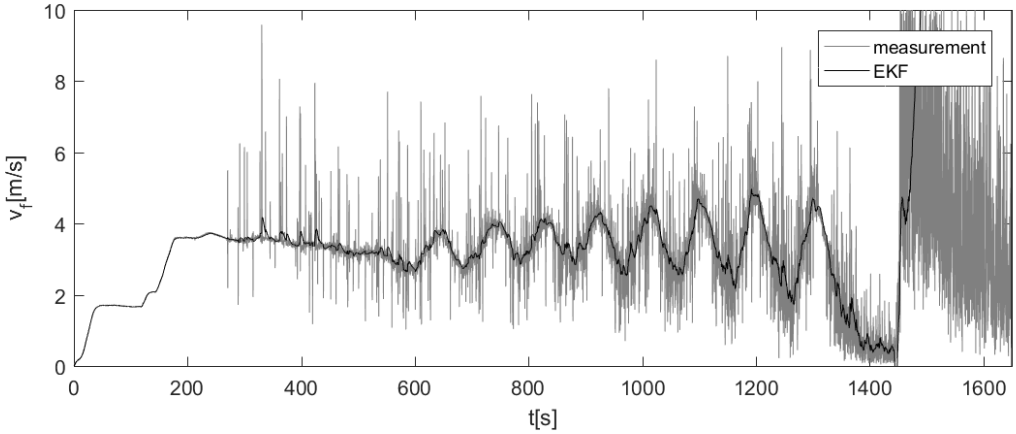

Figure C-5: Estimated fluid velocity $(v_f[m/s])$, measurement 5

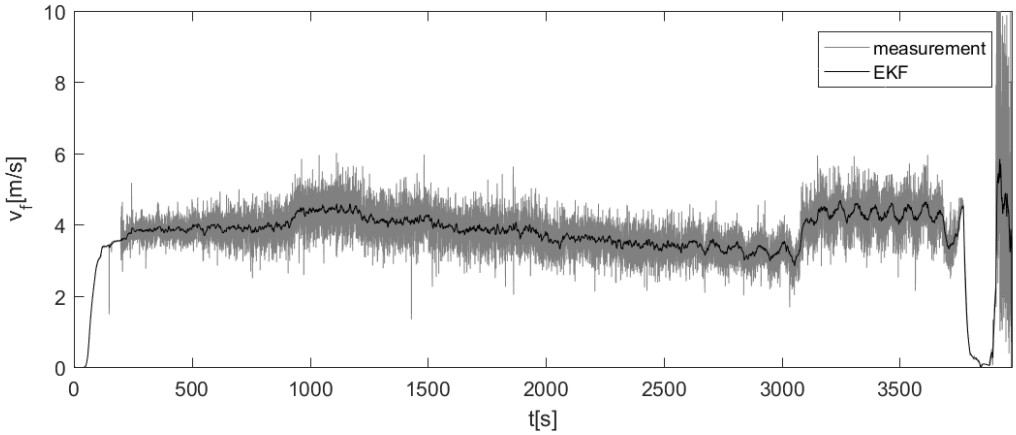

Figure C-6: Estimated fluid velocity $(v_f[m/s])$, measurement 6

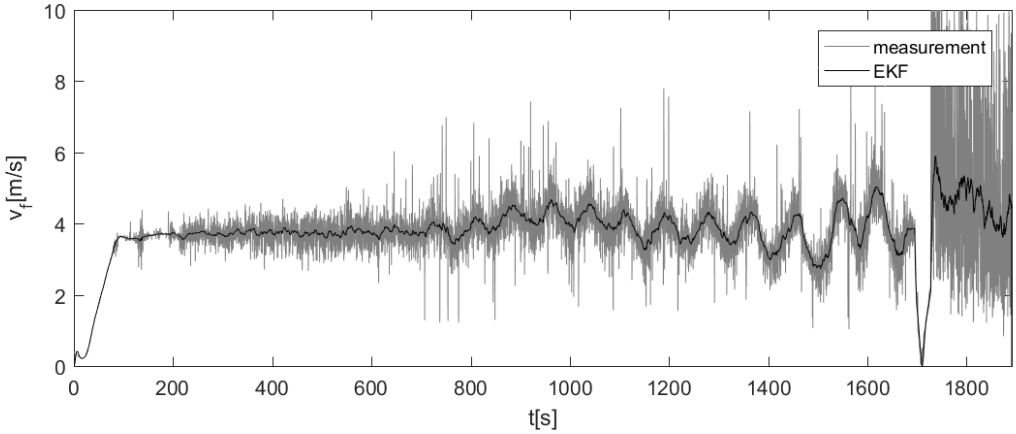

Figure C-7: Estimated fluid velocity $(v_f[m/s])$, measurement 7

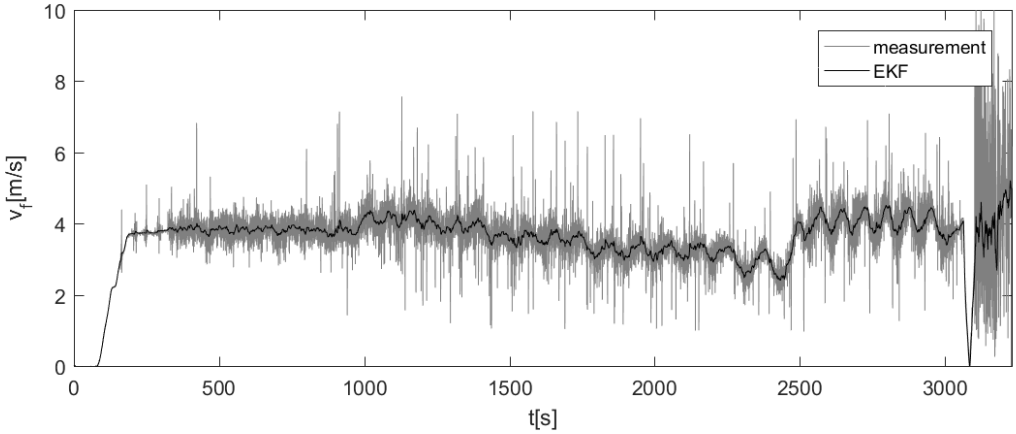

Figure C-8: Estimated fluid velocity $(v_f[m/s])$, measurement 8

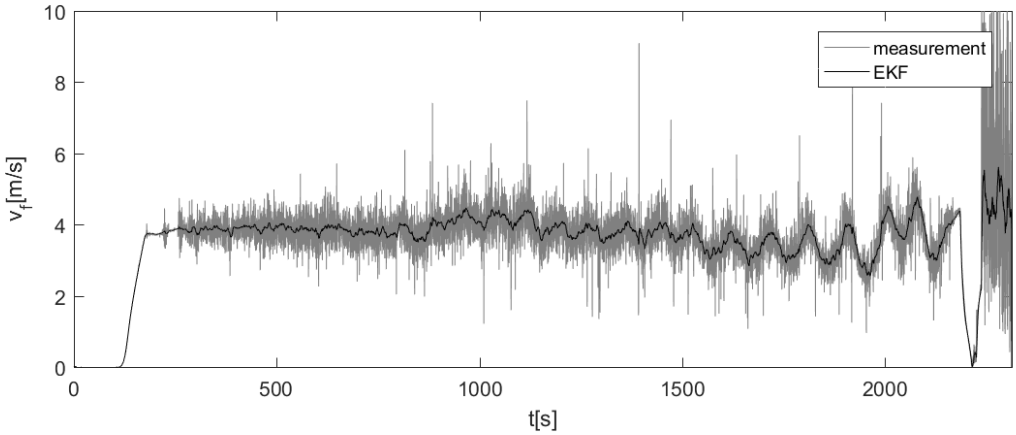

Figure C-9: Estimated fluid velocity $(v_f[m/s])$, measurement 9

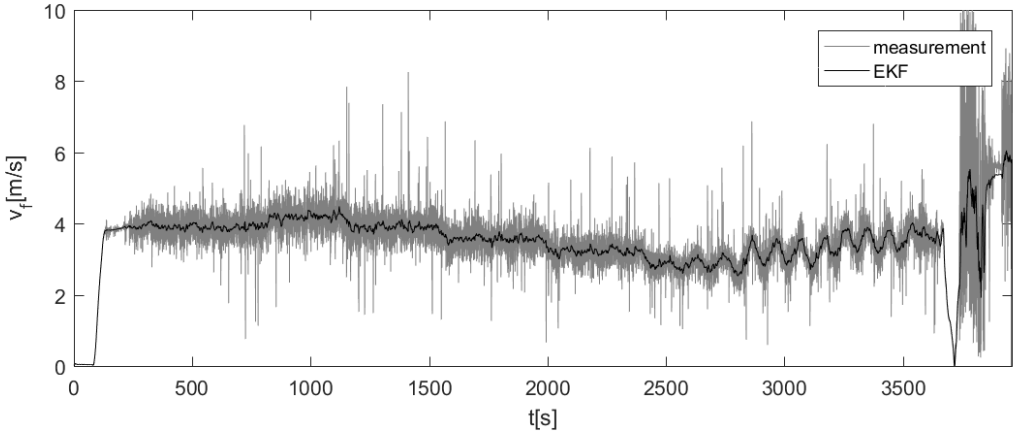

Figure C-10: Estimated fluid velocity $(v_f[m/s])$, measurement 10

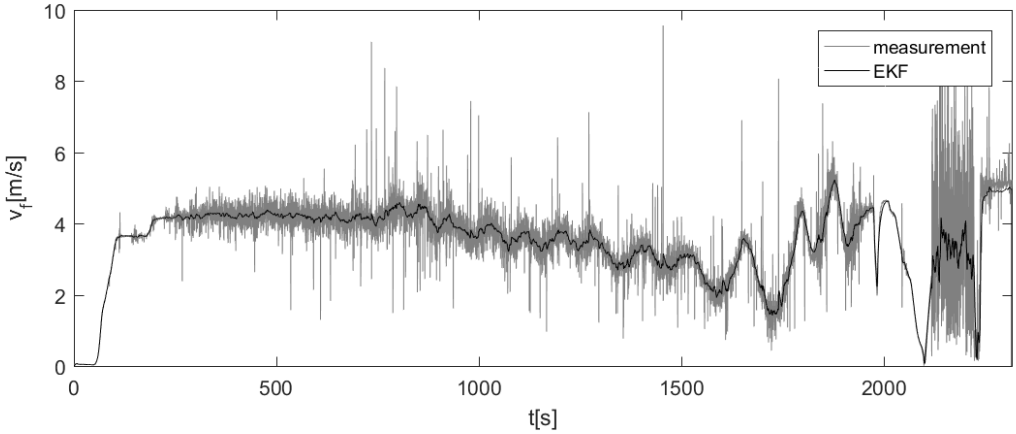

Figure C-11: Estimated fluid velocity $(v_f[m/s])$, measurement 11

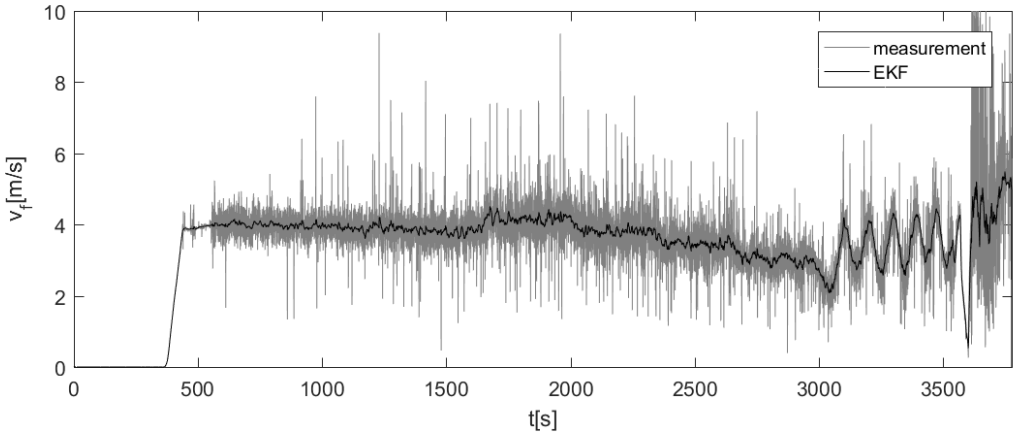

Figure C-12: Estimated fluid velocity $(v_f[m/s])$, measurement 12

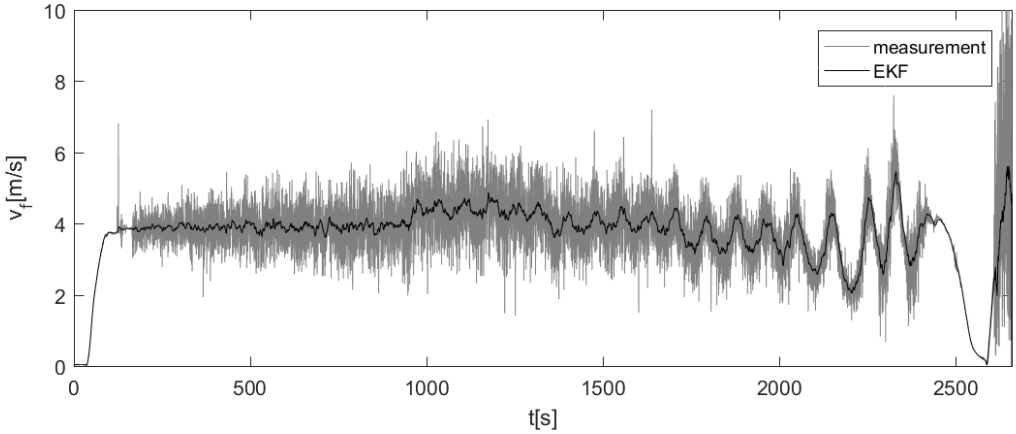

Figure C-13: Estimated fluid velocity $(v_f[m/s])$, measurement 13

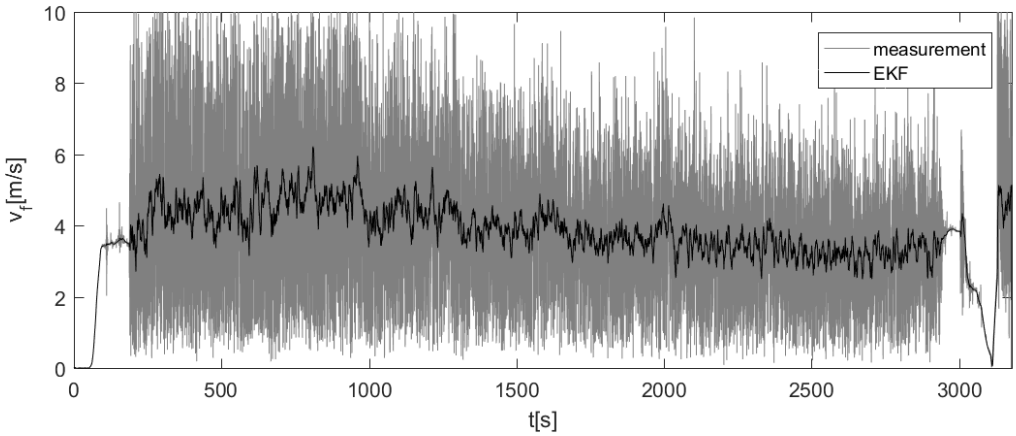

Figure C-14: Estimated fluid velocity $(v_f[m/s])$, measurement 14

Appendix D

Particle Diameter Observation (EKF)

The observer for the particle diameter designed in chapter 5 is adjusted and tested on the measurements. Since the particle diameter is directly related to the settling velocity, it is attempted to measure the settling velocity in order to prevent problems with negative estimated values..

D-1 Approach

The model to observe the particle diameter for the most optimal situation has been described in equation 5-14. It was written in a form that it was easy to apply on the simulations. The model is rewritten in order to be suitable for the measurements, mass fluxes are now considered in kg/s. The revised model is depicted in the appendix. The assumption is made that $v_{fi} = v_{fo}$ (for v_f a moving average filter is used) and that $n_{rz} = 1.4$.

$$\begin{aligned} m_{tot}(k+1) =& \Delta t \cdot (v_f(k) - w_t(k) \cdot (1 - c_{vi}(k))^{1.4}) \cdot (\rho_s \cdot c_{vi} \cdot A_p) - \\ & \Delta t \cdot (v_f(k) - w_t(k) \cdot (1 - c_{vo}(k))^{1.4}) \cdot (\rho_s \cdot c_{vo} \cdot A_p) + m_{tot}(k) \\ & \Delta t \cdot v_f \cdot (\rho_f \cdot (1 - c_{vi}) \cdot A_p - \rho_f \cdot (1 - c_{vo}) \cdot A_p) \\ w_t(k+1) =& w_t(k) \end{aligned} \tag{D-1}$$

First it is attempted to estimate the settling velocity, this saves computational power due to the reduction in the complexness of the Jacobian. The goal is to estimate this parameter by observing the ingoing and outgoing flux of a chosen section. $\Delta p_{12,11}$ and $\Delta p_{02,01}$ are used to measure the inlet and outlet concentration respectively. The mass of the section is measured using $\Delta p_{11,02}$.

D-2 Results

The observer is tested on all measurements. The best results, found for measurement 3,4 and 13 are shown in figure D-1.

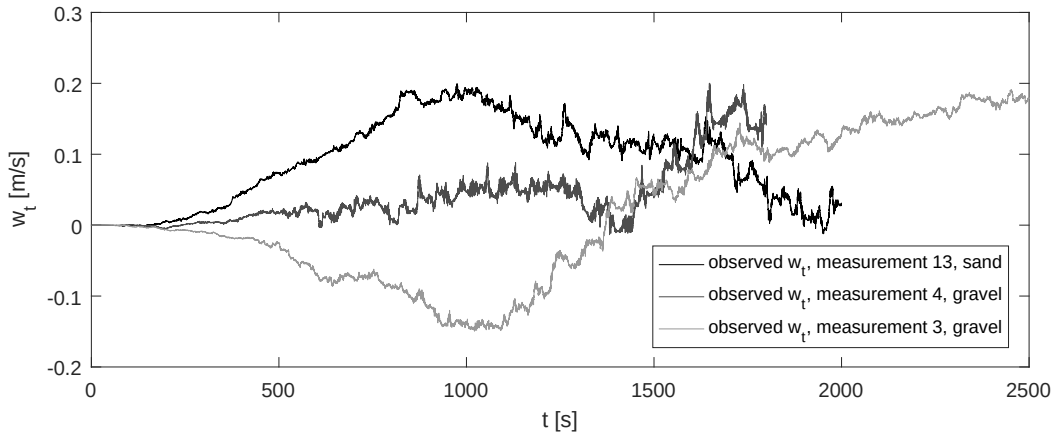

Figure D-1: d_m

It can be seen that after a period of time the settling velocity of the gravel measurements was found larger than the found value for sand measurements. However in between negative values are estimated. For most measurements the observed value oscillates and a clear steady state was not reached. Different EKF configurations (Q,R) and Δp configurations were tested, but a configuration yielding a clear output for all measurements (1:14) was not achieved.

D-3 Conclusion

It was already concluded that the particle diameter observer is very sensitive. The observer is tested using Δp measurements and It is found that the density measurements in combination with the fluid velocity measurements does not provide a clear observation of the settling velocity using the model that was constructed.

Appendix E

Concentration Observation

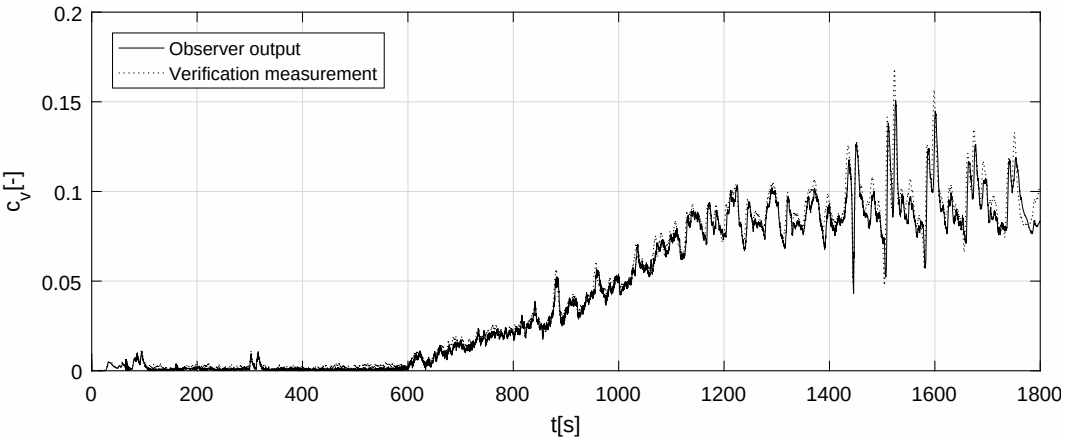

Figure E-1: Estimated concentration ($c_v[-]$), measurement 1

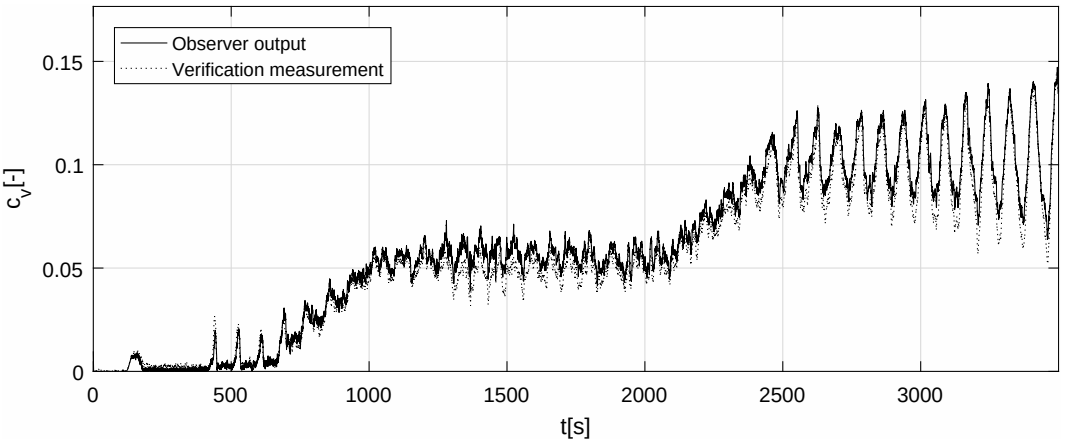

Figure E-2: Estimated concentration ($c_v[-]$), measurement 2

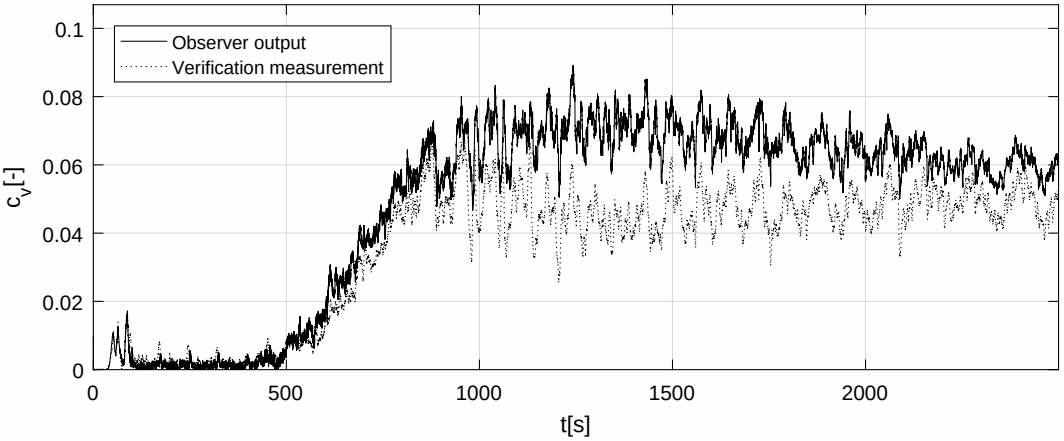

Figure E-3: Estimated concentration $(c_v[-])$, measurement 3

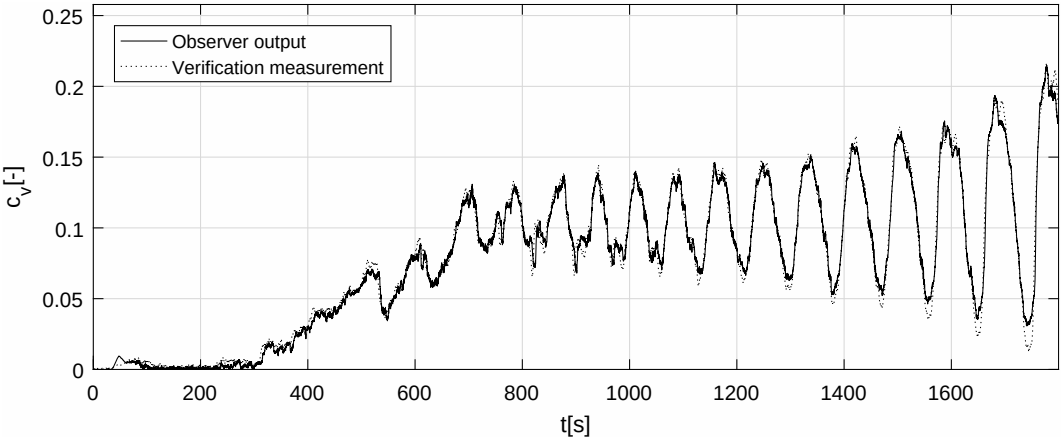

Figure E-4: Estimated concentration $(c_v[-])$, measurement 4

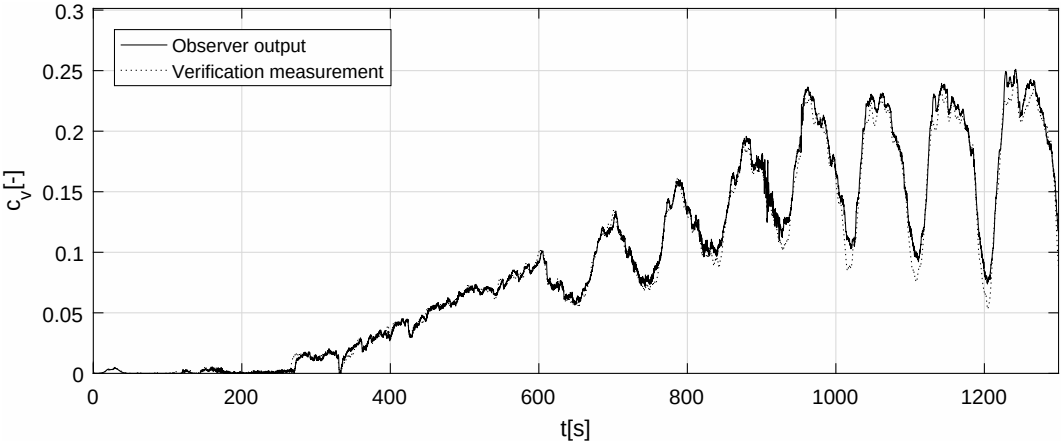

Figure E-5: Estimated concentration $(c_v[-])$, measurement 5

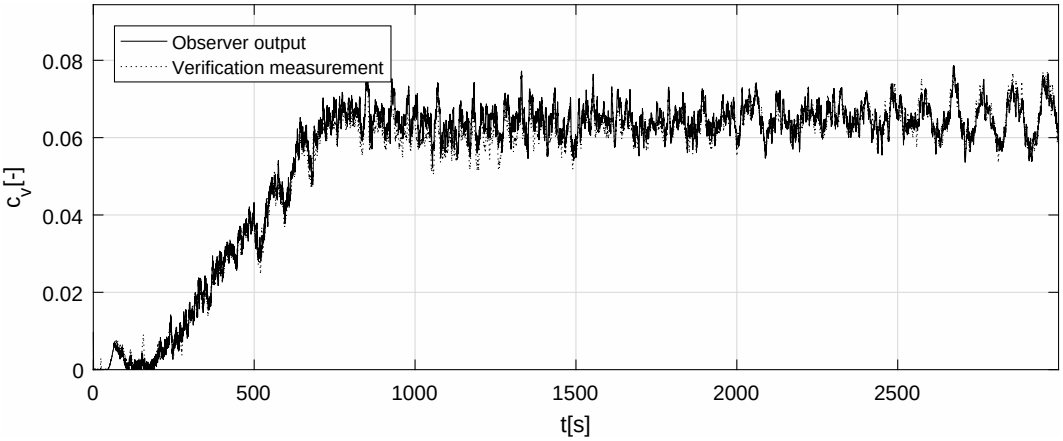

Figure E-6: Estimated concentration $(c_v[-])$, measurement 6

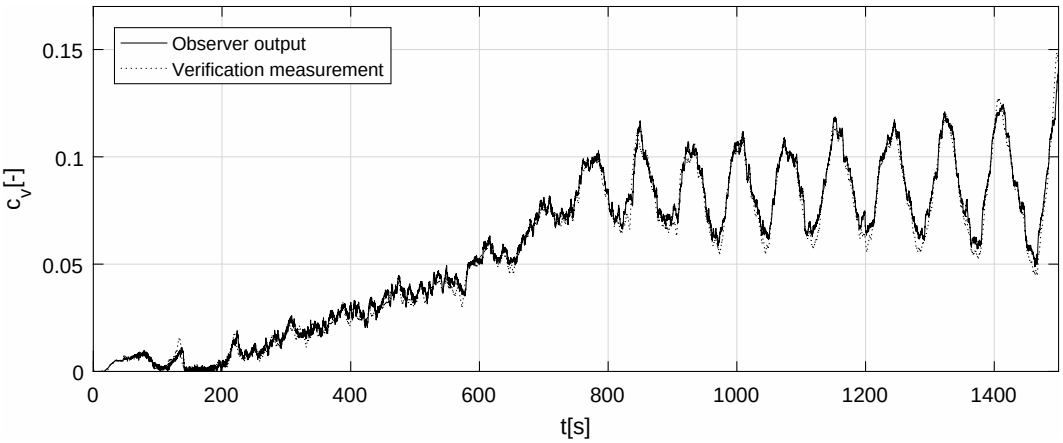

Figure E-7: Estimated concentration $(c_v[-])$, measurement 7

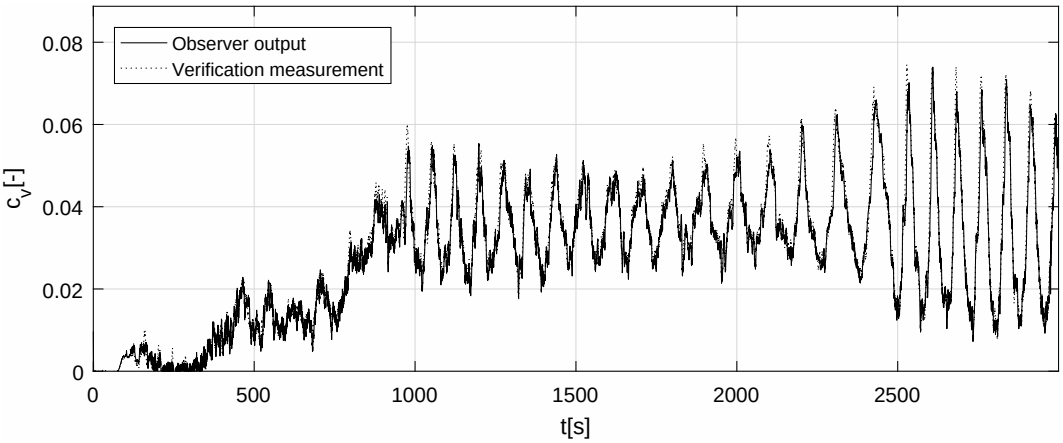

Figure E-8: Estimated concentration $(c_v[-])$, measurement 8

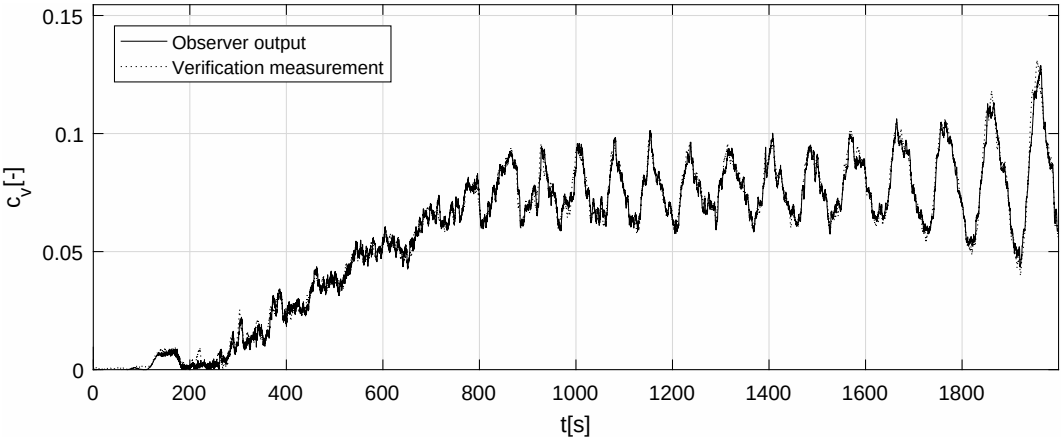

Figure E-9: Estimated concentration $(c_v[-])$, measurement 9

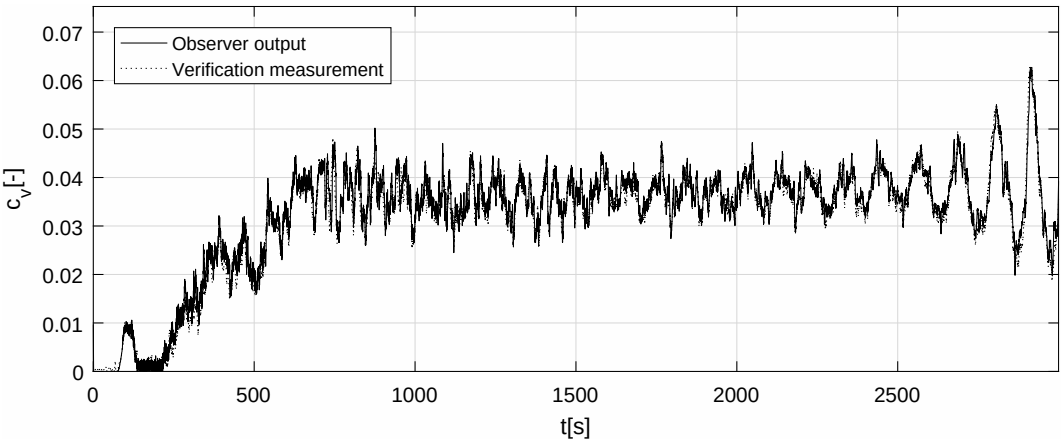

Figure E-10: Estimated concentration $(c_v[-])$, measurement 10

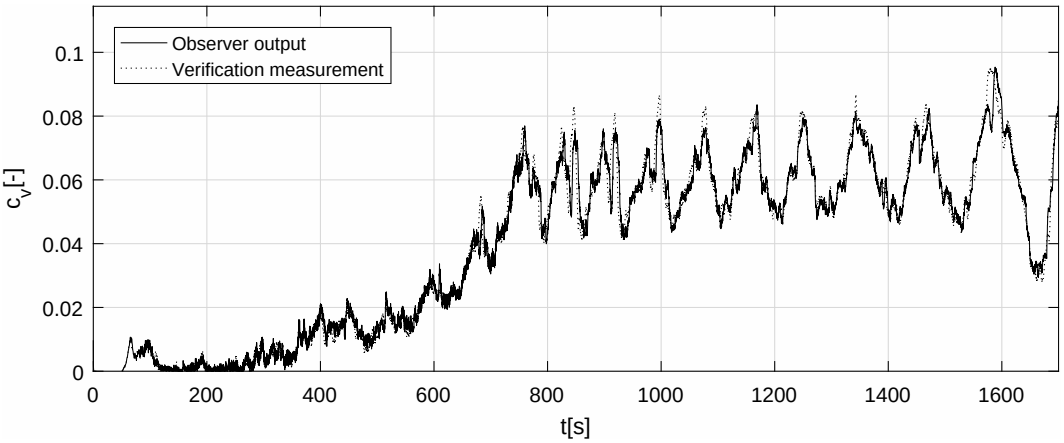

Figure E-11: Estimated concentration $(c_v[-])$, measurement 11

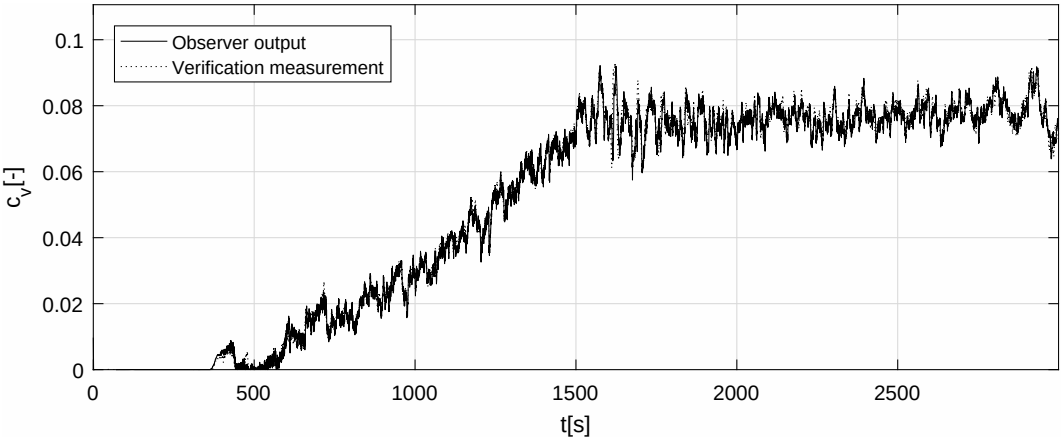

Figure E-12: Estimated concentration $(c_v[-])$, measurement 12

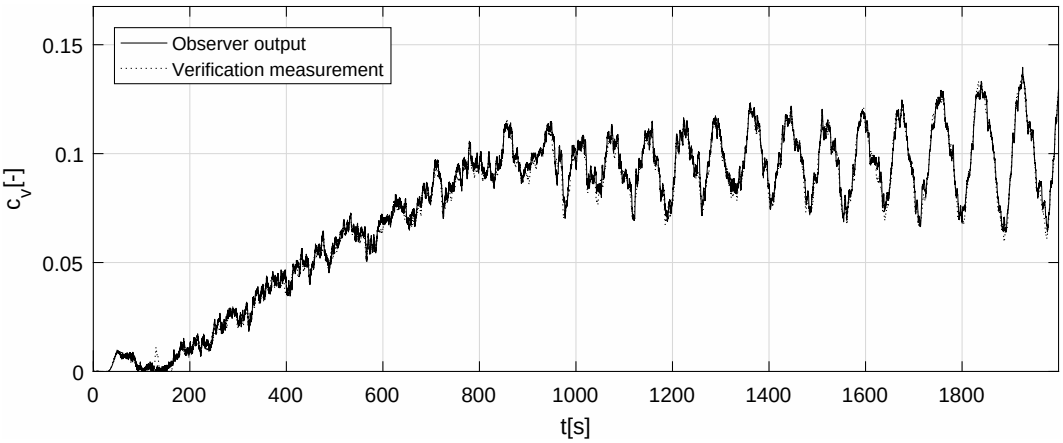

Figure E-13: Estimated concentration $(c_v[-])$, measurement 13

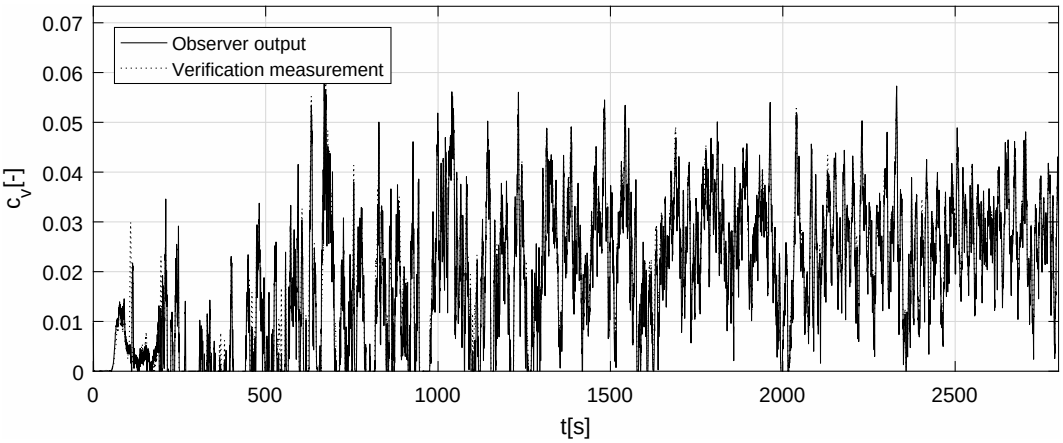

Figure E-14: Estimated concentration $(c_v[-])$, measurement 14